

DEVELOPMENT OF A THERMALLY ACTIVATED PYROTECHNIC  
INITIATOR BASED ON FABRICATION OF LOW TEMPERATURE  
CO-FIRED CERAMIC COMPONENTS

A Thesis

Presented in Partial Fulfillment of the Requirements for the

Degree of Master of Science

with a

Major in Nuclear Engineering

in the

College of Graduate Studies

University of Idaho

by

Lee E. Fuller

December 2013

Major Professor: John C. Crepeau, Ph.D.

## Authorization to Submit Thesis

This thesis of Lee E. Fuller, submitted for the degree of Master of Science with a major in Nuclear Engineering and titled "Development of a Thermally Activated Pyrotechnic Initiator Based on Fabrication of Low Temperature Co-Fired Ceramic Components," has been reviewed in final form. Permission, as indicated by the signatures and dates given below, is now granted to submit final copies to the College of Graduate Studies for approval.

Major Professor:

\_\_\_\_\_ Date: \_\_\_\_\_  
Dr. John C. Crepeau

Committee  
Members:

\_\_\_\_\_ Date: \_\_\_\_\_  
Dr. Karl K. Rink

\_\_\_\_\_ Date: \_\_\_\_\_  
Dr. Fred D. Barlow III

\_\_\_\_\_ Date: \_\_\_\_\_  
Dr. Gabriel P. Potirniche

Department  
Administrator:

\_\_\_\_\_ Date: \_\_\_\_\_  
Dr. John C. Crepeau

Discipline's  
College Dean:

\_\_\_\_\_ Date: \_\_\_\_\_  
Dr. Larry Stauffer

Final Approval and Acceptance by the College of Graduate Studies:

\_\_\_\_\_ Date: \_\_\_\_\_  
Dr. Jie Chen

## Abstract

Pyrotechnic initiators are commonly employed as primary charges for initiating combustion of less sensitive energetic compounds. Such devices must maintain reliable operation throughout their working lifetimes and require the utmost care during manufacturing. Implementation of low temperature co-fired ceramic in initiator design provides a reliable, versatile, and low cost material readily capable of mass production using existing equipment. Standard practice for industrial production of initiators requires the application of multiple safety measures when handling the highly volatile compounds required for initiator manufacturing. Incorporating a new design capable of negating the use of dangerous compounds during fabrication will lead to a cost effective and safe method for the construction of initiators. The proposed design could be fabricated in a nonreactive state and thermally activated at any time prior to initiation, leading to reduction of required safety measure. Evaluation of a prototype initiator meeting such specifications requires careful consideration in design and testing procedures. The necessary reliable operation of initiators is largely based in the ability for such a device to maintain a hermetic seal. Careful analysis through the use of red dye penetrant, helium mass spectrometry, and radioisotope leak detection (Radiflo®) will result in a comprehensive study of the proposed initiator package and mechanism of electrical initiation. A fully functional prototype is intended to be a proof-of-concept design that could be optimized for any specific application applicable to initiator operation.

## Acknowledgements

I would like to thank the following:

The Nuclear Regulatory Commission (NRC) for providing the funding necessary to make my time in graduate school possible.

Dr. Karl Rink for giving me the time, effort, and advice to develop this idea as well as tireless effort and continuous optimism needed to keep going.

Dr. Fred Barlow for providing me with laboratory space as well as training the advice needed to fabricate necessary components.

Dr. Crepeau for providing me with exactly the support necessary to make this research come together in the face of adversity.

Dr. Gabriel Portirniche for having confidence in my abilities and including me in research work beyond this thesis.

Bryce Gill for the help with producing code capable of solving everything necessary.

Russ Porter and Robert Fuhrmann for all of the advice, technical support, and machining essential to successfully conducting tests.

Molly, Elaine, and Becky for their patience and for providing me with the best administrative support anyone could ever ask for.

All of my family, friends, and fellow graduate students. Without supporting one another, nothing would ever get accomplished.

## **Dedication**

I dedicate this thesis to my loving wife MJ  
You are my inspiration in all things

## Table of contents

Authorization to Submit Thesis .....	ii
Abstract.....	iii
Acknowledgements.....	iv
Dedication.....	v
Table of contents.....	vi
List of figures.....	ix
List of tables .....	x
Chapter 1. Introduction.....	1
Chapter 2. Objectives.....	3
Chapter 3. Review of literature.....	4
3.1. Definition of Micro-Electro-Mechanical Systems (MEMS) .....	4
3.2. Low Temperature Co-Fired Ceramic (LTCC).....	4
3.2.1 LTCC component fabrication.....	6
3.2.2. CNC punch forming .....	7
3.2.3. Screen printing .....	9
3.2.4. Via interconnect .....	10
3.2.5. LTCC combustion system fabrication.....	10
3.2.6. Hermetic packaging of LTCC .....	11
3.3. Pyrotechnic initiator potential failure .....	13
3.4. Leak rates .....	17
3.4.1. Viscous flow.....	20
3.4.2. Molecular flow .....	22
3.4.3. Transitional flow .....	24
3.4.4. Flow regime systems.....	25
3.5. Leak detection methods .....	27
3.5.1. Helium Mass Spectrometry (HMS).....	29
3.5.2. Radiflo® leak rate detection.....	30
3.5.3. Dye penetrant inspection (DPI) leak detection.....	32
3.6. Back pressurization .....	34

3.6.1. HMS technique: molecular flow approach.....	38
3.6.2. Radioisotope technique: molecular flow approach .....	39
3.6.3. Radioisotope technique: Radiflo® equation .....	40
3.6.4. Iterative solution to back pressurization approach .....	41
3.7. Leak test limitations .....	42
3.7.1. Variation in dwell time and internal volume.....	44
3.7.2. Variation in tracer gas concentration.....	47
3.7.3. False negatives and the necessity of gross leak detection .....	51
Chapter 4. Design theory .....	52
4.1. Initiator design capabilities .....	52
4.1. Cavity seal methodology.....	53
4.2. Central layers .....	54
4.3. Lid interface .....	55
4.4. Base layer.....	56
4.5. Ceramic assembly .....	58
4.6. Prototype design.....	59
Chapter 5. Materials.....	60
5.1. LTCC material .....	60
5.2. Interconnect material.....	60
5.3. Adhesive material .....	61
5.4. Reactive compound.....	62
Chapter 6. Experimental design and evaluation methods.....	65
6.1. Experimental overview .....	65
6.2. Experimental methods.....	65
6.2.1. Dye penetrant test.....	66
6.2.2. Radiflo® leak rate test.....	68
6.2.3. Helium mass spectrometer leak rate test .....	71
6.2.4. Initiator firing test.....	73
6.2.3. Error Analysis.....	74
Chapter 7. Results .....	77

7.1. LTCC-via specimens.....	77
7.1.1. LTCC-via Radiflo® analysis.....	78
7.1.2. LTCC-via helium mass spectrometer analysis.....	79
7.1.3. LTCC-via dye penetrant analysis.....	80
7.2. LTCC initiator prototype .....	81
7.2.1. Initiator fabrication results .....	82
7.2.2. Initiator spark gap results .....	83
7.2.3. Initiator dye penetrant inspection results.....	86
7.2.4. Radiflo® test results.....	88
7.2.5. Full component initiation test results .....	90
Chapter 8. Conclusion .....	95
Chapter 9. Future work .....	97
Bibliography .....	100
Appendix A.....	104
Appendix B.....	107
Appendix C.....	109
Appendix D.....	112
Appendix E .....	115
Appendix F .....	120
Appendix G.....	125
Primary function: accept inputs and process data.....	126
Secondary function: refine data point associated error.....	127
Secondary function: export data to excel document .....	130
Appendix H.....	131

## List of figures

Figure 1. LTCC fabrication flow diagram.....	7
Figure 2. Ridged edges on LTCC punched profile.....	8
Figure 3. LTCC screen printed solder pad with via.....	9
Figure 4. Typical bridge-wire initiator excluding non-essential body components .....	14
Figure 5. Expanded view of bridge-wire initiator .....	15
Figure 6. Dye penetrant test on LTCC prototypes.....	34
Figure 7. Effect of dwell time on gross leak rate analysis.....	45
Figure 8. Effect of internal volume on leak rate analysis .....	46
Figure 9. Effect of initial internal partial pressure on leak analysis .....	49
Figure 10. LTCC initiator central layer .....	54
Figure 11. LTCC initiator top layer.....	56
Figure 12. LTCC initiator dimpled lid.....	56
Figure 13. LTCC initiator base layer.....	57
Figure 14. LTCC initiator layer assembly .....	58
Figure 15. LTCC initiator fully assembled cutaway view.....	59
Figure 16. LTCC-via specimens containing 1 and 16 vias respectively .....	77
Figure 17. Dye penetration in LTCC-via specimen.....	81
Figure 18. Spark gap (left: pre firing, right: post firing) .....	83
Figure 19. Cracked spark gap specimen .....	84
Figure 20. JB Weld gross leak specimen.....	88
Figure 21. LTCC post heat treatment .....	91
Figure 22. LTCC fully functional test specimen 1 .....	92
Figure 23. Hole observe in test specimen 2.....	92
Figure 24. Burnt remains of spark gap on interior of specimen 2 .....	93
Figure 25. Square top cavity front: (A), Square top cavity back: (B), Circular top cavity front: (C), Circular top cavity back: (D).....	106
Figure 26. Ruthberg standards plot [29].....	113

## List of tables

Table 1. Adhesive selection criteria.....	62
Table 2. Alcatel HMS experimental error .....	76
Table 3. Radiflo® test comparison .....	78
Table 4. Spark initiation voltage.....	84
Table 5. DPI adhesive result comparison .....	86

## **Chapter 1. Introduction**

Manufacturing initiators or detonators generally requires the use of energetic materials. Multiple safety implementations are used to properly handle these materials and ensure both the safety of the operators as well as equipment used for assembly. Energetic materials are sensitive to contact, friction, or heat and can easily be mishandled with undesirable consequences. The safety requirements meant for control of these materials are expensive and ultimately increase the individual cost of each initiator or detonator device. The opportunity to employ methods for eliminating the direct involvement of energetic materials in fabrication provides a potential for significant cost reduction while simultaneously and significantly decreasing the risk involved in manufacturing. Design of an initiator or detonator and development of a manufacturing method for a thermally activated device could alleviate or eliminate the necessity for certain safety procedures required during assembly.

Envision an initiator that could be completely assembled without the need to work with energetic compounds and then thermally activated to become “live” at any time after assembly, prior to, or even after shipment. At any time before thermal activation, the initiator/detonator would behave as a non-reactive and completely inert device utterly incapable of premature firing. The effective implementation of this device with proper supporting equipment would allow activation to occur at any time following manufacturing, long term storage, shipment, or even installation prior to initiation. The materials necessary for this device are readily available for industrial mass production and require a minimum of special tooling.

Preliminary fabrication of this device implements low temperature co-fired ceramic (LTCC) printing technology for production of multiple test prototypes. LTCC technology is primarily used for the construction of micro-electronic devices, a market that is not only driven extensively by low cost production, but also contains design flexibility that can easily be adapted for fabricating initiator components. The availability of LTCC coupled with the ease of design manipulation provides an ideal platform for rapidly building both initiators and detonators capable of post fabrication heat treatment. Naturally this particular design is not without its own pitfalls which necessitate the use of various testing techniques to ensure proper functioning, implementation, and potential longevity of the initiator device. However, implementation of such a device can lay the ground work for a revolutionary upgrade in the initiator manufacturing field.

## Chapter 2. Objectives

The objective of this research is to demonstrate proof-of-concept for the fabrication and operation of a multilayered ceramic thermally activated initiator. For completion of this research, data pertaining to the hermetic properties of LTCC substrate must be obtained and quantified, repeatability of an LTCC based initiator spark gap must be acquired, and testing the performance of a fully assembled prototype initiator must be conducted. The goals outlined in this research are:

- Development of a prototype LTCC based spark gap initiator
- Experimental quantification of leak rates through LTCC and prototype
- Qualified evaluation of prototype components including: base, lid, spark gap, solder pads, adhesive
- Estimation of potential leak rates using classical leak rate theory and the aid of dye penetrant, Helium Mass Spectrometry, and radioisotope leak rate detection methods
- Comparison of results to predicted values based on previously defined information found in existing literature.

The intention of this work is not to qualify any specific products for the repeated assembly of an LTCC initiator, but rather to provide a proof-of-concept for each of the necessary components as well as an understanding of the component's expected reliability. While the innovative initiator system can potentially make use of any energetic compound, a suitable surrogate reactive material is used for demonstration purposes.

## **Chapter 3. Review of literature**

### **3.1. Definition of Micro-Electro-Mechanical Systems (MEMS)**

The branch of technology that incorporates an integration of electrical and mechanical components as a characteristically small device is referred to as Micro-Electro-Mechanical Systems (MEMS). Despite the term “micro,” MEMS devices encompass the range of devices between nanometer and millimeter scale in size [1] but are often used to describe the entire field of small electro mechanical devices ranging into the centimeter scale [2]. The term “MEMS” is used in industry to describe a small device that utilizes both mechanical and electrical components for proper function [1, 2]. In the course of this work, the electric spark gap initiator designed from materials commonly employed in MEMS fabrication is considered to be a MEMS device.

### **3.2. Low Temperature Co-Fired Ceramic (LTCC)**

Low Temperature Co-Fired Ceramic (LTCC) consists of a ceramic substrate intended to form a foundation for microelectronic circuits. The LTCC provides the substrate used for depositing conductive or resistive materials onto a single board with the potential for creating multilayered components. Furthermore, the relatively non-reactive ceramic can be utilized as the basis for a chemical reaction chamber, combustion passage, or a number of other complex systems [3]. The ability to easily form the material into varying and specific geometry is just one more important quality that makes LTCC a good platform for the development and continual production of LTCC based MEMS devices.

Converting the LTCC into a useable component requires the material to be formed into desired shapes by any suitable means. In application, LTCC substrate has demonstrated

the capability of being rolled into tubular form to create tubular shaped ceramic components [3]. In most processes, however, the LTCC is utilized as in a “flat” configuration which is more suitable for manufacturing procedures. In the “flat” configuration, the ability to fabricate channels or cavities inside the device has been developed for a multitude of specific applications, especially relevant to the continued development of this research. Layers are connected together by metal filled holes referred to as “vias” which pass from one LTCC surface to another, providing a conductive bridge between layers. The surface of any ceramic layer can utilize screen printed conductive circuitry, widely customizable for any application.

Once all circuit components have been incorporated into the design, a lamination process is used to bond each LTCC layer together. During the lamination process, alignment is of the utmost importance due to potential failure in maintaining via connections between layers. Error in alignment propagates as discontinuities between conductive materials that result in failure to transmit electricity through multiple layers, or even transmission of electrical power to an undesired component. Once completed, the ceramic components are placed in a furnace to undergo a two-step firing process which removes the organic binding agent and sinters the ceramic structure together [4]. Depending on the complexity of a ceramic component, no further processes may be necessary. However, surface metal deposition, chemical etching, and dicing are among a few of the additional actions that can be conducted on fully fired, hard ceramic product.

Mass production of LTCC is well suited to the industrial process since all aspects of production can be easily automated. The geometry forming punch process discussed in Section 3.2.2 can be supplemented or replaced by CNC laser operation to reduce fabrication

time with no consequences to the final product. Similarly, custom punches can be utilized to minimize the number of operations required for finalizing the product geometry, either method serving to decrease production time. Additionally, the many substrate materials available are designed for firing in a belt oven, a device commonly employed in assembly line production. Since mass production of LTCC based products has already been utilized and proven a viable solution to circuit board fabrication, only minor changes to existing production procedures are required to make production of LTCC initiators a reality.

### **3.2.1 LTCC component fabrication**

Some aspects of ceramic substrate fabrication are difficult due to the high processing temperature necessary to form material into a suitable product. This is overcome with the addition of organic binding glasses which have lower melting temperature and promote sintering [4]. LTCC by nature is a lower temperature processed ceramic and contains substantially more organic binding glasses than other ceramic materials. This facilitates a sintering process at roughly 850° C compared to traditional high temperature co-fired ceramics at around 1500° C [4]. The lower temperature processing permits use of many conductive materials unavailable in high temperature ceramic processing. LTCC is generally factory-produced in the form of a highly malleable tape available in many sizes. The tape used in the development of an LTCC initiator is DuPont 951 “Green Tape” at approximately 6 inches square and 10 mils thick (0.01 in). A flow chart showing the steps involved in producing useable LTCC tape is shown in the Figure 1 below.

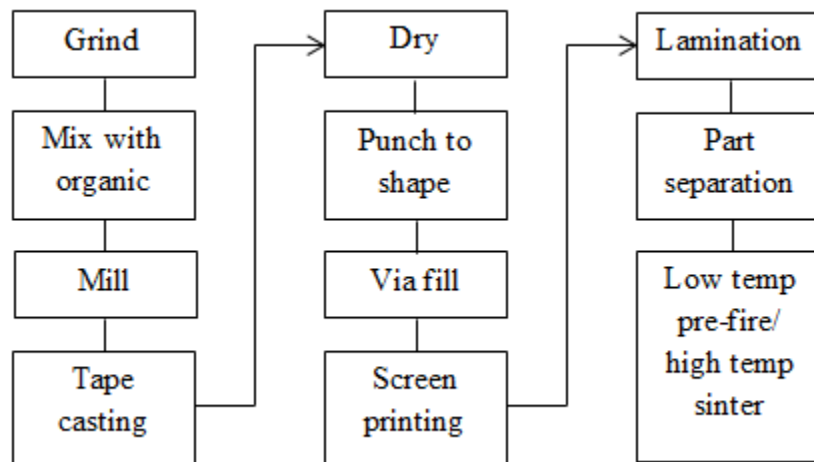


**Figure 1. LTCC fabrication flow diagram**

The majority of LTCC fabrication occurs after the tape casting/drying phase shown in Figure 1 which is usually completed by the material manufacturer. Once the tape has been cast and dried, a computer controlled pneumatic punch or laser cutting device can be utilized to form the LTCC layers to the desired shape. Following punch forming, vias are filled and/or screen printing operations are performed. The utmost caution is exercised when handling the tape at this stage due to the possibility of easily damaging the material prior to firing. Once the intermediate steps are completed, a short lamination process is utilized to combine multiple layers followed by “firing” in a box oven at the appropriate temperature [4]. The firing process results in shrinkage of 12.7-15% due to burn off of the organic binder and sintering of the ceramic which must be accounted for in design [5].

### **3.2.2. CNC punch forming**

To incorporate the geometry necessary for an interior cavity, precision pneumatic punch forming of the LTCC tape is required. The CNC process utilized in this work requires

AutoCAD to create and easily manipulate the desired punch profile. A two dimensional representation of each ceramic layer constituting the final assembly is developed to fit the pneumatic punch machine's working parameters. The CAD profile is converted into a series of coordinates that represent the location for holes and is input into the punch controller. The punch size used in development of the initiator is 0.0169" (0.4293 mm) in diameter and capable of a rapidly punching hundreds of holes under computer control.

The geometric design is completed by punching a series of small holes to produce larger geometric shapes. In this manner a large quantity of more complex shapes can be created with the repetitive use of the same tool. Viewing an LTCC structure once the punch profile has been completed reveals consistent roughness surrounding nearly every location where the punch was used. While an individual punched hole results in a relatively clean cut, stacking punch operations next to one another results in a ridge effect along the edges of larger geometry as shown in Figure 2 below.

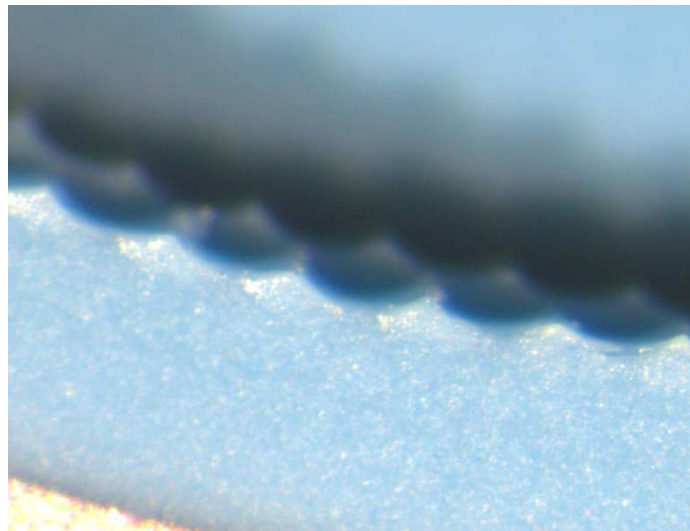


**Figure 2. Ridged edges on LTCC punched profile**

Methods employed to mitigate the presence of punch formed ridges include the use of a laser cutting device or a drastic increase in the number of holes used to punch out the profile. Both methods are capable of decreasing the size of the ridges, yet practical limits must be taken into consideration. While in some applications these ridges may result in potentially detrimental effects, no issues are perceived when incorporated into the design of the novel LTCC initiator.

### 3.2.3. Screen printing

Screen printing technology is a method of coating the surface of a substrate in a predefined pattern of desired material. In the case of circuit design, the coating material generally consists of a conductive paste used to interconnect features along the surface of the circuit as in Figure 3. Screen printing is accomplished by pressing the metallic paste through a screen at locations pre-determined by the design of the screen [4]. The screen at such locations is modified to allow material to easily pass through, creating a duplicate of the screen design on the surface of a substrate.

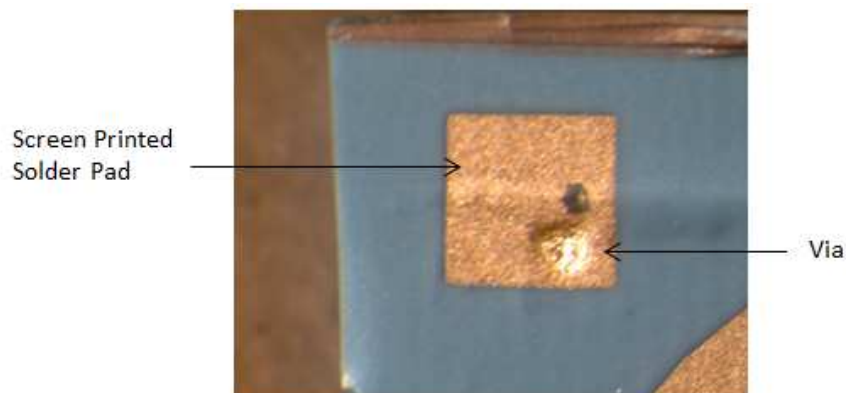


**Figure 3. LTCC screen printed solder pad with via**

The screen printing process has been developed over a vast period of time and with proper calibration can be extremely accurate and repeatable. Careful considerations must be taken to ensure proper alignment of the screen with the substrate, especially when multiple interconnecting vias are present or alignment based failure can occur.

#### **3.2.4. Via interconnect**

Vias are created in the ceramic substrate as a method for interconnecting multiple layers of circuitry deposited on different ceramic surfaces. A via is produced by punching a hole through one ceramic layer and filling the hole with conductive silver/glass frit paste prior to the screen printing process [4]. The results of via fill underneath a screen print can be seen in Figure 3. The “bulge” present at the via location is a common occurrence due to an approximately 15% reduction in ceramic height during the firing process with little to no reduction in via material dimensions [5]. This results in a difference in via height relative to the LTCC material height that is difficult to control during fabrication but is often not considered detrimental to design.

As an added precaution with the use of vias in multi-layered designs, it is desirable to incorporate screen printed pads at locations above and below each via. The pads offer an extended surface for via contact that can account for a larger error in alignment while maintaining uninterrupted contact throughout each layer. This reduces the sensitivity required when aligning any screen printing geometry as well as lamination alignment.

#### **3.2.5. LTCC combustion system fabrication**

The application of LTCC components for use in combustion based devices has been studied extensively in the development of micro-thruster technology for micro satellite

applications [6-8]. Multilayered ceramic components have been fabricated for deployment of controlled combustion utilizing a variety of energetic compounds intended to supplement microsatellite maneuverability [7]. A screen printed spark gap was successfully incorporated to initiate the combustion process of a bi-propellant mixture for the purpose of generating a measure of thrust [8]. In operation, the LTCC design consisted of multiple layers making up the thrust nozzle, combustion chamber, and fuel reserve as well as an adhered viewing window to observe reactions. The tests were successful to varying degrees and prove the viability of LTCC components in a system used to employ combustible materials, although without the intention of operating as an initiator.

### **3.2.6. Hermetic packaging of LTCC**

Packaging of MEMS devices can require high quality hermetic properties to ensure components have long working lives in often varying environments. Unfortunately, a large body of research into the hermetic properties of specifically LTCC alone does not appear to be presently available. Helium mass spectrometry has been utilized to determine leak rates in via filled LTCC components with an adhered quartz layer [9]. Unfortunately, the presence of a Benzo-Cyco-Butene (BCB) bonding compound which the researchers identify as the most likely proponent of leakage, limits the potential leakage of the via filled LTCC structure to  $10^{-7}$ - $10^{-8}$  (atm cm<sup>3</sup> s<sup>-1</sup>) [9], (see Section 3.4 for description of units).

Furthermore, the inclusion of data appears to show no correlation between bonding temperature and leak rate, in partial opposition to prior research [10]. The discrepancy between both sets of research suggests (but does not verify) that the role of BCB as the primary leaking component in the structure may not be trivial. While it is postulated that

LTCC may not contribute to leakage at this level, the collection of data can only reveal that the LTCC component has a lower bound of at least  $10^{-7}$  -  $10^{-8}$  ( $\text{atm cm}^3 \text{ s}^{-1}$ ).

It is particularly important to note, that in a complex system, generally the leak detection method is unable to locate the leak path, or to determine which specific component results in the leak. Since the system can only be identified with one leak rate, the system can essentially only be described by its least hermetic component, or a combination of the least hermetic components. The observation of a complex system comprised of various components and materials cannot identify specific leaks associated with specific materials or components. It remains unknown as to which component provided the leak, a lack of information which can be partially understood by conducting individual leak tests on each component or material. At this point, only suspected leaking components can be accounted for. However, the complex interaction between all components and materials still largely remains unknown, thus the true cause of the leak is still not certain. With leak detection capabilities, only an upper leak limit of the whole system can be determined, leading to a similarly defined upper leak limit for each component.

Some of the pitfalls of testing hermetic devices with either extremely small or “zero” internal cavity have been previously discussed in great detail [11-16]. With small cavities and relatively large leaks, the potential for the tracer gas to completely leak out of the cavity following the tracer gas bombing time must be accounted for, especially with the use of HMS testing. Careful measurement of all necessary parameters is paramount when trying to accurately quantify the hermetic properties of small systems. Methods to alleviate the issues surrounding zero-cavity leak detection have been addressed by Neff and Rink [11-13]. The presence of similar occurrences associated with the relationship between large leak rates and

internal volumes is mentioned in research conducted on a complex MEMS system [10]. An undefined region between fine and gross leak analysis detection methods is noted and determined primarily by the internal volume of a device. The undetermined region can be much larger than a “zero cavity” volume as is noted in later sections [10]. However, in practice, noting these limitations and acting accordingly can ensure that the “undefined region” is not applicable to analysis through the use of proper test methods when available.

In multilayer ceramic fabrication it is common practice to incorporate vias for connecting electrical components between layers of LTCC. If a via contacts both interior cavity and exterior environment, it provides the means for a potential leak path simply due to material discontinuity. However, the via paste material contains both conductive metal as well as small pieces of glass known as “glass frit” which serve as a hermetic bonding agent with the ceramic discussed in greater detail in Section 5.2 [4]. Testing initially suggested that there may be little to no difference in hermetic properties of LTCC encapsulated cavities with or without vias which is discussed in Section 7.1. However, testing and analysis of thermally shocked LTCC substrate still must be completed to determine how cyclic thermal expansion of the via metal will affect the hermetic properties of the LTCC substrate over time.

### **3.3. Pyrotechnic initiator potential failure**

Pyrotechnic initiators are produced in mass quantities in a cost driven market [17-18] and subject to multiple inspection criteria to ensure an absolute minimum of potential component failure. Regardless of inspection criteria, specific areas of concern pertaining to non-hermetic devices remain. Properties such as hermeticity, strength, corrosion resistance, electrostatic safety, rapid development, and low cost are the driving features behind initiator

design [17]. Fabrication of a complex electromechanical system requires the application of multiple different material types to perform different functions for initiator operation as shown in Figure 4. Different materials are required for protective housing, electrical insulation, and electrical leads which result in multiple areas of material interface and thus potential for hermetic or corrosion based failure modes.

Two primary failure modes associated with the design of an initiator can result in a “no-fire” situation. The first of these can be classified by failure to initiate due to physical damage sustained by the firing mechanism, likely during manufacturing. The second is associated with a hermetic failure leading to damage of the firing mechanism (often bridge-wire), or loss of pyrotechnic compound through the leak orifice if applicable. However, since both of these methods are likely to begin during fabrication, careful quality control methods can be applied to limit potential failure in this manner.

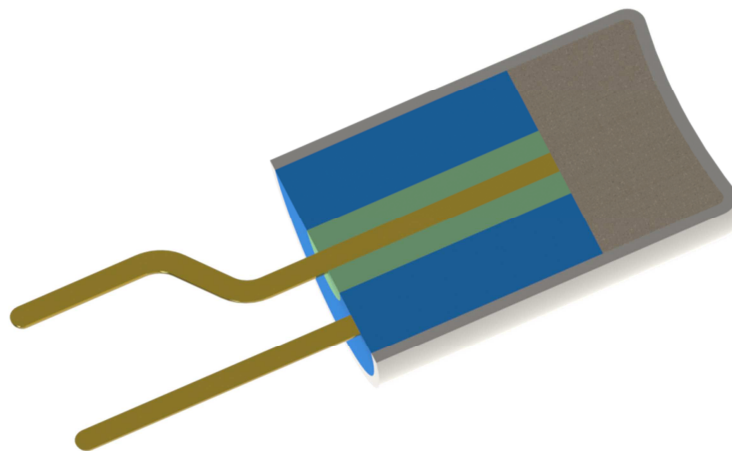


**Figure 4. Typical bridge-wire initiator excluding non-essential body components**

Of the two modes mentioned above, the more prominent means for failure of an initiator is due to corrosive attack on the bridge-wire component [13,19-21]. The presence of leak paths leading to both pyrotechnic compound and electrical components enables moisture penetration into the device, followed by possible degradation of the bridge-wire or the pyrotechnic itself. Even when extreme care is taken in the preparation of initiators, the potential for failure cannot be ignored and methods for qualifying and quantifying leak rates are required. Development of cheap yet effective methods for creating hermetic seals in the device has previously resulted in the application of the Glass-To-Metal Seal (GTMS) component shown in the exploded view of a common bridge-wire initiator in Figure 5.

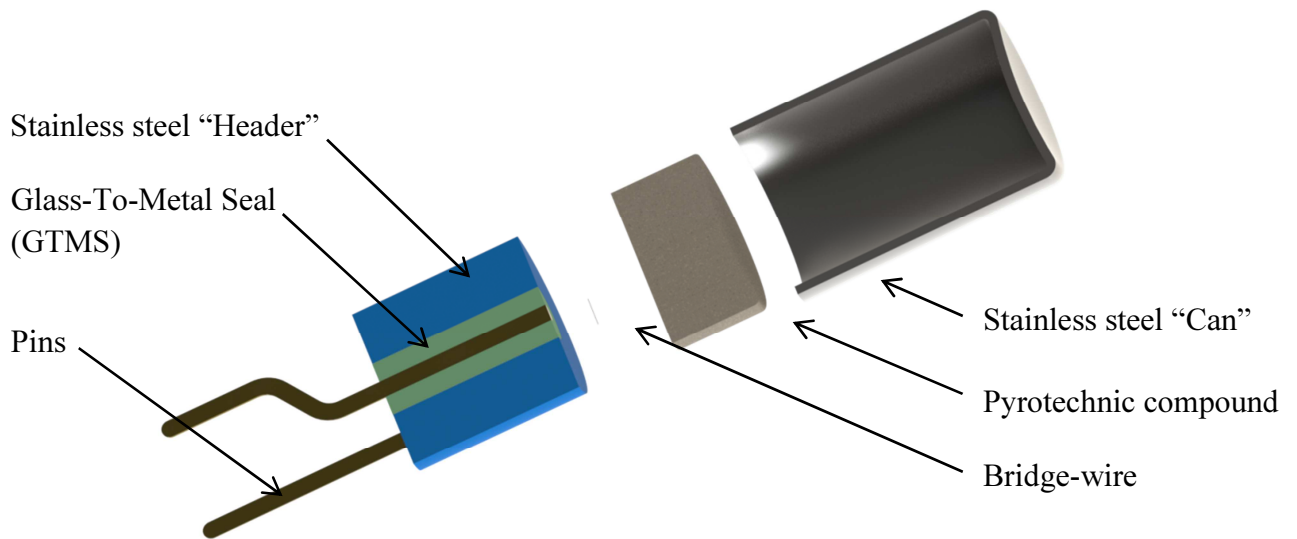


**Figure 5. Expanded view of bridge-wire initiator**

A GTMS is a component commonly employed in initiator design to form an insulated hermetic bond between electronic "pins" and metal housing (Header) [13, 18-22]. Glass is employed in this role because it can act as an electrical insulator, is non-reactive with pyrotechnic compounds, bonds well with metals, and can be made to closely match thermal expansion characteristics of other initiator materials [21]. These characteristics are

the governing criteria for selection of specific glass used in a GTMS [22]. The bonding process between glass and metal results in a high quality seal since the mechanism is a combination of chemical bonding and mechanical interlocking which occurs at high temperature [21]. However, while the GTMS excels in performing all the functions necessary for operation, multiple studies still have shown that GTMS can be prone to thermally and mechanically induced cracking during installation and requires extensive testing to reduce failures [13,19-25].

Leaks in initiators have been studied extensively by [13, 19-25], noting the necessity of the GTMS for initiator design as well as the intrinsic difficulty with preventing the formation of leak paths. One such study was conducted by utilizing helium mass spectrometers for quantifying leak rates in failed initiators [25]. Additional studies in crack growth and thermal stresses in stressed glasses result in similar conclusions that favor GTMS cracking as a prominent failure mode [13, 19, 20, 24]. The findings generally identify the presence of leak paths possibly due to the formation of cracks in the GTMS as the result of thermal gradients present in the initiator during laser welding. However, the presence of improper seal formation between metal and glass components, as well porous welding operations used to seal the “header” to the “can” are also cited as potential leak path locations [13].

While the GTMS is an essential component of common initiators, it can be completely eliminated with the application of LTCC technology. LTCC fabrication incorporates metallic interconnects containing glass frit that bonds with the ceramic across the ceramic-metal interface as well as within the metal conductor. This forms a pseudo glass-to-metal-to-ceramic seal created in situ when the LTCC is fired at designated

temperatures. The seal formed in this manner can result in highly hermetic bond formation that appears to show limited signs of sensitivity due to thermal shock [26]. However, continual study may be required for further verification of this phenomenon.

### 3.4. Leak rates

It is generally accepted that any container, regardless of design, is incapable being completely hermetic [27]. A device operating over a certain length of time is then required to perform through its working life, lending to acceptable levels of hermeticity that can be used as threshold parameters during production testing [27]. A quantification of the hermetic properties for a device results in a parameter commonly described as the “leak rate” which is typically measured in units of ( $\text{Pa m}^3 \text{ s}^{-1}$ ) or in the bulk of American literature ( $\text{atm cm}^3 \text{ s}^{-1}$ ) [15-16, 28-29]. The common ( $\text{atm cm}^3 \text{ s}^{-1}$ ) is primarily used in the mathematical applications presented in this work.

$$1 (\text{Pa m}^3 \text{ s}^{-1}) = 9.87 (\text{Atm cm}^3 \text{ s}^{-1})$$

The units of a leak rate are equivalent to units of power where ( $\text{Pa m}^3 \text{ s}^{-1}$ ) reduces to the common unit of a Watt ( $\text{N m s}^{-1}$ ). Therefore, as a leak progresses over time, the integration of the leak rate with respect to time yields the amount of work done by or to a system based on the direction of flow. The leak rate with respect to time thus describes the flow work applied to a system where the portion of flow work influenced by thermal input is often considered negligible as the result of assumptions used to provide mathematical relations to define a specific flow. More specifically, the units ( $\text{atm cm}^3 \text{ s}^{-1}$ ) describe the volume of tracer gas capable of flowing across a boundary per unit time with respect to a generalized standard atmospheric pressure (1 atm).

A mathematical approach to leak rates results in categorization of flow regimes in which a leak resides as determined by the governing equations of the specific flow. The three prominent flow regimes are continuum (viscous) flow, molecular flow, and transitional flow and the relation between Knudsen number and flow regime is described in Sections 3.2.1-3.2.3 below [27, 30-32]. Together, the three regions loosely describe leak behavior encompassing the majority of leak study. A dimensionless parameter known as the Knudsen number is used to distinguish between flow regimes and describes the ratio between mean free path and leak path cross section [30-32]:

$$\text{Kn} = \frac{\lambda}{d} \quad (3.4.1)$$

$\lambda$  = the molecular mean free path (m)  
 $d$  = characteristic dimension of leak (m)

The mean free path of a fluid particle can be described as a function of the cross section of fluid particles and the number of number of molecules per unit volume [33]:

$$\lambda = \frac{1}{\sqrt{2}n\pi d_p^2} \quad (3.4.2)$$

$n$  = number of gas molecules per unit volume ( $\text{m}^{-3}$ )  
 $d_p$  = cross section of fluid particle ( $\text{m}^2$ )

By invoking the ideal gas assumption, the number of gas molecules per unit volume can be directly related to the pressure through properties of the fluid. The Knudsen relation can then be described in terms of fluid pressure and the characteristic dimension. By applying the properties of air flow at room temperature, the Knudsen relation for air flow under ideal conditions can be reduced to the empirical relation [30]:

$$\lambda = \frac{5.09}{P_{\mu}} \rightarrow Kn = \frac{5.09}{P_{\mu}d} \quad (3.4.3)$$

$P_{\mu}$  = the pressure of the air in ( $\mu\text{m Hg}$ )

Thus, as described above, the Knudsen number can be influenced both by the pressure of the flowing fluid, and the characteristic dimension of the flow path. Therefore flow driven by a time dependent pressure differential (as with leaking volume) could potentially pass through each flow region, provided the path geometry remains constant. The assumption of constant geometry during flow is usually invoked because in most cases the geometry is unknown, and has little probability of ever being fully established. Furthermore, in the many cases, accurately describing a leak path may lead to extremely complicated mathematical relations which are difficult to accurately apply. As a result, a series of assumptions, such as constant leak geometry, are required to perform analysis on a system and geometry terms present in the mathematical relations describing a leak are lumped together as described below.

A term known as “flow conductance,” commonly denoted as “F,” is often used to describe specific aspects of a flow system. The flow conductance is used to identify similarities between the mathematical relations governing flow and the well-known relations describing the flow of electricity. By singling out conductance in equations used in each flow regime, the effects that fluid properties and flow path geometries have on the flow can be easily described. The general form for describing a flow with respect to the flow conductance is [29-31, 34]:

$$Q = F(P_2 - P_1) \quad (3.4.4)$$

$Q$  = the flow rate ( $\text{Pa m}^3 \text{ s}^{-1}$ ) ( $\text{atm cm}^3 \text{ s}^{-1}$ )

$F$  = flow conductance ( $\text{m}^3 \text{ s}^{-1}$ ) ( $\text{cm}^3 \text{ s}^{-1}$ )

$P_1$  = downstream pressure (Pa) (atm)

$P_2$  = upstream pressure (Pa) (atm)

### 3.4.1. Viscous flow

Viscous flow or continuum flow occurs when the mean free path is two orders of magnitudes less than the characteristic dimension ( $\text{Kn} < 0.01$ ). This condition can be the result of either large flow paths, high pressure fluid, or both. This flow regime consists primarily of fluid-fluid interactions rather than fluid-channel wall interaction, where the fluid properties dominate flow characteristics. One of the fundamental assumptions with analysis of the viscous flow region is application of the no-slip condition. This assumption is enacted along the wall boundary which results in a velocity gradient between the wall and the flow path central axis. While viscous flow incorporates both turbulent and laminar conditions, the low flow rate often associated with small leaks requires analysis of the laminar conditions only and the more complex turbulent systems can thus be neglected.

Since some aspects of fluid flow through a medium are dependent on the geometry of the path (volumetric flow rate), each individual path with its own individual geometry must be evaluated separately. A series of equations used to model viscous flow were developed on the basis for generic flow geometry conditions. The most common equation, known as the “Poiseuille Equation,” provides a description for flow through a straight tube with circular cross section and is depicted below [30-31, 35]:

$$Q = \frac{\pi a^4}{8\eta l} \bar{P}_a (P_2 - P_1) \quad (3.4.5)$$

where:

$Q$  = Flow rate (Pa m<sup>3</sup> s<sup>-1</sup>) (atm cm<sup>3</sup> s<sup>-1</sup>)

$a$  = Tube radius (m) (cm)

$l$  = tube length (m)(cm)

$\eta$  = viscosity of the gas (Pa s) (atm s)

$\bar{P}_a$  = mean pressure (Pa) (atm)

$P_1$  = upstream pressure (Pa) (atm)

$P_2$  = downstream pressure (Pa) (atm)

A detailed derivation of Poiseuille's equation which also describes the necessity of assumptions required for valid use of the relation is available in existing literature [35]. The assumptions include incompressible fluid, fully developed flow, laminar flow, and the no-slip condition [30, 35].

The first assumption requires that the flow's Mach number (flow velocity relative to the local speed of sound) is less than 0.3. Compressible flow induces variation in the fluid's density throughout the flow path which in turn affects additional fluid properties at specific locations in the flow. Generally, the low differential pressure associated with leak rates provides instances where the flow's Mach number will not exceed 0.3 and for most instances this assumption is valid.

The three additional assumptions are related to one another and begin with the requirement of small path radius compared to length. Furthermore, the laminar flow condition must be assumed to proceed with the fully developed flow condition. Development of flow describes the behavior of a fluid as the velocity profile changes from relatively uniform at the entrance of the flow channel, towards a constant profile at some point downstream. The constant profile for laminar flow appears parabolic in nature with

the highest flow velocity aligned with the central axis of the channel and zero flow velocity at the channel walls. The zero flow velocity at the wall is associated with the no-slip assumption. The length of flow development is dependent on the Reynolds number of the flow and the radius of the channel [30]. If a specific flow contains a lengthy developing region, the effects of the developing region on the overall flow cannot be ignored.

In the Poiseuille equation, the flow conductance is described as:

$$F = \frac{\pi a^4}{8\eta l} \bar{P}_a \quad (3.4.6)$$

This description is clearly dependent on the mean pressure  $\bar{P}_a$  which correlates with the understanding of how viscous flow is primarily dependent on fluid properties. Fluid properties are generally dependent on the state of the fluid, i.e. pressure, temperature, and density to name a few.

### 3.4.2. Molecular flow

Molecular flow occurs when the mean free path of the fluid is on the order of or greater than the characteristic dimension i.e.  $Kn > 0.5$  [30-31]. This results in the condition where the majority of molecular interaction occurs between the fluid molecules and the walls of the leak path. The assumption of random scattering when describing fluid molecule-channel wall interaction is required to derive the components of flow conductance for a molecular flow system [31]. Molecular flow is dependent primarily on the geometry of a flow channel and requires adjustments be made for each mathematical model to account for specific geometry. However, in most leak detection situations the path geometry will remain unknown, leading to incorporation of an unknown variable (flow conductance) that cannot

easily be solved for. Flow through a short circular constant cross section tube can be modeled by the equation [30]:

$$Q = \frac{\pi \bar{v}_a a^2}{4} (p_2 - p_1) \quad (3.4.7)$$

where:

- Q = flow rate ( $\text{Pa m}^3 \text{ s}^{-1}$ )
- a = tube radius (m)
- $p_1$  = upstream partial pressure (Pa)
- $p_2$  = downstream partial pressure (Pa)

The mean molecular speed  $\bar{v}_a$  ( $\text{m s}^{-1}$ ) is described as [30]:

$$\bar{v}_a = \left( \frac{8R_o T}{\pi M} \right)^{\frac{1}{2}} \quad (3.4.8)$$

- $R_o$  = universal gas constant ( $\text{m}^3 \text{ Pa K}^{-1} \text{ mol}^{-1}$ )
- T = gas temperature (K)
- M = molecular mass of fluid particle ( $\text{Kg mol}^{-1}$ )

The assumptions required for deriving molecular flow relations consists of the random scattering assumption described above and the ideal gas behavior assumption. Random scattering describes the interaction between fluid particles and the channel wall and is based on kinetic theory. It is an assumption that the direction in which a molecule travels after interaction with the channel wall is independent of the direction initially traveled. This assumption notes the uncertain surface geometry of materials on a molecular level, and assumes that a fluid particle's interaction with the channel wall is similarly uncertain and therefore random. The ideal gas law is enacted for modification of flow equations to utilize a (known) pressure term rather than the likely unknown number of particles per unit volume.

For flow through a short tube orifice, the flow conductance containing the variables described in Equation 3.4.7 is [30]:

$$F = \frac{\pi \bar{v}_a a^2}{4} = \frac{\pi a^2}{4} \left( \frac{8R_o T}{\pi M} \right)^{\frac{1}{2}} \quad (3.4.9)$$

This description, unlike with viscous flow, is clearly independent of the fluid pressure at any specific point in the flow path. Instead, it is dependent on the average speed of the fluid particle and the geometry through which the fluid is traveling. Additional relations have been developed for other flow conditions which are described in detail for other flow geometries each containing the similar lack of pressure dependence [30].

### 3.4.3. Transitional flow

Transitional flow occurs between a Knudsen number of 0.5 and 0.01 where the dynamics of the flow are often described as a mixture of both viscous and molecular flow conditions. There are no flow equations in the transition range that have been derived from base principles and only empirical relations are used to describe transitional flow [30]. Many references cite Knudsen's original work which resulted in an empirical relation describing the flow conductance for transitional flow through a long cylindrical channel:

$$F = F_v + \left( \frac{1 + 2 \frac{a}{\eta} \left( \frac{M}{R_o T} \right)^{\frac{1}{2}} \bar{P}_a}{1 + 2.47 \frac{a}{\eta} \left( \frac{M}{R_o T} \right)^{\frac{1}{2}} \bar{P}_a} \right) F_t \quad (3.4.10)$$

$F_v$  = viscous flow conductance (no slip)

$F_t$  = molecular flow conductance

Unlike other flow regimes, the empirical relation describing flow conductance in the transitional region is dependent on the viscosity, mean pressure, and the temperature of the fluid which shows the influence of each other flow regime. The end of transitional flow nearing viscous flow conditions identifies large error in viscous flow model calculation due

to invalid use of the no-slip condition. Since the no-slip condition is one of the primary assumptions used for development of viscous flow models, a slip-correction factor must be utilized to incorporate significant contributions to the flow conductance under transitional flow conditions. Similarly, on the lower end of the transitional region (near molecular flow), the fluid-fluid interaction contributes significantly to the flow conductance and cannot be neglected [30].

A number of mathematical relations have been developed to describe the transitional region; however these largely rely on empirical relations formulated by Knudsen or others to describe specific flow conditions. Due to the complexity of models describing transition flow, a general aversion to transition flow analysis has occurred [36]. Therefore, in practice, flow conditions which are somewhat time dependent can be tailored to either viscous or molecular flow in any system, presenting the use of much less complicated relations without a loss of accuracy.

#### **3.4.4. Flow regime systems**

Analyzing leak path networks propagating through various components in a device can result in multiple unknown parameters. For example, it is unlikely that an accurate description of the flow conductance for a leaking device can be developed. It may also be unlikely for the flow conductance in such a device to show significant change under repetitive test conditions. However, thermal or mechanical changes to the leak network deviating from the “repetitive” nature of testing can easily result in changes to the flow conductance and must be accounted for. Furthermore, a complex system composed of multiple individual leak paths could feature any or all of the flow conditions previously

mentioned which provides additional uncertainty in an accurate description of a leak network.

Test procedures standardized by MIL-STD 883J and 750F [37-38], generally imply that viscous leaks often appear larger in magnitude than molecular leaks, and are inapplicable to fine leak measurement. An in depth justification for use of only molecular flow theory to describe fine leaks is provided by Goswami & Han [14]. The driving factors behind viscous flow require conditions either unattainable in small cavity devices or nearly impossible to detect using current leak detection techniques [14]. It could easily be possible for multiple molecular leak paths to resemble a single viscous leak path in leak rate magnitude since leak paths in small devices are more likely to be through cracks and fissures rather than large holes [36]. A case which would result in an improper mathematical approach for analyzing acquired data. There is simply no practical way for the majority of leak detection methodologies to address this potential discrepancy. In most cases it may be impossible to determine the composition of all leak paths associated with a complex device and ultimately assumptions must be used.

The application of MIL-STD methodologies for leak analysis requires flow regime assumptions to apply mathematical relations. A molecular flow based equation is used in MIL-STD procedures as the basis for leak rate analysis and is capable of providing a mathematical solution to both gross and fine leak rates [29]. However, care must be taken to ensure proper application of the equation, as it only accounts for molecular flow. Blind acceptance of the molecular flow assumptions for gross leak rate quantification is not accurate, as viscous and transitional flow must also be considered to form an accurate representation of the gross leak rate. Due to the association between gross leaks and

hermetic failure, in many leak analyses, a threshold is used at which a leak rate higher than said threshold is noted and regarded as a failure. The inability of identifying gross leak flow characteristics a priori coupled with the difficulty in accurately quantifying gross leaks in small cavities has resulted in a lack of viscous and transitional flow data for small devices.

### **3.5. Leak detection methods**

Leak detection in small electronic components can be conducted in multiple different ways in accordance with the accepted methods of MIL-STD-883J.1014 for determining the effectiveness of a sealed device [37-38]. The common unit used to describe a leak rate is ( $\text{atm cm}^3 \text{ s}^{-1}$ ) which is applied to differing leak rate terminology. A leak rate initiates a change in pressure differential across the leak path and the rate of leak is dependent on the pressure differential. The leak rate is thus a time dependent phenomena which decreases with respect to time. The common leak rate used to describe hermeticity of a device is referred to as the “initial apparent leak rate” which is a function of test parameters specific to the test specimen [14]. The “initial apparent leak rate” is taken from the first test conducted and used to determine the true leak rate [14] as discussed in Section 3.6.1.

Procedures are outlined in both MIL-STD-883J and MIL-STD-750F for eight different leak test methods for either quantifying a leak rate, or more applicable to production, a pass fail qualifying method. The establishment of these methods include helium mass spectrometer (HMS), radioisotope ( $^{85}\text{Kr}$ ), perfluorocarbon (bubble test), optical, dye penetrant, weight gain, and cumulative helium leak detection (CHLD) discussed in further detail below[37-38].

The perflouorocarbon and weight gain methods are used to analyze gross leaks only and can be considered as “destructive” tests under most circumstances. In each case, an

attempt is made to force some amount of tracer fluid into interior cavities under high pressures. The perfluorocarbon test is then associated with observing bubbles emitting from the interior if a sufficient amount of tracer has filled the cavity. However, large leaks may obscure the observation of bubble streams [37-38] and an upper limit of detectability where bubbles cannot be observed must be considered. In contrast, the weight gain technique takes advantage of a noticeable difference in weight before and after a device is submerged in the high pressure tracer. An increase in weight indicates a similar amount of tracer gas has made its way into the cavity and a leak is present [37-38]. In both cases these tests are used as pass/fail criteria and accurate quantification of a leak rate is generally not achievable.

The optical leak detection method is applicable to electronic devices and hinges on the ability to determine deflection in a lid or cavity wall, provided a differential pressure is applied to the system [37-39]. An optical interferometer is used to monitor lid deflection as a differential pressure is applied, or the external pressure is held constant. If a gross leak is present, a state of hydrostatic equilibrium is observed and deflection, dependent on external-internal pressure differential, will not be observed. If deflection is observed but is not proportional to the pressure change, a fine leak is present. Furthermore, change in deflection over time when the external pressure is held constant is an indication that the pressure inside is equalizing with the external pressure and therefore a leak exists [39]. While not included in MIL-STD procedures, it can be inferred that a geometrical understanding of the monitored device must be in place to correlate deflection with leak rate. In most instances geometrical edge effects are nontrivial, which leads to a limit of detectability at approximately  $10^{-10}$  (atm cm<sup>3</sup> s<sup>-1</sup>), and may require the application of computational finite element analysis methods to perform leak analysis in some instances.

The Cumulative Helium Leak Detection technique (CHLD) can be considered as a variation to traditional HMS detection methods discussed in later sections. The CHLD system employs a cryo-pump as well as a different measurement approach for leak detection which is capable of extending the range of accurate leak rate quantification [37-39]. This detection technique is capable of freezing a tracer gas inside an internal cavity prior to testing with the application of a cryo-cooling system. The retention of tracer gas during a test chamber evacuation stage allows gross leaking components to accurately be tested up leak rates of  $1 \text{ (atm cm}^3 \text{ s}^{-1})$  [39]. The non-traditional approach which determines the leak rate by correlation with the observed change in helium count as a function of time can reportedly employ the natural concentration of helium in air to measure leak rates without traditional bombing. While stating accuracy in leak rate calculation on the order of  $10^{-13} \text{ (atm cm}^3 \text{ s}^{-1})$ , an issue arises with the lack of calibrated leak standards available for leaks of that magnitude [39]. Without the means to correlate detected leak rates in low ranges between the CHLD technique and other methods, the accuracy of such a system is subject to some scrutiny.

### **3.5.1. Helium Mass Spectrometry (HMS)**

One of the more widely used techniques for quantifying leak rate data employs variations of a helium mass spectrometer (HMS). The HMS device is designed to extract helium from the internal cavity of a sealed vessel, ionize the gas under high vacuum, and essentially quantify the rate at which helium atoms strike a target. The quantified ions are then correlated to an indicated leak rate “R” (initial apparent leak rate) which is a function of the pressure differential and geometrical properties of the leaking specimen. The initial apparent leak is processed to provide a true leak rate through the application of the

molecular flow assumption [14, 29, 37-38]. While heavily dependent on internal volume, the short time require for the gross loss of tracer gas between bombing and analysis in a small cavity device requires careful consideration to accurately determine the magnitude of a gross leak. However, simple procedures for indication of gross leakers can be followed, assuming that further analysis is applied where appropriate [29].

Application of the HMS system for leak testing LTCC systems has resulted in associated leak rates on the order of  $10^{-9}$  to  $10^{-7}$  ( $\text{atm cm}^3 \text{ s}^{-1}$ ) for systems containing both LTCC and BCB as a bonding agent [9-10]. The test methodology applied in both cases is MIL-STD-883 and each offer a comprehensive analysis of the leak system beyond producing simple leak rate magnitudes. However, the work neglects to mention any application of HMS test correction methods [29] although it is assumed to be applied based on their adherence to the MIL-STD protocol [9-10]. Additionally, while not explicitly stated, it is assumed that the methods employed leak standards on the order of  $10^{-11}$  ( $\text{atm cm}^3 \text{ s}^{-1}$ ) to comply with the MIL-STD. Gross leak tests to back up the HMS data in the BCB system research consisted of using fluorocarbon liquids for visual inspection.

### **3.5.2. Radiflo® leak rate detection**

The use of  $^{85}\text{Kr}$  as a tracer gas is another technique commonly employed by industry to quantify leak rates in small cavity devices.  $^{85}\text{Kr}$  is a chemically inert radioactive isotope that produces both beta and gamma radiation, the latter of which can be used to quantify the amount of tracer gas inside a device without extracting the gas [15, 28, 40]. The Radiflo® system provides accurate leak rate measurements on the order of  $10^{-12}$  ( $\text{atm cm}^3 \text{ s}^{-1}$ ), which is sufficient for comparison of the components analyzed in this thesis [15, 37-3, 41]. The radioisotope method of leak detection is generally accepted as one of the premier techniques

for testing hermetically sealed components, with capabilities extending from fine to gross leak analysis.

Tests conducted with the Radiflo® Mk V Leak Detection System are used to present quantifiable leak rate data for analysis of fine leaks. The radioisotope leak rate detection method is often employed on industrial scale analysis [28, 41] and has test procedures outlined in MIL-STD 883J alongside HMS procedures. The Radiflo® uses a mixture containing diluted radioactive isotope  $^{85}\text{Kr}$  as the tracer element. In operation, the  $^{85}\text{Kr}$  gas mixture is forced into the interior of a device based on a specified length of time or a defined test sensitivity discussed in Section 3.6.3. Subsequently, withdrawal of specimens from the Radiflo® is typically followed by gamma emission quantification with a thallium-doped sodium iodide (NaI) scintillation crystal capable of determining the quantity of  $^{85}\text{Kr}$  remaining in the device [15, 41].

Similar to the HMS, the partial pressure of  $^{85}\text{Kr}$  is an important aspect in accurately determining a leak rate. For the purpose of leak detection, highly concentrated  $^{85}\text{Kr}$  is not required due to high detectability of  $^{85}\text{Kr}$  gamma emission with the application of appropriate scintillation counters. Furthermore, since the  $^{85}\text{Kr}$  is only produced as a byproduct of nuclear fission in commercial reactors through fission product separation methods applied to waste components, the  $^{85}\text{Kr}$  by itself is expensive. Therefore,  $^{85}\text{Kr}$  used for leak detection is utilized in a diluted mixture primarily consisting of either dry air or a nitrogen mixture.

Determining the amount of krypton present in the tracer gas mixture is directly related to the specific activity of the gas (SA). The SA relates the activity of pure krypton at a specified pressure and temperature to the activity of the gas mixture used for leak

detection. Since the amount of  $^{85}\text{Kr}$  inside a cavity is quantified through gamma detection, and the specific activity is known, or can easily be quantified, an accurate reading of the partial pressure can be determined without the assumptions required in HMS internal partial pressure predictions. This principle eliminates a major portion of the uncertainty associated with HMS back pressurization leak detection.

A method used to conduct gross leak analysis takes advantage of the adsorption properties of krypton gas when in contact with an adsorbent medium [11-13, 28]. When exposed to a carbon based material, krypton atoms form a Van Der Waals bond with the surface of the carbon, enabling “adherence” to the surface and retention during the evacuation phase of the test cycle. Studies have identified that the application of steam activated coconut husk charcoal as the carbon source results in a high adsorption relation partially due to a large natural surface area to volume ratio [42-43]. Inclusion of such carbon based particles on the inside of a hermetic package prior to final assembly can eliminate “false rejects” associated with gross leakers. If inclusion of charcoal is not permissible in device fabrication, the application of additional methods for verification of gross leaking components may be necessary to satisfy testing specifications.

### **3.5.3. Dye penetrant inspection (DPI) leak detection**

Dye penetrant testing utilizes a liquid tracer agent to perform a visual, qualifying examination for potential leaks. Magnaflux® red dye has low viscosity and exhibits low surface tension which allows it to penetrate into and propagate through entire crack systems with the appropriate application of a pressure differential. However, the application of liquid tracers is capable of clogging leak paths, effectively rendering other leak testing data inaccurate [44-45]. The upper limit of detectability for dye penetrant testing is approximated

on the order of  $1 \times 10^{-4}$  ( $\text{atm cm}^3 \text{ s}^{-1}$ ) where path clogging begins to occur [45]. The presence of dye penetrant is often detrimental to a fully assembled electrical component and thus it is considered to be a destructive test method.

Care must be taken to ensure that a proper understanding of a dye penetrant system is applied to inspection before drawing conclusions regarding to the nature of a potential leaker. Essentially, the dye will readily seep into any crack or porosity present in a device once it is applied without regards to the nature of the surface discontinuity. If a material is porous, a large amount of dye will appear to seep out from the porous material following the test, providing a potentially false notion that a gross leak is present [44]. Generally, it is wise to employ methods for observing the interior of a device cavity before making any final determinations.

To conduct a test, the specimen must be cleaned, exposed to red dye, cleaned again, and assisted in drawing the remaining dye out of any present cracks. Dye penetrant testing is an easy procedure for initial testing of the initiator apparatus and employs the back pressurization method discussed in Section 3.6. The device is placed inside a sealed compartment and subject to vacuum conditions with the intention of reducing internal pressure. Once an allotted vacuum time has been achieved, the device is removed from the vessel, submerged in a container of red dye, and placed in a pressure tank. Pressurization time and pressure should follow the procedures outlined in MIL-STD 883J 1014 with some discretion allowed for devices incapable of maintaining high pressures.

The procedure works on the potential of hydrostatic pressure applied to the system resulting in a pressure differential between the interior and exterior of a tested component.

The pressurized dye bath should drive the penetrant into the cavity if sufficiently sized leak paths are present. After a specified pressure bombing time has been achieved, the specimens and dye container are removed from the pressure compartment. Each specimen is cleaned profusely for continued observation [37-38]. Although not specified in MIL-STD procedure, it is beneficial to place each specimen on an absorbent cloth, allowing time for specimens to show signs of leakage. Over time, if the cloth is stained red, a significant leak may be indicated as shown in the Figure 6. If the cloth does not show stains from the dye, a gross leak may not be present. Dye penetrant testing is applicable to gross leaks only with the application of a length pressurization time and has no well-defined lower limit resulting in use as a pass/fail test method [37-38]. With either case, it is beneficial to cut each specimen open to observe if any dye has been deposited at interior locations.



**Figure 6. Dye penetrant test on LTCC prototypes**

### **3.6. Back pressurization**

Historically, preloading a tracer gas into a device has been commonly employed for leak detection. Another widely used technique for detecting relatively small leaks in microelectronic devices, back pressurization, is another way to introduce tracer gas into a component. Back pressurization requires forceful introduction of tracer gas into a

component's interior by an applied differential pressure between exterior and interior. Once this is completed, the tracer gas is either quantified in situ or extracted through opposing differential pressure and quantified by external means. Both HMS and Radiflo® leak detection techniques can utilize the back pressurization technique and a method for processing acquired data is based on the molecular flow assumption [16, 29, 40]. The molecular flow method is derived from principles first put forth by Knudsen [34] and generally is used for HMS analysis. However, a slightly different mathematical relation is used in Mil-Spec 883J for proper application of the radioisotope approach [37-38, 46].

Molecular flow is assumed to be the primary mode for mass transfer in describing fine leaks in small cavity devices. The ability to neglect viscous flow contributions in favor of molecular flow is the result of viscous flow dependence on a high pressure differential or large leak path [14]. It is generally accepted that viscous flow in small cavity devices would not be observable during leak detection due to loss of tracer gas [14, 36]. Thus the molecular flow method of gas transport is applicable and leak can be described by the equation [16, 29-30]:

$$V \frac{dp}{dt} = F(p_e - p) \quad (3.6.1)$$

$V$  = internal free volume( $m^3$ ) ( $cm^3$ )

$\frac{dp}{dt}$  = change in internal pressure with respect to time( $Pa s^{-1}$ ) ( $atm s^{-1}$ )

$F$  = flow conductance( $m^3 s^{-1}$ ) ( $cm^3 s^{-1}$ )

$p_e$  = external bombing partial pressure of tracer gas ( $Pa$ ) ( $atm$ )

$p$  = internal volume partial pressure of tracer gas ( $Pa$ ) ( $atm$ )

When conducting tests on multiple different devices, the flow conductance, a function of geometry, will likely differ between each device. Furthermore, it is highly

unlikely that quantification of flow conductance could occur at all, which lead to incorporation of a variable called the standard leak rate [29]:

$$L = FP_0 \quad (3.6.2)$$

$L = \text{standard leak rate}(\text{Pa m}^3 \text{ s}^{-1}) (\text{atm cm}^3 \text{ s}^{-1})$   
 $P_0 = 1 (\text{Pa}) (\text{atm})$

The standard leak rate “L” is defined as the flow rate observed between a 1 atm pressure differential across a leak channel with zero downstream pressure [29]. A leak rate is a function of the flow conductance associated with a leak path and flow conductance is a function assumed dependent on only the path geometry. By assuming that flow path geometry remains constant for a given leaking device, flow conductance and thus “L” is also a constant parameter. Incorporating the standard leak rate into the flow rate equation allows either a graphical or iterative approach to quantifying the flow rate in a leaking device through variation of “L” described in Section 3.6.4. Refining the mathematical description of the flow equation by applying the standard leak rate yields:

$$V \frac{dp}{dt} = \frac{L}{P_0} (p_e - p) \quad (3.6.3)$$

Separation of the differential equation can be followed by integration from time “T<sub>0</sub>” to “T”, ranging from the initial time “0” to the time at which tracer gas pressurization ceases. During this time, the tracer gas internal partial pressure progresses from an assumed initial pressure of “p<sub>0</sub>” towards a final partial pressure “p.” The ramifications of an assumed initial partial pressure are discussed in Section 3.7. Separation of variables and integration yields the following equation [16, 29] and a more detailed description included more complex bombing situations are provided in Appendix E.

$$p = p_e \left[ 1 - \exp\left(-\frac{LT}{P_o V}\right) \right] \quad (3.6.4)$$

$p$  = internal partial pressure (atm)  
 $P_e$  = external partial pressure (atm)  
 $T$  = pressurized bombing time (s)

The value of “ $p$ ” is representative of the internal partial pressure of the tracer gas at the time a leaking vessel is removed from high pressure immersion and differential pressure (likely) changes direction. The time that passes between removal from pressurization and analysis in a test chamber is referred to as the dwell time. An expression to evaluate the decrease of internal tracer gas concentration during the dwell time can be derived by treating “ $p$ ” as a constant value for continued integration resulting in the expression below.

Reference Appendix E.

$$p_n = p_e \left[ 1 - \exp\left(-\frac{LT}{P_o V}\right) \right] \exp\left(-\frac{Lt}{P_o V}\right) \quad (3.6.5)$$

$p_n$  = internal partial pressure after dwell (atm)  
 $t$  = dwell time (s)

To solve for the standard leak rate, the quantities for internal volume, external bombing partial pressure of helium, bombing time, and dwell time must be known. Clearly, if a device has been previously subjected to a tracer gas bombing, additional modification to the value for “ $p_n$ ” needs to be utilized. This is discussed in Section 3.7 and in Appendix E. The equation mentioned above yields the internal partial pressure at the time of the test based on known test parameters and the standard leak rate “ $L$ ”. The solution method for determining the true leak rate diverges for the HMS and Radiflo® techniques beyond this point as described below.

### 3.6.1. HMS technique: molecular flow approach

The helium mass spectrometer test procedure results in a key piece of information known as the “initial apparent leak rate” [14] or the “indicated leak rate” and defined as the variable “R” [29]. The nomenclature used by Ruthberg [29] is applied to additional equations for convenience. The indicated leak rate is time dependent, read directly from the HMS machine, and is equal to the left hand side of the general form flow equation from Section 3.4 [29]:

$$R = F(p_n - p_d) \quad (3.6.6)$$

$p_d$  = helium partial pressure inside the detector (Pa) (atm)

R = indicated leak rate ( $\text{atm cm}^3 \text{s}^{-1}$ )

$p_d$  = HMS vacuum pump pressure (Pa) (atm)

The HMS vacuum pump pressure is maintained within the HMS machine and considered negligible in comparison to the assumed helium partial pressure inside the test specimen which results in the simplified equation below.

$$R = Fp_n \quad (3.6.7)$$

Ruthberg suggests that since most tests for leakage are conducted shortly after device fabrication, the initial internal partial pressure is essentially equal to zero leading to a secondary relation:

$$p_n = R \frac{P_o}{L} \quad (3.6.8)$$

With the application of Equations 3.6.7 and 3.6.8, a graphical technique may be employed to solve for gross and fine leak rate magnitudes largely dependent on the internal volume of test specimens. The approach used by Ruthberg makes use of terms called the “relaxation rate” and “internal fractional partial pressure” to simplify equations which can

be referenced in Appendix D. The basic form of the molecular flow leak rate approach has been presented in comparison without application of the simplifying terms used by Ruthberg. A numeric code has been developed to quickly solve the HMS system based on the graphical approach employed by Ruthberg shown in Appendix D and discussed in Section 3.6.4.

### 3.6.2. Radioisotope technique: molecular flow approach

The radioisotope approach to leak rate analysis relies on the quantification of radioactive gas to determine the partial pressure of  $^{85}\text{Kr}$  inside a device. Therefore, the initial partial pressure can be known explicitly, eliminating error associated with the prediction of internal partial pressure based on extraction of gas back through the leak channel.

Ruthberg's approach to a solution for the radioisotope method differs from the method outlined by MIL-STD883 [37, 41] in the application of assumptions relating to the flow.

For the radioisotope technique, the key piece of information is the gamma count " $R^*$ " acquired by an appropriate scintillation counter. The method relies on understanding that the gamma count associated with  $^{85}\text{Kr}$  directly relates to the quantity of  $^{85}\text{Kr}$  in a device at a specific temperature by invoking the ideal gas assumption and incorporating the counting efficiency of the thallium doped NaI scintillation crystal:

$$R^* = p_i V A K \quad (3.6.9)$$

$R^*$  = gamma count (counts  $\text{min}^{-1}$ )

$p_i$  = internal partial pressure of krypton (Pa) (atm)

$V$  = internal volume of part ( $\text{m}^3$ ) ( $\text{cm}^3$ )

$A$  = activity of pure krypton ( $\mu\text{Ci m}^3 \text{Pa}^{-1}$ ) ( $\mu\text{Ci cm}^3 \text{atm}^{-1}$ )

$K$  = counting efficiency of detector (counts  $\mu\text{Ci}^{-1}$ )

Note that the partial pressure of the  $^{85}\text{Kr}$  in the tracer gas is related to the total pressure of the tracer gas mixture by [29]:

$$P = \frac{S}{A} p^* \quad (3.6.10)$$

$P$  = pressure of tracer gas mixture (Pa) (atm)

$p^*$  = partial pressure of radioactive gas component (Pa) (atm)

$S$  = specific activity of tracer gas mixture ( $\mu\text{Ci Pa}^{-1} \text{m}^{-3}$ ) ( $\mu\text{Ci atm}^{-1} \text{cm}^{-3}$ )

$A$  = activity of pure radioactive gas component ( $\mu\text{Ci m}^3 \text{Pa}^{-1}$ ) ( $\mu\text{Ci cm}^3 \text{atm}^{-1}$ )

The relation above is used to resolve the partial pressure of  $^{85}\text{Kr}$  in the tracer gas mixture either internally or externally under the assumption that the gas remains mixed. The gamma count can then be related to the internal pressure of the system with all variables described above.

$$P_i = \frac{R^*}{\text{VSK}} \quad (3.6.11)$$

The internal  $^{85}\text{Kr}$  partial pressure of the system is then directly related to the external partial pressure by Equation 3.6.5. Following the procedure used in the HMS method, the standard leak rate “L” can be used to find an internal tracer gas pressure that holds true for both Equation 3.6.5 and Equation 3.6.11.

### 3.6.3. Radioisotope technique: Radiflo® equation

The Radiflo® method utilizes an equation that is not derived from the molecular flow theory. As such, the same assumptions do not apply and in effect, the system of equations is much easier to utilize. The MIL-STD approach [37-38] recommends the application of this methodology for conducting tests over the molecular flow method. The two equations applicable to this method are [37-38, 41, 46]:

$$Q = \frac{R_{\text{reject}}}{\text{SKPT}} \quad (3.6.12)$$

$$L_r = Q \left( \frac{R^* - R_{\text{bg}}^*}{R_{\text{reject}}} \right) \quad (3.6.13)$$

$Q$  = leak test sensitivity ( $\text{Pa m}^3 \text{ s}^{-1}$ ) ( $\text{atm cm}^3 \text{ s}^{-1}$ )  
 $R_{\text{reject}}$  = set reject level above background ( $\text{counts min}^{-1}$ )  
 $S$  = Specific activity of tracer gas ( $\mu\text{Ci Pa}^{-1} \text{ m}^{-3}$ ) ( $\mu\text{Ci atm}^{-1} \text{ cm}^{-3}$ )  
 $K$  = scintillation crystal counting efficiency ( $\text{counts min}^{-1}$ )  
 $\bar{P} = P_e^2 - P_o^2$   
 $T$  = bomb time (s)  
 $R^*$  = gamma count ( $\text{counts min}^{-1}$ )  
 $R_{\text{bg}}^*$  = background gamma count ( $\text{counts min}^{-1}$ )  
 $L_r$  = leak rate ( $\text{Pa m}^3 \text{ s}^{-1}$ ) ( $\text{atm cm}^3 \text{ s}^{-1}$ )

While it is obvious that this system can be reduced to one equation, the concept of test sensitivity with respect to bomb time is important for test application. From the relation above, the bomb time and test sensitivity are seen to be dependent on one another. In industrial application, often a sensitivity level is set and the bomb time associated with it will be calculated and applied. However in laboratory setting, a bombing time may be more convenient to set, and sensitivity is then mathematically determined. Either method is acceptable to perform tests up to the known sensitivity level.

The other important parameters consist primarily of constants associated with the specific activity of the tracer gas, counting efficiency of the scintillation crystal, and background radiation levels. The reject level is a parameter often used as a convenient threshold value to distinguish between acceptable and non-acceptable leak rates serving as the pass fail criteria for mass produced parts.

#### **3.6.4. Iterative solution to back pressurization approach**

A code presented in Appendix G employs a numerical approach which closely follows the methods utilized by Ruthberg's graphical solution. In the iterative approach, a series of discrete points are solved in each equation, and areas of interest are refined to increase accuracy. Comparatively, Ruthberg's method for solving the aforementioned system of equations is nontrivial and requires approximations based on a graph of standards

and corresponding differences between standard data and test condition data. He notes that there is no simple way to solve the inseparable exponential equation and reverts to a graphical method.

Both the code and the graphical approach exclusively use molecular flow theory, where the flow conductance “F” is assumed to be based entirely on the geometry of the leak flow channel. Thus, the flow conductance and consequently the standard leak rate “L” can be perceived as unknown constants. Both the numerical approach and graphical method hinge on the application of varying the standard leak rate over a wide range of values and finding intersecting points for both system equations. From the intersecting points, the pressure difference across the flow, standard leak rate, and the magnitude of the flow conductance can be determined. The standard flow rate equation taken from flow theory can then be applied to find the leak rate of the system simply by:

$$\text{True leak rate} = FP_n \quad (3.6.14)$$

The method applied to finding intersections between each relation consists of noting the difference in value between each consecutive point and identifying when the difference approaches a set minimum difference. The corresponding value is then recorded and used in additional calculations. Input and output data for the code is packaged in an easy to use fashion that results in simple and organized data returned for both fine and gross leaks. Each of the leak rate methods mentioned in earlier sections can be independently solved for and compared.

### **3.7. Leak test limitations**

The back pressurization technique has both upper and lower limits of detectability for any specimen with a range of approximately  $10^{-5}$  to  $10^{-11}$  (atm cm<sup>3</sup> s<sup>-1</sup>) [44]. With either

limit, the need to properly calibrate equipment as well as the identification and quantification of potential error is paramount when attempting to conduct accurate leak rate analysis. Each differing method discussed below has its own limiting factors and the approximate leak range described above is representative of both practical and technical limitations to performing tests.

The lower limit of detectability for HMS testing, approximately  $10^{-11}$  (atm cm<sup>3</sup> s<sup>-1</sup>) is the result of both minimum test resolution as imposed by available equipment and is compounded by the miniscule presence of helium in the atmosphere for HMS testing. Additionally, leak standards two orders of magnitude below the minimum detectable limits as necessitated by MIL-STD protocol are simply not available, providing yet another limiting factor to fine leak analysis [16, 37-38]. A HMS detector quantifies helium ions and is unable to determine where the helium originates from, remaining unable to distinguish between desorption and leak based helium sources. Complete elimination of all potential non-leak related helium in a system cannot be easily overcome without extreme measures and is simply impractical in the majority of test conditions.

Limitations imposed on the lower limit of detectability are not confined to the HMS alone and background radiation present in radioisotope analysis hinders leak test accuracy in all but the most extreme cases. Additionally, limitations imposed by scintillation counting accuracy, detector shielding, and improper handling of specimens must be considered. The effects of background radiation, largely reduced by shielding, still results in fluctuating readings which, at best, provide only a small reduction in accuracy. It should be noted that the attenuation of gamma radiation through a shielding medium theoretically cannot reduce

detectable background radiation to zero [47]. The energy associated with background gamma observed by a shielded detector is thus a function of the shielding medium's thickness and a realistic shield thickness must be used. An additional limitation specifically related to the internal tracer gas concentration after bombing with the Radiflo® technique is discussed in Section 3.7.2.

The upper limit of detectability approximately  $10^{-5}$  ( $\text{atm cm}^3 \text{s}^{-1}$ ) is essentially determined by the potential for gas to escape in the time between pressurized bombing and quantifying data with each respective method [10, 14, 39]. However, this is also heavily dependent on the internal volume of any device under analysis and the upper limit is subject to change. In a leaking system both the length of dwell time and the internal volume can have the most significant impact on leak rate analysis as shown in Figures 7 and 8. With smaller internal volumes, the large leak rates can support the transfer for a much larger proportion of gas present in a cavity compared to each other combination of large/small leaks with large/small volumes. Thus, unless specific techniques are utilized, small cavity devices maintain the possibility for tracer gas to completely evacuate the internal volume during the dwell time as discussed further in Section 3.7.3.

### **3.7.1. Variation in dwell time and internal volume**

The dwell time associated with application of molecular flow leak rate analysis has a significant impact on calculating the magnitude of a gross leak [29, 37-38]. The graph in Figure 7 shows the impact of dwell time on the relaxation rate and normalized internal helium partial pressure "E" used in the Ruthberg approach when all other parameters are held constant.

$$R_r = \frac{L}{P_o V} \quad (3.7.1)$$

$R_r$  = relaxation rate ( $s^{-1}$ )

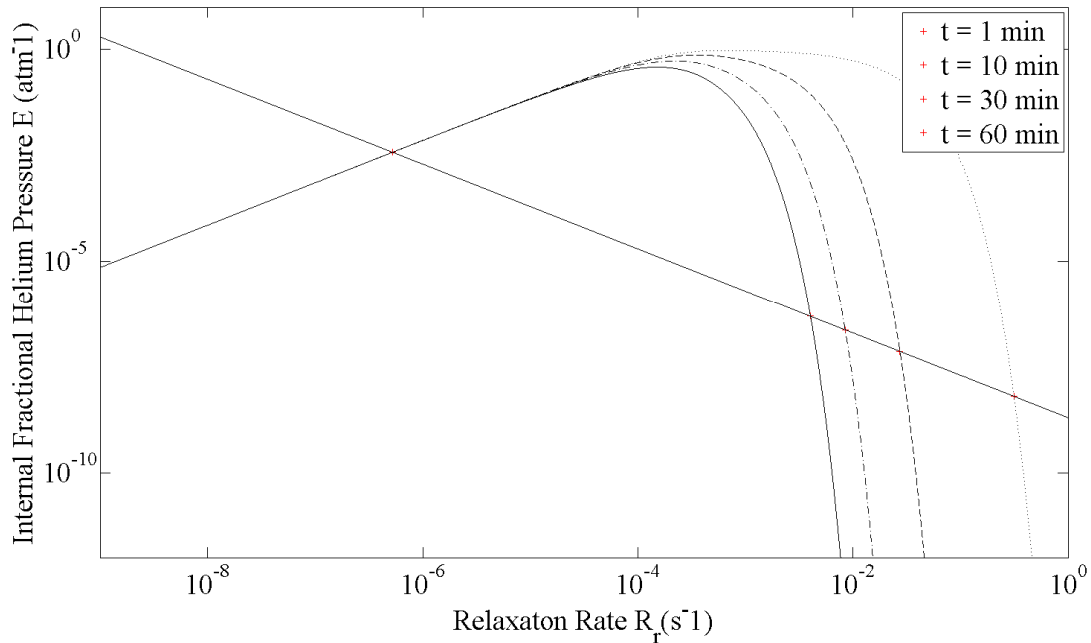


**Figure 7. Effect of dwell time on gross leak rate analysis**

In the figure above, the indicated leak rate is assumed to be  $10^{-10}$  ( $\text{atm cm}^3 \text{ s}^{-1}$ ), with and internal volume of  $0.1$  ( $\text{cm}^3$ ). Note that intersection in fine leak region (left hand side) indicates that dwell time is an insignificant factor in fine leak calculation, with an approximate true fine leak rate of  $6.2 \times 10^{-10}$  for any circumstance. The gross leak region (right hand side) shows variance of nearly two orders of magnitude with respect to the relaxation rate with gross leak magnitudes spanning  $1.6 \times 10^{-2}$  to  $2.3 \times 10^{-4}$  ( $\text{atm cm}^3 \text{ s}^{-1}$ ).

The effect of internal volume size on the internal partial pressure and relaxation rate observed after completion of pressurized bombing is shown in Figure 8. For this example, all variables other than internal volume are held constant, in this case the indicated leak rate

is held at  $10^{-10}$  ( $\text{atm cm}^3 \text{ s}^{-1}$ ) and dwell time is set at 10 minutes. A variation of internal volume spanning four orders of magnitude corresponds to a two order of magnitude variance in both the relaxation rate and the predicted internal partial pressure. Similarly, the calculated true fine leak rate ranges from approximately  $2.0 \times 10^{-9}$  to  $6.2 \times 10^{-11}$  with a corresponding gross leak range from  $1.6 \times 10^{-2}$  to  $1.2 \times 10^{-5}$  ( $\text{atm cm}^3 \text{ s}^{-1}$ ).

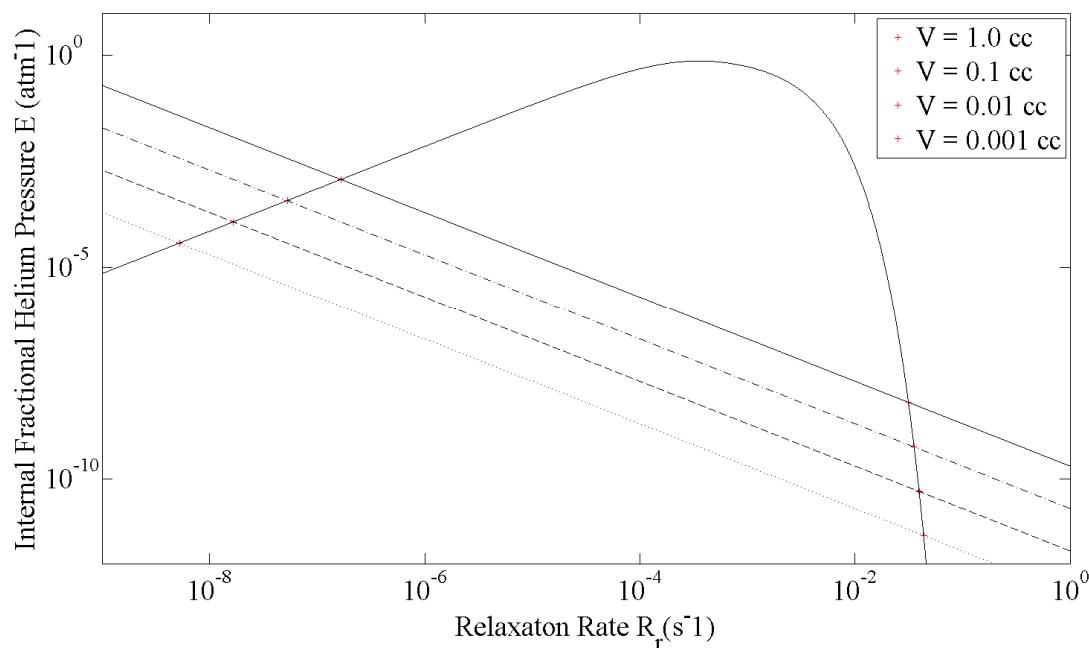


**Figure 8. Effect of internal volume on leak rate analysis**

Once a device is removed from high pressure bombing, the tracer gas immediately begins to leak out from the interior at an unknown rate leading to the two possible case dependent leak rate conclusions shown in the figures above. The loss of tracer gas can skew results by identifying a smaller leak than actually present which necessitates the use of dwell time, requiring the application of Equation 3.6.5 in favor of Equation 3.6.4 for molecular flow analysis. To distinguish between a fine leak and gross leak, a follow up reading can be taken at a later time. Large changes in reading represent additional loss of significant tracer

gas due to a gross leak while minimal change represents a fine leak [29]. However, this method is not deemed sufficient to determine the presence of a gross leak and should be augmented with the application of suitable gross leak detection methods.

### 3.7.2. Variation in tracer gas concentration

Potential error in the back pressurization approach to leak detection can be attributed to uncertainty in the initial concentration of tracer gas within a device prior to testing [16]. Since the HMS quantifies helium ions exiting the interior of a cavity to determine leak rate, the concentration of helium in the gaseous mixture must be known. Slight error in estimating internal helium concentration leads to large errors in perceived leak rates [48]. Without knowing the size of the leak path, which is the unknown parameter of interest, the full amount of gas present inside a device can only be estimated. Thus, if the interior gas concentration is unknown, the crack size cannot be determined without some degree of uncertainty.

The potential for error due to variation in helium concentration is described by a simple comparison of Equation 3.6.4 with the modification required to incorporate an initial internal gas concentration described by Ruthberg. By following the procedure for identifying leak rates based on previously defined methods, the internal partial pressure at the end of high pressure bombing can be modeled by:

$$p_n = p' + (p_e - p')[1 - \exp(-R_r T)] \quad (3.7.2)$$

$p'$  = initial partial pressure (Pa) (atm)  
 $R_r$  = relaxation rate from 3.7.1 ( $s^{-1}$ )

If the initial internal partial pressure is assumed to be negligible at the beginning of high pressure bombing, Equation 3.7.2 reduces to Equation 3.6.4 provided again for convenience.

$$p_n = p_e[1 - \exp(-R_r T)]$$

When the initial partial pressure is acknowledged, in addition to providing a pseudo-minimum partial pressure it affects the pressurization rate during the bombing time as well. Clearly, as the bombing time or leak rate is increased, the internal partial pressure approaches the external partial pressure of the tracer gas. Therefore the initial partial pressure has a diminished effect on the overall tracer gas concentration at the end of bombing. However, since there must be a reasonable limit to the length time allotted for pressurized bombing [28], with suspected fine leak rates, bomb time must increase substantially to reduce the significance of the initial partial pressure on a reading. This is particularly relevant to use of the Radiflo® method which results in a drastic increase in bombing times associated with a small increase in the test sensitivity limit. The sheer amount of time required to force  $^{85}\text{Kr}$  into a device suspected of a leak rate below  $10^{-12}$  ( $\text{atm cm}^3 \text{ s}^{-1}$ ) makes repeated testing increasingly expensive and impractical. Other techniques such as pre-filling components with tracer gas are commonly applied to mitigate this occurrence [40].

In the case of the radioisotope method, any assumptions associated with the initial partial pressure can be eliminated by quantifying the initial activity reading of any test specimen. The internal partial pressure assumption in HMS application is often nontrivial and revolves around knowledge of the environment in which the device was fabricated. Unless sealed in a controlled environment where the helium content is exactly known, any

initial reading, regardless of the circumstance, would require an assumption of initial internal helium partial pressure. Even atmospheric concentrations can be observed to deviate by 10% over relatively short amounts of time [37].

Making such assumptions can easily lead to large error in fine leak detection accuracy with only small deviations in the initial back pressure. However, the error remains somewhat proportional to the size of the leak rate detected as shown in Figure 9 below. The variation in calculated internal partial pressure after a typical two hour bombing time at 5 (atm) is observed over a range of fine and gross leaks. Each data set represents different observed initial helium concentrations in an internal cavity including the typical concentration of helium under standard atmospheric conditions (5 ppm) [37].

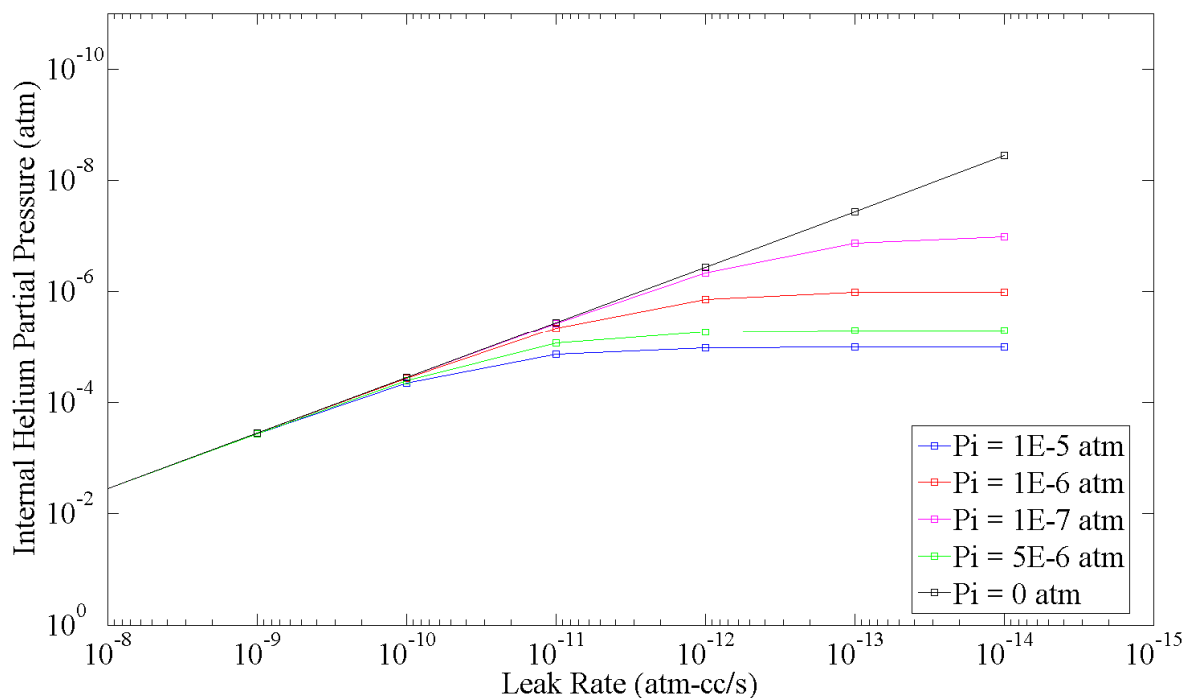


**Figure 9. Effect of initial internal partial pressure on leak analysis**

The internal helium partial pressure observed at the end of tracer gas bombing is both a function of the initial concentration and the leak rate. The initial concentration of tracer gas may be inconsequential in a device exhibiting larger leak rates since the internal atmosphere has ample time to reach equilibrium with the bombing chamber atmosphere. However, if such equilibrium is only reached by transfer of gas through the leak rate, smaller leak rates require additional time to reach equilibrium proportional to the size of the leak indicated by the divergence of different test conditions in Figure 9.

Considering that highly sensitive HMS devices are often rated to a minimum detectability of  $5 \times 10^{-12}$  (atm cm<sup>3</sup> s<sup>-1</sup>) [44] and some CHLD helium detectors are rated to  $10^{-13}$  (atm cm<sup>3</sup> s<sup>-1</sup>) or even  $4 \times 10^{-14}$  (atm cm<sup>3</sup> s<sup>-1</sup>) [37-38] For detecting leaks at this low rate, the initial partial pressure becomes the most significant factor describing the atmosphere inside a device upon completion of bombing. The rate at which helium can be introduced into the interior of a device is directly dependent on the leak rate where increasingly small leak rates result in increased time requirements to produce acceptable results.

With respect to the Radiflo® <sup>85</sup>Kr detection system, the aforementioned issue is a moot point. The presence of krypton inside a device can be determined by quantifying radioactivity following immersion in the Kr-N or Kr-air mixture. Measuring the radioactivity determines exactly the amount of krypton present. There is no need to first understand the concentration of krypton within an interior cavity so long as the concentration of krypton in the tracer gas is already known [48]. However, as mentioned in earlier paragraphs, there is a practical limit to the allotted bombing time for back pressurization analysis which results in a similar lower limit of detectability that must be considered in all leak detection techniques.

### **3.7.3. False negatives and the necessity of gross leak detection**

As mentioned in Section 3.6.1, one issue with gross leaking components is associated with the ability to lose the majority of tracer gas between bombing and detection. This manifests itself as the potential for “false negative” readings with regard to gross leakers. It remains entirely possible for either all or most of a tracer gas to be evacuated from the interior volume during the dwell time of any specimen.

In HMS operation, a device is bombed at high pressure and then generally subject to atmospheric conditions for the majority of its dwell time. This results in decreasing the tracer gas concentration towards atmospheric levels. However, this is further compounded by a pump-down procedure utilized at the beginning of detector operation. An HMS detector cell must hold near vacuum pressure to operate and quantify helium ions to eliminate failure of the ionizing filament [32, 44]. This manifests itself as a pump down procedure prior to analysis and could also result in further reduction of tracer gas n provided a large gross leak is present in the device being tested. This practice is not limited to the HMS, as a high vacuum pump down is present in the Radioisotope technique following the pressurization period [28]. A procedure required to recover the radioactive tracer gas utilized during bombing. In either case, additional measures ensuring that gross leaks are accounted for must utilized to can accurately describing a leaking system.

## Chapter 4. Design theory

### 4.1. Initiator design capabilities

Similar in design to current bridge-wire or spark gap initiators, the primary characteristics of this device consist of an enclosed cavity, filled by a reactive compound, coupled with a method for initiation. In this case, the initiation type explored implements a spark gap method for fabrication simplicity. However, existing equipment is more than capable of creating a bridge wire initiator with similar performance and at a similar cost that remains compatible with the system employed.

Ideally, the design of an initiator would incorporate simple manufacturing constraints and the utmost simplicity of each constituent component to decrease the potential for failure. Of a lesser, yet present concern is the desire for maximum volume ( $V$ ) to surface area ( $SA$ ) ratio built into the design. When vying for primacy with simplicity in construction, the  $V/SA$  ratio does not hold precedence. The most effective design in regard would incorporate a spherical cavity providing the maximum volume to surface area attainable while eliminating (or at least limiting) the presence of stress concentrations at certain locations. However, the techniques used for creating the initiator with spherical geometry were not reasonable and succinctly detrimental to the primary design criteria.

An earlier attempt was made to incorporate a more spherical design into the project by introducing a series of decreasing cavity radii in each layer of the LTCC structure. This design is summed up in Appendix A. The ceramic printing process provides a method for constructing an initiator in a series of layers. Each layer allows the fabrication of its own internal geometry as well as incorporation of metal filled vias acting as a built in electronic wire feed-through system. In this method, complex cavity shapes can be developed while

maintaining the ability to incorporate a spark gap or bridge-wire and almost any location. All designs share common features such as a lid, base, and central layers. Subsequently, the final design can be analyzed as a series of subsections consisting of the central section or cavity wall, the non-ceramic lid, and base containing the spark gap.

#### **4.1. Cavity seal methodology**

The primary issue with the design of any initiator resides in hermetically sealing a cavity, after it has been fabricated. In practice, this equates to a sealing process between a component acting as a lid and corresponding component acting as a container. The unique requirement for low temperature sealing with high temperature operations, the necessity of which is discussed in Section 5.4, severely limits the possibilities for performing the lid sealing task. The operation must involve a sealing method such as laser welding, soldering, application of adhesive, or TLP bonding prior to the “thermal activation” heat treatment operation required to make the energetic compound reactive.

The post fabrication high temperature process in excess of 240° C renders soldering useless in this application for two reasons. If a high temperature solder is used, activation of the energetic material could potentially occur during the soldering process, leading to a potentially dangerous situation and eliminating the primary purpose for application of the proposed compound. The same situation occurs if laser welding is applied unless significant optimization of the welding operation is applied. If a low temperature solder is used to eliminate potential thermal activation, the solder would re-flow during the heat treatment process and present an unacceptable potential mode for failure during fabrication. Thus low curing temperature adhesive materials or TLP bonding is required for sealing the initiator.

However, when considering adhesives, the thermal conductivity differences between the adhesive, lid, and ceramic in a dynamic thermal environment can be an issues. Additionally, repetitive, successful TLP alloy bonds in anything other than a clean room environment are extremely difficult. Only through extensive leak rate testing of initiators subject to thermal cycling, can the selection of appropriate sealing method occur.

#### 4.2. Central layers

The initiator requires the presence of a hermetically sealed interior cavity to contain the reactive material used as the primary explosive. Ideally the interior cavity would contain approximately 1 (cm<sup>3</sup>) of volume; however limitations imposed by available equipment set the volume attainable through stacked ceramic layers at a much smaller size. The LTCC design utilizes a layered process which allows each central layer making up the bulk of the cavity to be essentially identical in configuration. Figure 10 shows the basic design of the interior layers which create the major ceramic portion of the initiator volume. The scales of some features such as the vias are increased for illustration purposes.

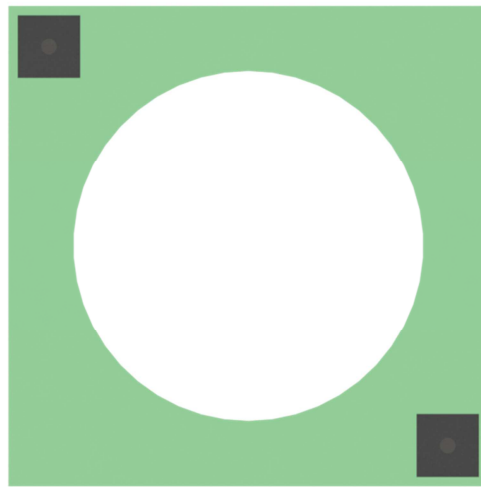


**Figure 10. LTCC initiator central layer**

From Figure 10, the via holes are observed to be in opposite diagonal corners relative to one another. Initial designs had these placed along the center of opposing sides. However, in the interest of increasing the available space for the internal cavity, the via were relocated towards the corners, where bulk “unused” space is present. With the vias in the corners, the diameter of the internal cavity could be slightly expanded, which directly results in an increase in the internal volume.

### **4.3. Lid interface**

The lid interface section of the design consists of two separate layers providing initial access to the interior, and complete sealing upon final assembly. The layer shown in Figure 11 is the top most ceramic piece containing a few features dissimilar to the central cavity layers. The notable features are the soldering pads which cover the top of each via and the metal ring encircling the interior void. The soldering pads provide the means to solder lead wires to the initiator in preparation for electric initiation. The concentric ring serves as a metallic surface to aid bonding between the lid and the top of the ceramic piece. The ring itself is bonded to the ceramic during the high temperature co-firing process due to glass frit contained within the metallic ink.

The lid consists of a metal disk slightly larger than the central cavity diameter and capable of adhering to the top ceramic layer. To increase the interior volume, the lid is significantly dimpled in the center as depicted in Figure 12. The dimple provides a large increase in volume without altering the bonding surface. While not covered in this analysis, the lid should be easily capable of implementing common pressure concentration techniques such as cruciform stamping to increase the likelihood of predicted rupture upon initiation.

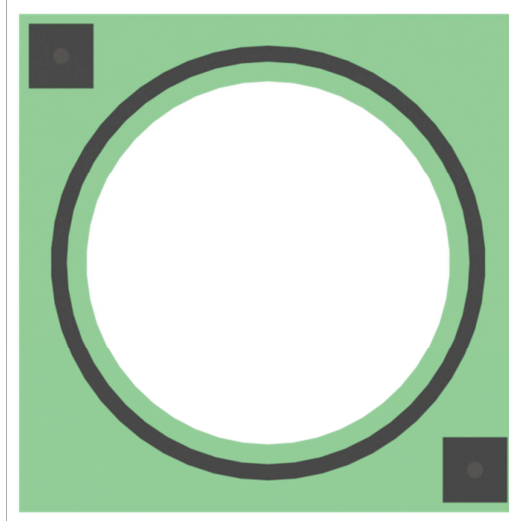


**Figure 11. LTCC initiator top layer**

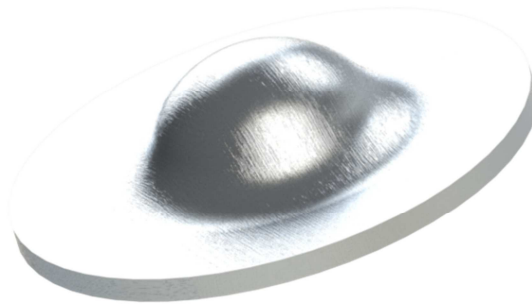


**Figure 12. LTCC initiator dimpled lid**

#### **4.4. Base layer**

The base layer consists of a method for electrical initiation of the energetic compound contained in the interior cavity. This design utilizes either a spark gap or bridge-wire initiation method, both of which could be easily manufactured with current technology compatible in LTCC component fabrication. The spark gap is created by precise determination of the distance between each “leg” shown below in Figure 13. These are embedded in the ceramic by utilizing a simple screen printing technique. In spark gap

initiation, a high voltage difference proportional to the spark gap distance is applied across the circuit and a spark forms between the contacts once the dielectric's breakdown voltage is reached. In many cases the acting dielectric material is air, or has similar properties to air. The spark achieves extremely high local temperatures in an extremely short period of time and initiates a chemical reaction in the energetic compound.

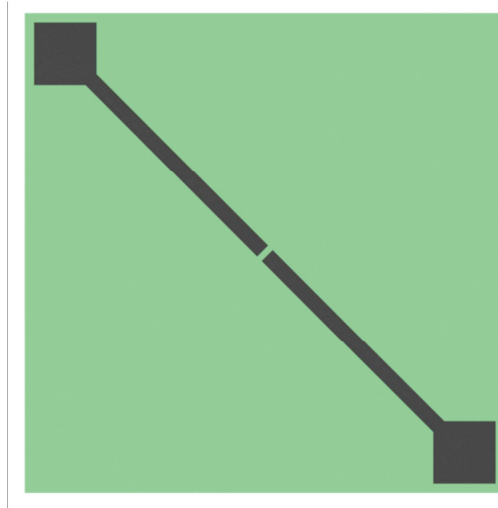


**Figure 13. LTCC initiator base layer**

Fabrication of a bridge wire requires the use of an additional machine capable placing a small “fine” protruding wire between both the “legs” of the spark gap. When current is applied to the system, the fine wire heats up rapidly to the point where it either melts or initiates the intended chemical reaction. Constantly applied current is required for the bridge-wire to heat up which eliminates the potential for static discharge misfire (a potential failure for spark gaps). However, the thin wire must be in contact with the energetic compound and thus provides an additional potential for corrosive failure depending on the electrochemical interaction between the metal wire and the energetic compound.

#### 4.5. Ceramic assembly

Each layer is assembled in a specific vertical fashion prior to being fired at higher temperatures. By increasing the number of layers present in a single initiator, both the cavity volume and number of ceramic sheets required increases. This leads to a more acceptable interior volume but also drives an increase in the individual cost of the initiator. As revealed with the dimpled lid, the volume of the ceramic interior can be augmented by modification to the lid, which can help to reduce the number of layers required for a specific volume. Once the desired number of layers has been determined, they are each stacked together, laminated, and fired. Following the lamination stage, the ceramic layers effectively behave as a single solid bonded piece. Figure 14 shows a representation of the ceramic assembly post lamination [4]. A cut away view of a fully assembled, fired LTCC initiator including the lid piece is shown in Figure 15 below. Note that during the firing process the DuPont green tap changes from a green color to a light blue and the increased internal volume from the dimpled lid can easily be seen.

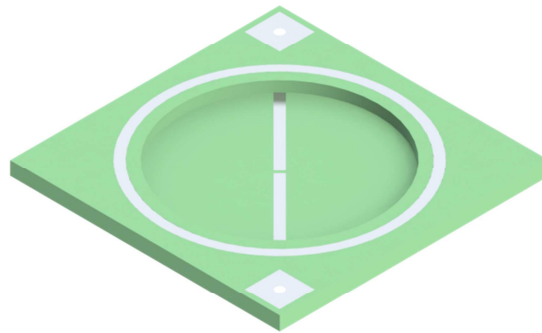


**Figure 14. LTCC initiator layer assembly**



**Figure 15. LTCC initiator fully assembled cutaway view**

#### **4.6. Prototype design**

The cost driven design of a prototype initiator for conducting initial test of both hermetic sealing between the lid and top layer as well as spark gap initiation was completed with a four layer approach. The theory behind this design assumes that both the top seal and bottom spark gap/bridge wire layers of the LTCC can be manufactured with little regards to the number of internal layers present. The top and bottom layers contain the areas of interest in the device while the central layers effectively contribute only to the linear scalability of the cavity volume. A prototype can easily represent the functionality of the initiator with relatively few layers. Functionality of the top and bottom pieces for the co-fired design is of utmost importance for failure criteria analysis, and any design representation of a finalized device should employ a fully functional representation of each important feature. Design of a prototype consisting of four layers was implemented to reduce the amount of material used by promoting fabrication of a fully functional initiator with only one piece of DuPont ceramic tape. Utilizing this method to rapidly create a number of prototype initiators resulted in hermetic testing and concept validation with minimal material requirements.

## **Chapter 5. Materials**

### **5.1. LTCC material**

Selection of materials for fabrication of the LTCC initiator is based on the material cost, availability, and the capability of equipment available to the University. The ceramic material used in the initiator fabrication is DuPont 951 Green Tape which comes from a versatile product line providing a selection of layer thicknesses [5]. A thick tap at 254  $\mu\text{m}$  (10 mils) is used to maximize internal volume by increasing the height of each stacked layer, and thus increasing the overall height of the layered cavity. Consequently, utilizing a thinner tape would require an increased number of layers to achieve similar volumes, which drives up cost and makes fabrication more difficult. Regardless of tape thickness, the assembly process is conducted in a clean room environment to minimize the potential introduction of contaminants that could hinder the fabrication process.

### **5.2. Interconnect material**

Vias are utilized to provide an electrical connection between layers in a multilayered ceramic device. The via-fill material consists of a conductive metal coupled with glass frit and takes the form of a paste. With the application of low temperature ceramics leads to a wide selection of materials which can be utilized as the primary conductor in the paste. The via fill material can then potentially be optimized for corrosion resistance and conductivity while being closely matched with the thermal expansion characteristics of the ceramic material. For hermetically sealed components, matching thermal expansion characteristics is important to limit potential thermally induced crack growth [4], one of the same issues seen in current initiator designs.

The purpose of glass frit embedded in the metallic paste is to promote bonding between the via metal and the ceramic while maintaining conductivity. The glass frit has a lower melting temperature than the ceramic substrate and promotes sintering with the LTCC material to form a solid, sintered, semi-ceramic/metallic region which provides a high quality bond between ceramic and metal. Additionally, the paste is required to have a relatively high viscosity since it is expected to remain in its intended location during the firing process [4], although surface tension provides some mitigation of creep affects during high temperature firing.

### **5.3. Adhesive material**

Selection of the adhesive material is initially determined by the availability, usability and cost for individual adhesive types, with additional criteria applied for more specific screening process. The criteria for selection of adhesives center on their operating temperature, curing temperature, coefficient of thermal expansion (CTE), glass transition temperature and their long term storage characteristics. The primary selection criteria for desirable adhesive characteristics are shown in the table below:

When using any material as an adhesive, various material properties must be taken into account. Normal thermal fluctuations will force the initiator (and its components) to expand and contract proportional to the coefficient of thermal expansion. The use of multiple materials leads to the possibility of failure due to differences in thermal expansion rates. Minimization of failure due to cracking along material transition boundaries can be achieved by attempting to match the CTE of all materials involved in the transition [23]. However, since an adhesive is primarily use to bind two dissimilar materials together, matching both materials is often not possible.

**Table 1. Adhesive selection criteria**

1.	Cure temperature less than 200° C
2.	Cure time minimization
3.	Relatively low coefficient of thermal expansion
4.	Relatively high glass transition temperature
5.	Continuous operating temperature above 150° C
6.	Intermittent operating temperature above 250° C

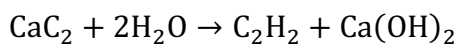
The glass transition temperature (GTT) of adhesive materials presents additional concern with components operating over a large temperature range. The thermal expansion problem is compounded by the presence of the GTT since it acts as a threshold where the adhesive's CTE increases substantially. This is of particular concern when dealing with many epoxy-resin based adhesives since the transition temperature is low enough to be crossed over multiple times during the operating life of the initiator. When using cyanate ester based adhesives, the transition temperature is relatively high in comparison to the operating temperatures and is therefore not of concern. While the CTE plays an important role in selection of an adhesive, other characteristics such as usability and cost cannot be ignored.

#### **5.4. Reactive compound**

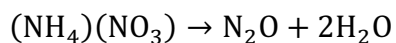
The material utilized as the reactive compound falls under some specific criteria which limit selection. The compound must be capable of combusting when high temperature is applied to the system via spark gap or potentially bridge-wire, and must remain chemically inert until thermally activated. As previously mentioned, current fabrication of

bridge-wire initiators is both tedious and expensive, requiring a large amount of safety equipment and large handling expenses during production. While it is not yet known if initiators using a thermally activated compound could perform on the same level as current primary explosive compounds, they could easily be used as a low cost alternative to initiate an exothermic chain reaction.

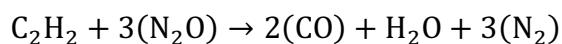
While many thermally activated energetic materials could likely be produced, a simple reaction is proposed for the proof-of-concept purpose of this demonstration. The reaction hinges on the well-known formation of acetylene ( $C_2H_2$ ) and calcium hydroxide ( $Ca(OH)_2$ ) by the chemical interaction between calcium carbide ( $CaC_2$ ) and water ( $H_2O$ ).



Since the calcium carbide reacts upon contact with water, it must be handled under dry conditions to avoid premature acetylene production. Controlled application of water to the system and the gaseous reactive compound are two of the reasons hermetic packaging is necessary. In either case, the water must come from a reaction that can be controlled and in this application a post fabrication heat treatment is applied. The decomposition of ammonium nitrate between the temperature ranges of 200° C to 250° C results in production of primarily water and nitrous oxide ( $N_2O$ ).



Once the ammonium nitrate has been thermally decomposed and the water has reacted with the calcium carbide, an exothermic reaction between the acetylene with nitrous oxide as an oxidizer can occur.



The inert compound used in testing the initiator device was based on a stoichiometric homogeneous mixture of calcium carbide and ammonium nitrate. A chemical equilibrium analysis of the exothermic reaction containing one mole of acetylene is included in Appendix F which applies the NASA CEA program. In application, the amount of acetylene in the reaction would be much less, however simple molar concentrations are used for CEA analysis.

## **Chapter 6. Experimental design and evaluation methods**

### **6.1. Experimental overview**

Each experiment contains a series of independent and dependent variables which are combined and arranged to allow a complete analysis of the given system. The controlled variables are related to material selection and fabrication processes. The primary quantifiable dependent variables are the leak rate and the voltage required for creating a spark in each initiator. Additionally, pass/fail qualifying analysis is required in lieu of accurate gross leak measurement capability, serving as a go/no go benchmark for the various adhesive/lid combinations. The first iterations are utilized to determine if the design method works and are followed by additional device fabrication in the event of success.

The cost associated with the batch creation of the LTCC initiators is relatively low while the time requirements are much higher. Each batch (9-18) initiators requires approximately a day to complete with the capabilities available in the prototyping laboratory. To reduce the amount of LTCC material required for initial hermeticity tests and thereby reduce the time requirements, the number of test specimens was supplemented with the addition non LTCC specimens when applicable. Specifically, aluminum cavity devices were fabricated using the same adhesive material to provide additional samples for testing the viability of using specific adhesives. Elimination of undesirable material combinations from further study is used to focus research efforts towards fabrication of a fully functional design.

### **6.2. Experimental methods**

To successfully fabricate the proposed initiator, each component is isolated and evaluated individually based on appropriated methods. The permeability of each component, unsupported in literature, is evaluated prior to implementation in the final design when

applicable. A series of tests conducted with helium mass spectrometry, Radiflo®, and dye penetrant inspection were applied to a number of small LTCC cavity devices representing the LTCC-via interface. Due to a lack of information regarding the adhesion of a lid with the LTCC ceramic material, leak tests were conducted to assess the viability of specific adhesives for further study. However, since proof of concept remains the purpose of study, optimization of adhesive material was not continued beyond successful measures. Finally, the spark gap deposited on each device was analyzed to determine if the design proved repeatability in results. A description of each experiment is depicted in the following sections.

#### **6.2.1. Dye penetrant test**

The apparatus involved in dye penetrant testing include Magnaflux® red dye, a large pressure vessel with a secure sealing door, a vacuum pump capable of maintaining vacuum pressure at 30 (mm Hg), and an air compressor capable of maintaining pressures greater than 60 (psi) (4 atm). The equipment was assembled in such a way that both the roughing vacuum pump and air compressor were connected to the pressure chamber and capable of individual isolation. During operation, either vacuum or pressure reservoir were isolated from the pressure chamber and used only during appropriate times. Additionally, the pressure chamber incorporates a valve controlled venting line used for equalizing tank pressure upon completion of each individual test. It is important to note that the dye penetrant test should be the last hermetic test conducted, since immersion in dye will interfere with results of other test methods.

Initially, each specimen is placed within a sealed vessel and exposed to vacuum pressure for a specified amount of time. Following completion of the vacuum pump-down,

the specimens are submerged inside a container of red dye. This is then placed inside the sealed vessel which is held at an elevated pressure for a specified amount of time, following MIL-STD procedure for final analysis. Finally, the specimens are removed from the vessel, carefully cleaned, and placed on an absorbent cloth. Once cleaned, the appearance of any dye penetrant is an indication of gross leak, although further verification by gaining access to the interior of a tested device is required. In the case of small devices where cutting is not an option, extensive cleaning coupled with destructive fracture is utilized to observe interior portions of each component.

The first batch of initiators along with aluminum adhesive samples using Ablebond JM7000 cyanate ester adhesive was subject to dye penetrant testing following complete fabrication. The samples were placed in a vacuum chamber and held at vacuum pressure for 15 minutes, placed in dye, and pressurized to 4 (atm) for an additional 15 minutes. While not complying with MIL-STD procedure, the analysis was intended to provide only initial determination of adhesive permeability. Following appropriate time to observe leaks, the specimens were then opened for interior inspection. This process was repeated exactly for a second round of testing with the application of JB Weld epoxy resin adhesive. The second round of testing utilized the back side of the same ceramic components with JB Weld and a new batch of aluminum specimens.

A selection of 7 LTCC-via specimens was taken from the 68 originals while testing procedures outside the scope of this research were conducted on a number of the other specimens. The MIL-STD procedure was followed exactly with a 10 hour dye bombing period at 4 (atm) due to concern of material failure under higher pressure testing. The via specimens were then extracted from the dye, cleaned, and set aside for a number of days.

Since no available tools capable of cutting open the small ceramic components without compromising the results of the test were available, each individual sample was fractured to reveal the interior cavity.

### **6.2.2. Radiflo® leak rate test**

Operation of the radioisotope method for leak rate detection requires the use of a Radiflo® Mark V. leak detection system. The Radiflo® detection system uses  $^{85}\text{Kr}$  diluted in air as the tracer gas. The system utilizes an accessible isolation pressure chamber for placement of test specimens with a self-contained tracer gas storage and recovery system [41]. Operation permits specification of desired bomb time and gas pressure while displaying any and all information pertinent to the test systems current operation. Detailed information on specific components of the device can be found in multiple texts provided by IsoVac Engineering [41].

After test specimens have been removed from the Radiflo® device, a thallium doped sodium iodide scintillation crystal capable of counting the emission of  $^{85}\text{Kr}$  gamma activity is utilized to quantify  $^{85}\text{Kr}$  present in the system. The scintillation crystal utilized in this test procedure is a “well” design which is encased in a lead shield to reduce background radiation. The well crystal is accessible through a removable lid incorporated in the lead shield.

To operate the Radiflo® and obtain leak rate data, initial determination of either the bombing time associated with specific test sensitivity, or the test sensitivity associated with a desired bomb time is required. Drawing from the equations described in Section 3.6.3, this relation can be obtained with the following.

$$Q = \frac{R}{(SK\bar{P}Tt)} \quad (6.2.1)$$

or

$$T = \frac{R}{(SK\bar{P}Qt)} \quad (6.2.2)$$

In this application, Q is defined as the test sensitivity while T is the bomb time while all other parameters are specific to the test equipment and discussed in Section 3.6.3. Once these parameters are determined the specimens are sealed inside the test chamber and the Radiflo® unit is set to operate. Upon completion of the time associated with the tests, the tracer gas is evacuated back into its storage container and the test chamber is equalized with the atmosphere. At this point, the samples can be removed from the Radiflo® device and taken to an appropriate counting device. Each individual specimen is placed within the scintillation “well” crystal where the activity is quantified and the dwell time is associated with each device is noted. As discussed in earlier sections, the dwell time does not provide large effects to fine leaking devices, and subsequently is not associated with the mathematical approach for quantifying a leak rate with the Radiflo® method.

If gross leak measures are taken into consideration, steam activated coconut husk charcoal placed inside the interior cavity prior to final assembly is used as a krypton retainer [41]. The carbon acts as an adsorbent medium [43-44], referred to as a “getter,” [15] which holds the <sup>85</sup>Kr in place during the length of the dwell time. The presence of a “getter” also reduces the significance of dwell time on gross leaking devices and provides the means for gross leak detection. If any specimen is shown to contain excess activity, appropriate means for disposal must be employed in accordance with radioactive waste disposal regulations.

A number of LTCC specimens were fabricated containing a small internal volume and varying number of vias for the purpose of hermetic analysis. A batch of 68 such specimens were subject to multiple Radiflo® fine leak tests designed to identify extremely small leak rates potentially present in each sample. Initially each of the samples was placed inside the Radiflo® bombing chamber for approximately 400 hours at 4 (atm) in a tracer gas consisting of dry air and  $^{85}\text{Kr}$  with specific activity of  $142 (\mu\text{Ci atm}^{-1}\text{cm}^{-3})$ . The bombing time was selected to yield a test sensitivity on the order of  $1 \times 10^{-11} (\text{atm cm}^3 \text{s}^{-1})$ . The specimens were removed and processed by a thallium doped NaI scintillation crystal with a counting efficiency of 14500 (counts/min). Due to atypical laboratory conditions the associated dwell time for this test ranged between 45 and 90 minutes, where under normal circumstances the dwell time would be much less. An additional analysis conducted at a later date with the same specimens followed the exact same procedures as outlined with a bombing time of approximately 800 hours corresponding with a test sensitivity on the order of  $5 \times 10^{-12} (\text{atm cm}^3 \text{s}^{-1})$ .

A selection of 6 fully assembled ceramic initiators along with 3 aluminum adhesive samples was also subject to Radiflo® analysis. The initiators were placed in the Radiflo® test chamber for 18 minutes at 2.7 (atm) with test sensitivity on the order of  $1 \times 10^{-8} (\text{atm cm}^3 \text{s}^{-1})$  with other parameters similar to the other Radiflo® tests. A longer dwell time of approximately 7 hours between removal from bombing and analysis with the scintillation crystal was implemented. Prior to final assembly, steam activated coconut charcoal was placed inside the interior cavity of the initiators and aluminum samples. The charcoal “getter” material reduces the effect of dwell time on accurate quantification of leak rates.

However, incorporation of the “getter” was not possible in the small LTCC-via specimens tested earlier, leading to a well-defined upper limit of detectability.

Due to the relatively large dwell time associated with the Radiflo® analysis, the upper limit of detectability is accounted for by applying methods described by Jourdain [10]. In the case of the small cavity LTCC-via specimens (internal cavity approx.  $5 \times 10^{-4} \text{ cm}^3$ ) the upper limit of detectability was found to be on the order of  $3.6 \times 10^{-7} \text{ (atm cm}^3 \text{ s}^{-1}\text{)}$ . When coupled directly with the dye penetrant analysis technique, an undefined range where both test methods are unable of providing analysis exists between roughly  $1 \times 10^{-4}$  and  $3.6 \times 10^{-7} \text{ (atm cm}^3 \text{ s}^{-1}\text{)}$ . Additional testing utilizing a helium mass spectrometer served to reduce the size of undefined leak region as described below due to reduced dwell time during each test. As mentioned earlier, under normal laboratory conditions, the Radiflo® is more than capable of conducting tests over the same range as the HMS. However, in the case of these specific tests, a longer dwell time was necessary during Radiflo® analysis.

### **6.2.3. Helium mass spectrometer leak rate test**

An Alcatel ASM 180T helium mass spectrometer (HMS) can employ multiple techniques for leak detection such as back pressurization and helium sniffing. The orientation of components within the ASM 180T consists of a roughing pump, hybrid turbomolecular pump, calibrated leak module, and analyzer cell connected to the detector inlet with appropriated automated valves. The detector inlet is connected to a small pressure chamber designed for easily introducing and removing test specimens. The auto calibration standard operates upon startup or at operator request and maintains appropriate calibration of the machine at all times. The detector inlet is capable of interfacing with larger test

chambers or external calibration standards which can provide supplementary calibration measures. Additionally, the HMS requires the application of external tracer gas high pressure bombing for specimens prior to operation. The pressure chamber described in Section 6.2.1 performs this operation with the substitution of a regulated pressure tank containing 95% purity helium gas in place of the air compressor. All other components of the pressure chamber apparatus remain unchanged for either operation.

When applying the back pressurization technique, the ASM 180T has a rated upper sensitivity limit  $2 \times 10^{-11}$  (atm cm<sup>3</sup> s<sup>-1</sup>) [49]. An internal leak standard on the order of  $1 \times 10^{-6}$  is used for single point auto-calibration and applied to the flexible leak detection technique. It should be noted that MIL-STD protocol states that leak standards two orders of magnitude below any tested leak rate must be provided for validation of results. A number of external standards ranging between  $1 \times 10^{-4}$  and  $5 \times 10^{-9}$  were applied to validate tests over an increased leak rate range with a maximum accurate upper detectable limit of  $5 \times 10^{-7}$  (atm cm<sup>3</sup> s<sup>-1</sup>) based on MIL-STD protocol. Additionally, following procedures outlined by Jourdain [10] for calculation of the maximum detectable leak rate, the upper limit of detectability for the small cavity LTCC-via specimens of approximately  $2 \times 10^{-6}$  (atm cm<sup>3</sup> s<sup>-1</sup>) based on the highest dwell time during the tests and the smallest possible cavity volume described below in Section 6.2.5. The resulting detectable range of the HMS is relatively small compared to other test methods yet serves to increase the overall leak detection range by an order of magnitude.

Test procedures utilized for helium mass spectrometer leak detection closely follow the guidelines imposed by MIL-STD 883 for the flexible method. A selection of 7 sample specimens were taken from 68 original LTCC-via devices and subject to 15 minutes of

vacuum pressure at 20 (mm Hg) to aid in outgassing any potential contaminants. The specimens were submerged in helium at 4 (atm) for 3 hours due to concerns about failure under higher pressures. Upon completion of the bombing operation, each specimen was removed from the pressure chamber and individually tested with the Alcatel ASM 180T HMS. The dwell time associated with each test ranged from 1 to 16 minutes, well within the 1 hour maximum dwell time outlined in MIL-STD protocol.

#### **6.2.4. Initiator firing test**

Equipment necessary for conducting examination and evaluation of spark discharge at the designed location as well as firing a fully functional initiator is applied to ceramic test specimens. The experimental system includes a variable voltage power supply, step-up transformer, digital multi-meter, appropriate conductive wire, and necessary safety equipment for handling a high voltage system. Lead wires are soldered to each initiator at the designated solder pads and connected to the high voltage output from the transformer. The low voltage input for the transformer is connected to the variable voltage power supply which employs its own protective fuse. To monitor the applied voltage, digital multi-meter is coupled to low voltage leads on the transformer. The variable voltage power supply is connected to an outlet and voltage is increased until a spark is observed. For a number of tests, video recording equipment is applied to allow a measure of post-test analysis. Due to the high voltage nature of the test equipment, care must be taken to ensure that all equipment is powered off between tests.

A number of LTCC spark gap specimens were examined for repeatability in firing under controlled conditions. The first batch consisting of 8 LTCC components contained screen printed spark gaps, three separate via layers, and solder pads. Once the appropriate

equipment had been assembled, individual initiators as soldered in place and tested one at a time. The voltage is slowly increased while simultaneously being monitored until spark is observed. Appropriate notes are taken, the test specimen is removed from the apparatus, and the process is repeated. The second and third batches of LTCC components lent an additional 5 specimens for analysis using the same procedures as outlined above.

Firing the 3 fully functional initiators incorporating the reactive compound mixture mentioned in Section 5.4 utilized the same equipment and procedure as the spark gap tests. Prior to firing, the initiators were filled with the reactive mixture, sealed with the appropriate adhesive, and cooked at 220° C for 4 hours to activate the energetic compound. Each specimen was connected to the spark apparatus and video recordings used to provide additional information for analysis. Voltage was increased in each case until an observable event occurred.

### **6.2.3. Error Analysis**

The dye penetrant inspection and initiator firing procedures described above consisted of pass fail style tests which provide little reason for numerical error analysis. However, in the case of both Radiflo® and HMS analysis, some error associated with both the leak rate of individual tests and the overall leak range for each method can be quantified. The error in both test systems relies on both the accuracy of calibration and the resolution of test equipment. Furthermore, in the case of individual tests, error relies heavily on dimensional uncertainty in the fabricated components. In the Radiflo® tests conducted on initiators containing the charcoal “getter” material, the internal dimensions have minimum effect on the analysis, as the “getter” provides the means for tracer gas retention. However,

deviation in internal volume and effects on test accuracy is pertinent to the small cavity LTCC-via specimens described below.

During the co-firing process in LTCC formation, the material shrinks both in the x, y, and z direction by  $12.7 \pm 0.3\%$  (x, y) and  $15 \pm 0.5\%$  (z) [5]. Additionally, the initial thickness of the thin DuPont 951 tape used in the small cavity LTCC-via specimens is approximately  $114 \pm 8$  ( $\mu\text{m}$ ) which corresponds to further deviation in the z-direction of the LTCC component [5]. The internal volume of the small cavity devices was designed with dimensions  $0.185 \text{ cm} \times 0.185 \text{ cm} \times 0.0228 \text{ cm}$  prior to co-firing. The intended final internal volume was  $5 \times 10^{-4} \text{ (cm}^3\text{)}$  resulting in variation of  $5.06 \pm 0.24 \times 10^{-4} \text{ (cm}^3\text{)}$ .

Tests conducted with the Radiflo® required the application of a scintillation counting crystal. While the crystal was heavily shielded against background radiation, a notable deviation in background levels at any given time was in the range of  $500 \pm 100$  (counts/min). Similarly, when conducting analysis on any given device, the deviation in readings also resulted in a range of  $\pm 100$  (counts/ min) likely due to variation in the background readings. The effect of this range is explored later in Section 7.1.1 and in Section 7.2.4.

Analysis with the Alcatel HMS applied the use of LacoTech leak standards which are rated at  $\pm 8\%$  accuracy including both external and internal leak standards used in calibration. The leak range associated with the HMS is between  $10^{-11}$  and  $10^{-2} \text{ (atm cm}^3 \text{ s}^{-1}\text{)}$  based on a single set point calibration on the order of  $10^{-6} \text{ (atm cm}^3 \text{ s}^{-1}\text{)}$ . Bias error associated with multiple leak tests conducted on two separate leak standards is summed up in table below describing analysis of two calibrated leak standards.

**Table 2. Alcatel HMS experimental error**

Standard Leak	Actual Leak Rate $\pm 8\%$ ( $\text{atm cm}^3 \text{ s}^{-1}$ )	Indicated Mean Leak Rate ( $\text{atm cm}^3 \text{ s}^{-1}$ )	Bias	Error
1	$3.27 \times 10^{-8}$	$1.4 \times 10^{-8}$	$1.87 \times 10^{-8}$	57.18%
2	$5.85 \times 10^{-9}$	$2.6 \times 10^{-9}$	$3.25 \times 10^{-9}$	55.56%

The bias error shown in the table is much larger than the error associated with the standard leaks during calibration and is considered in analysis. However, as revealed in Section 7.1.2, experimental data resulted in indication of leak rates outside of the available testing range.

## Chapter 7. Results

### 7.1. LTCC-via specimens

Due to a lack of hermetic property data for via-filled LTCC systems, a number of samples were created to conduct an analysis of the hermetic integrity of vias in LTCC. A population of 68 LTCC specimens containing zero, one, or sixteen vias were fabricated with an internal volume of approximately  $5 \times 10^{-4} \text{ (cm}^3\text{)}$  shown in Figure 16. These specimens were subject to Radiflo® testing which revealed that fine leaks were not present within a detectable range of  $3.6 \times 10^{-7}$  to  $5 \times 10^{-12} \text{ (atm cm}^3 \text{ s}^{-1}\text{)}$  based on the smallest possible cavity size and longest dwell time ( $4.82 \times 10^{-4} \text{ cm}^3$  and 90 min). Similarly HMS testing on 7 random samples revealed that no leaks were present between the range of  $2 \times 10^{-6}$  to  $5 \times 10^{-7} \text{ (atm cm}^3 \text{ s}^{-1}\text{)}$  based on smallest cavity size and largest dwell time ( $4.82 \times 10^{-4} \text{ cm}^3$  and 16 min). A combination of both equipment limitations and characteristics of the LTCC-via devices limited the ability to apply gross leak detection techniques to analysis with the HMS and Radiflo®. Since neither test was capable of conducting accurate gross leak analysis, dye penetrant inspection was applied the 7 specimens used in HMS analysis.

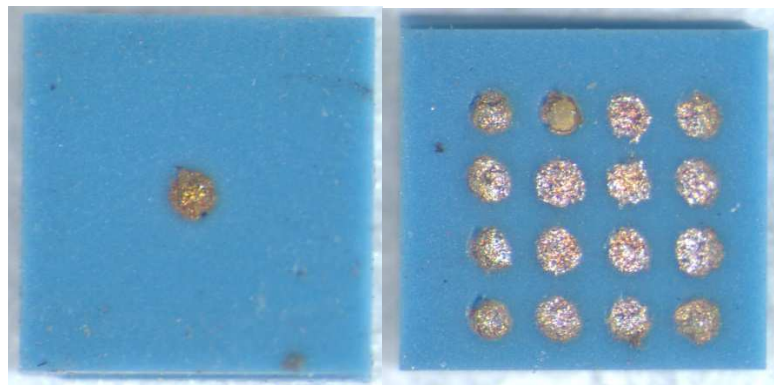


**Figure 16. LTCC-via specimens containing 1 and 16 vias respectively**

### 7.1.1. LTCC-via Radiflo® analysis

The Radiflo® analysis of the LTCC specimens consisted of two different attempts to perform a quantifiable leak rate analysis. The first testing consisted of a 14 day bombing time with a theoretical leak test sensitivity on the order of  $3 \times 10^{-11}$  ( $\text{atm cm}^3 \text{s}^{-1}$ ) when the Radiflo® equation was applied. Upon analysis with the scintillation rate meter apparatus, each of the samples showed no deviation in radioactivity when compared to normal background levels of  $500 \pm 100$  (counts/min). The second test conducted to increase the test sensitivity used a 33 day bombing time with theoretical test sensitivity on the order of  $5 \times 10^{-12}$  ( $\text{atm cm}^3 \text{s}^{-1}$ ). Once again, none of the specimens associated with the test contained activity greater than the observed background level as shown in Table 3.

**Table 3. Radiflo® test comparison**

Activity (counts/min)	Number of samples with activity level	
	Test 1	Test 2
400	8	11
450	13	7
500	28	26
550	12	11
600	3	12

The second test procedure produced a slightly increased number of specimens with higher activity levels. However, comparison between the individual samples in each test only indicated one sample exhibited 600 (counts/min) under both test conditions. While

unable to properly quantify a leak for each device the data indicates that leak rates within the detectable range of the Radiflo® were not present.

### **7.1.2. LTCC-via helium mass spectrometer analysis**

A small population of LTCC specimens was selected for HMS analysis. While not the specific objective of this research, the HMS test was implemented as a secondary method to increase the overall detectable leak range for analysis of the small cavity devices. With an accurate detectible limit of  $5 \times 10^{-7}$  (atm cm<sup>3</sup> s<sup>-1</sup>), no fine leaks for any specimen were observed within the detectable range. During the test, continual application of LacoTech leak standards indicated proper operation of the mass spectrometer and further reinforced the observations made.

Prior to analysis with the HMS, a time dependent discrepancy in background readings was observed. The HMS device was turned on and calibrated utilizing LacoTech procedure and tested against external standards until stability in readings was observed. Several tests conducted on an empty chamber (back ground) were implemented during this time which also demonstrated consistent readings. Once testing of individual devices was initiated and the high pressure helium bombing chamber was purged, a change in the recorded background level occurred. In order to find the root cause of this phenomenon, multiple background readings were recorded prior to, during, and after analysis of individual devices.

Based on the observation, it is believed that inadequate venting of helium from the bombing chamber resulted in increased helium concentration in the atmosphere surrounding the test device. Accumulation of helium in the local environment was then accounted for during all subsequent tests. In the presence of this phenomenon, analysis of each specimen

resulted in leak rates above the accurate detectable level and showed no deviation from background level readings taken at similar times during each test.

### **7.1.3. LTCC-via dye penetrant analysis**

Post DPI testing, the specimens were not allowed further access to the clean room due to potential contamination of the working area which limited the accessibility of the specimens to imaging and cutting equipment. Therefore, each LTCC-via specimen was fractured with a carbide scoring tool to observe potential dye accumulation in the internal cavity of each device. The DPI method revealed gross leaks in 4 of the 7 specimens observed with no indication of gross leaks in the remaining specimens. While the resolution available for magnified image capture of the LTCC-via samples was limited by equipment capability, the figures below depict specimens post DPI analysis.

As shown in Figure 17, dye appeared to collect externally along the vias of each sample analyzed, regardless of whether or not it was a leaker. Potentially revealing inadequate cleaning or ingestion of dye in the via- ceramic interface. This could be an indication of leak path formation in the material interface. However, in the case of non-leakers, due to misalignment between via and ceramic discussed in Section 3.2.4, this observance could be based simply on the difficulty of cleaning such an area. Once specimens were opened, dye was observed along the boundary between the LTCC substrate and the vias on both internal and external surfaces in the leaking specimens.

In one of the samples, the dye had penetrated between separate layers of LTCC, indicating improper lamination or de-lamination likely prior to the high temperature firing process. It is conceivable that both of these potential leak paths are a function of poor quality control during manufacturing.



**Figure 17. Dye penetration in LTCC-via specimen**

The dye penetrant testing is only capable of detecting gross leaks and is not capable of leak rate quantification. When coupled with the fine leak assessment conducted on each of the sample specimens, findings indicate that either a sample will tend contain a gross leak, or extremely fine leak. The fine leaking specimens, indicated by lack of internal dye, indicate the potential for fabrication of highly hermetic devices using LTCC material. Unfortunately the combination of tests conducted resulted in an undefined leak range between  $1 \times 10^{-4}$  and  $2 \times 10^{-6}$  ( $\text{atm cm}^3 \text{s}^{-1}$ ) which could only be accounted for with test methods unavailable at the time. Furthermore, the hermetic properties shown in the LTCC-via specimens are not necessarily representative of more complex devices such as the novel LTCC initiator analyzed in this study.

## **7.2. LTCC initiator prototype**

A total of 27 initiator prototype samples were fabricated for test purposes in two separate batches using similar designs. From these samples, the first batch of 9 was utilized for analysis and selection of appropriate sealing agent in the lid sealing process as well as to determine the functionality of a screen printed spark gap. After all tests on the initial batch were exhausted, an additional two batches consisting of 18 samples were fabricated. During

the fabrication process, an operator error based flaw in one of batches resulted in the inability for 9 initiators to fire. These samples were subsequently fabricated for the exclusive use in hermetic analysis.

### **7.2.1. Initiator fabrication results**

The cost and time associated fabrication of prototype initiators coupled with limited access to some of the equipment required for conducting leak detection procedures resulted in a relatively small sample population of prototype initiators. The results reported here represent the 27 prototype initiators and the existing LTCC-via specimens intended for hermetic study. Fabrication of LTCC based initiators proved to be time consuming due to limitations imposed by the equipment available for use. However, as noted in earlier sections, these time requirements could be severely reduced by equipment readily available in an industrial application. Fabrication consisting of minimal automated processes revealed repeatability in producing similar products with similar results when tested individually.

During fabrication one of the three batches exhibited some slight alignment issues with regards to the screen printing process which can be attributed to operator inexperience. The alignment issue resulted in a single batch lacking the ability to properly fire. Since the screen printing procedure is capable of automation, this error could easily be eliminated while simultaneously increasing production rate. Nevertheless, this failure highlights the importance of controlling the fabrication process and ensuring proper quality control during assembly.

### 7.2.2. Initiator spark gap results

All samples containing a spark gap were tested to demonstrate successful spark initiation. The initial 8 specimens utilized in testing were capable of creating a spark at the intended location in all cases. From the ceramic components considered in this test, two contained a spark gap imbedded between ceramic layers below the cavity floor. This occurred as a byproduct of a minor issue in fabrication, and was later corrected for fabrication of additional batches. However, unexpected favorable results provide a potential modification to the proposed design or even the possibility for an alternative design.

During five of the sample tests conducted on the surface spark gap specimens, the samples showed the spark formation at the intended location within a 315 (V) range at a mean value of 1125 (V) shown in Table 4. Due to a lack of amperage control with the equipment available, the intended printed gap material was quickly destroyed by the expanding spark. Figure 18 shows the spark gap of a specimen before and after conduction of the tests. The success of these ceramic components show that there appears to be no problem with the LTCC vias maintaining alignment through the firing process, and the ability for repeated successful initiation of the spark gap through electrical means.



**Figure 18. Spark gap (left: pre firing, right: post firing)**

**Table 4. Spark initiation voltage**

Test #	Gap location	Applied Voltage $\pm 10$ (V)
1	Surface	972
2	Surface	1440
3	Surface	1260
4	Surface	1170
5	Surface	954
6	Surface	954
7	Embedded	707
8	Embedded	810

Test specimen 2 had the only noticeably differing results when compared to the other specimens. During the test phase, at a relatively low voltage (compared to other tests) sparking began to occur at locations around the central cavity. Voltage was increased until a spark occurred at the intended location at a voltage higher than in other tests. At this time, the ceramic cracked along an irregular path partially aligned with the spark gap trace depicted in Figure 19.

**Figure 19. Cracked spark gap specimen**

Initially the crack did not extend completely through the piece but stopped short on one end of the primary cavity at the location with the material increases from one to four layers in thickness. However, after removing the specimen from the test apparatus separation occurred along the remaining portion of the crack which divided the ceramic into two pieces.

The behavior of this test is believe to be the cause of excessive material used in the via filling process. When the vias are filled, silver paste is forced into each via through direct physical application and excess material is difficult to remove in some situations. In more than one case, silver past was lodged along the inner edge of the primary cavity hole. It is thought that a buildup of this paste accumulating over multiple layers provided a route for current to flow from the spark gap line to the metallic ring present on the top layer. A similar occurrence happened at the opposite spark trace site leading to current flow around the intended spark site which manifested itself as a scorch mark on the ceramic. At each of these locations additional sparking was observed, leading to the conclusion that these locations essentially created a smaller spark gap distance capable of gaping at a lower voltage. Eventually with high enough applied voltage the primary gap area sparked, leading to destruction of the component, verifying that the spark can still occur at the intended location and concluding that the vias maintained proper alignment in all tests.

Tests conducted on the final two specimens did not have exposed spark gaps due to complications during fabrication. For an unknown reason, the CNC punch apparatus failed to punch out proper cavity profiles for two locations resulting in a layer of ceramic covering the top of the spark gaps in the two associated samples. The test results also showed that spark formed at the intended location although at a lower required voltage averaging 750

(V). However, there were only two tests to verify this behavior. While the ark was visible as a blue glow, presumably through the ceramic layer, it is not known if this configuration could still potentially initiate the primary energetic. If capable, this would eliminate direct contact between the vias and the inner surface of the initiator and effectively eliminate the potential leak path formed by the via-ceramic interface. Additionally, this would eliminate contact between the spark gap and energetic compound.

### 7.2.3. Initiator dye penetrant inspection results

Dye penetrant inspection was utilized to determine the feasibility of specific adhesives for use in continued testing. The adhesives used were ABLEBOND JM7000 cyanate ester and J-B Weld steel reinforced epoxy. The former consisted of a one part adhesive stored at low temperature and the latter is a commonly used two part resin which has previously shown superior performance as a sealant during HMS testing [25]. The results from Dye penetrant testing indicated that the JM7000 adhesive was ill-suited for this application. The results comparing both adhesive tests are summed up in the Table 5 below.

**Table 5. DPI adhesive result comparison**

Bonded material	Ablebond JM7000		JB Weld	
	# of specimens	Observed leakers	# of specimens	Observed leakers
Ceramic	8	8	7	2*
Aluminum	11	2	10	1
Stainless steel	10	4	-	-

\*One sample had physical damage occur prior to testing directly resulting in observable leak. Second sample also had physical damage prior to leak analysis discussed below

The 29 different JM7000 samples tested included ceramic, aluminum, and stainless steel components. Each of the ceramic pieces utilized an aluminum lid. As described in Table 5, sixteen JM7000 specimens leaked, including each of the 8 ceramic samples. Furthermore, upon separation of the lids and base, the adhesive was observed to form a noticeably weak physical bond between each lid and base combination. Separation of the adhered components along the adhesive boundary was conducted with minimal effort. A slight increase in the number of leakers was observed with the stainless steel specimens. Due to the additional difficulty in dimpled lid fabrication for the stainless steel lids, the material was not used in further testing.

The results from dye penetrant testing of the J-B weld specimens were favorable in comparison to the JM7000. As a result, 10 aluminum specimens coupled with 7 ceramic samples were analyzed using the same technique as previously employed. Upon completion of the red dye bomb testing procedure, none of the samples showed any indication of leaking when conducting observations with the naked eye. However, upon further inspection, one of the aluminum specimens revealed the presence of a gross leak from two separate orifices shown in Figure 20 below.

While this sample did not exhibit symptoms consistent with the leaking JM7000 specimens (i.e. visible red dye on cloth backing after two weeks), it is entirely feasible for the leak to have lost most of the red dye during the cleaning phase after dye bombing. With two potentially large leak paths, there would be no residual back pressure to hinder leakage, and the dye would have essentially been flushed out of the system by the cleaning agent.

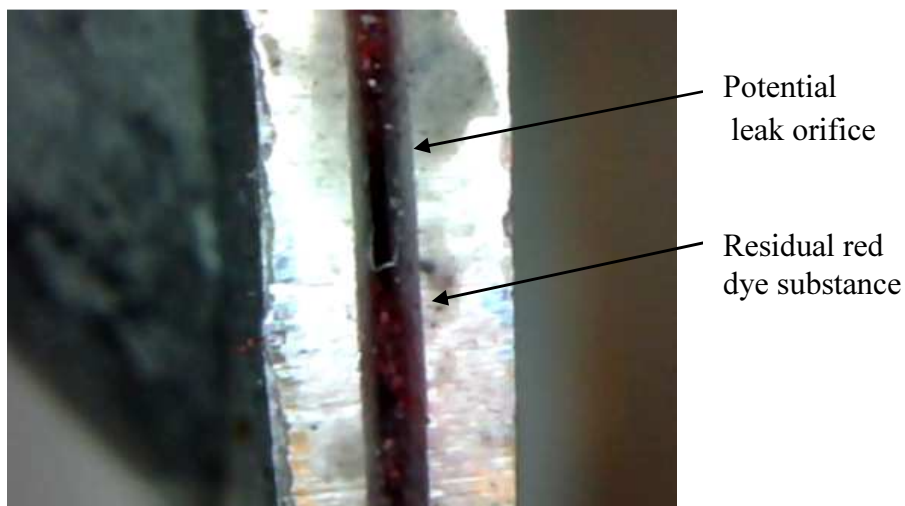


**Figure 20. JB Weld gross leak specimen**

The 7 ceramic samples that were tested resulted in 2 gross leak occurrences. In the case of one sample, fracture of the ceramic occurred during assembly and resulted in a large crack that appeared along the underside of the sample. This was observed prior to testing and was identified as the cause of the observed leak. The second leaking component also was unrelated to the adhesive. Prior to JB weld adhesive testing, the spark gap procedure outlined in Section 6.2.4 was conducted and resulted in damage to the ceramic at the location of the spark gap. While the specimen was being cleaned after pressurized bombing, a steady stream of dye appeared to flow from the center of the bottom layer, directly under the spark gap's location. Upon further inspection, no dye appeared to have penetrated through the adhesive ceramic or adhesive aluminum interface.

#### **7.2.4. Radiflo® test results**

Six initiators and three aluminum test specimens were subject to Radiflo® analysis with the application of steam activated coconut-husk charcoal. Two separate tests were conducted on the samples consisting of 18 and 36 minute bombing times with test

sensitivities of  $1.9 \times 10^{-8}$  and  $9.3 \times 10^{-9}$  ( $\text{atm cm}^3 \text{ s}^{-1}$ ) respectively with a reject level set at 250 (counts/min).

The initial test had a dwell time of 4 hours with inclusion of the charcoal negating the effect of dwell time on gross leak detection. Each of the six initiators along with one of the aluminum specimens produced activity readings approximately 150 (counts/min) above the observed background level ( $500 \pm 100$  counts/min). The remaining two aluminum specimens had larger readings of approximately 450 (counts/min) above the background level. Under normal conditions this indicates leak rates on the order of  $1.12 \pm 0.74 \times 10^{-8}$  and  $3.35 \pm 0.74 \times 10^{-8}$  ( $\text{atm cm}^3 \text{ s}^{-1}$ ) respectively. A second test was conducted under similar conditions with a bombing time of 36 minutes and dwell time of 45 minutes due to atypical laboratory conditions mentioned earlier. Each of the samples resulted in an activity level at approximately 300 (counts/min) above background with the exception of two aluminum specimens at 550 and 1050 (counts/min) above background which was reconfirmed by an additional reading following day. The readings indicate leak rates of approximately  $1.12 \pm 0.37 \times 10^{-8}$ ,  $2.05 \pm 0.37 \times 10^{-8}$ , and  $3.86 \pm 0.32 \times 10^{-8}$  ( $\text{atm cm}^3 \text{ s}^{-1}$ ) respectively. However, the inclusion of coconut husk charcoal as a “getter” material complicates this reading. Furthermore, at the time of testing, the  $^{85}\text{Kr}$  adsorption characteristics or the JB Weld adhesive remain unknown but are suspected of being the primary contributor to the activity reading for each device.

Based on observation and consideration of the data, it is believed that at least one of the aluminum specimens has a sizeable leak while the remaining specimens may be showing substantial krypton adsorption in the adhesive. Under these test conditions, observing no change in activity level between the readings of the second test indicates that the maximum

leak rate attainable in each specimen corresponds directly to the tests conducted above. The large amount of charcoal present inside each specimen is unlikely to have become saturated with  $^{85}\text{Kr}$  based on the activity recorded for each device and higher levels should have been observed if a gross leak was present. Furthermore, a decrease in activity level would have been observed if the charcoal had been saturated with krypton and excess tracer could leak out of a device. Since no change in readings was observed between tests, it is unlikely that this occurred. The initiator devices utilizing JB-Weld exhibited potential for fine leak packaging by MIL-STD standards, however it is advised that a more suitable adhesive material be implemented in future renditions of such a device.

#### **7.2.5. Full component initiation test results**

Due to a low number of available LTCC components, three initiators were fabricated while containing all necessary components for initiation including the energetic compound used exclusively in this device. Three additional specimens containing no energetic compound were also fabricated as a control group to contrast results with the fully functional initiators. These specimens were assembled in a clean room environment and sealed with the same JB Weld adhesive that was utilized in other tests. Once assembled, the three fully functional initiators were placed in a temperature controlled kiln and subject to  $220^{\circ}\text{C}$  for three hours to allow thermal activation of the energetic compound through chemical interaction between the compound's constituent components at elevated temperatures.

Upon removal from the kiln, the JB Weld had changed from a typical gray color to a darker black. Notably, an oily substance of the same color was observed on the exterior of all three specimens as shown in Figure 21 and in close proximity to the solder pads of two

different samples. The three control specimen's adhesive component maintained the typical grey color as expected. Since all three of the specimens had differing test results, they are each considered individually and contrasted with the results from the control group.

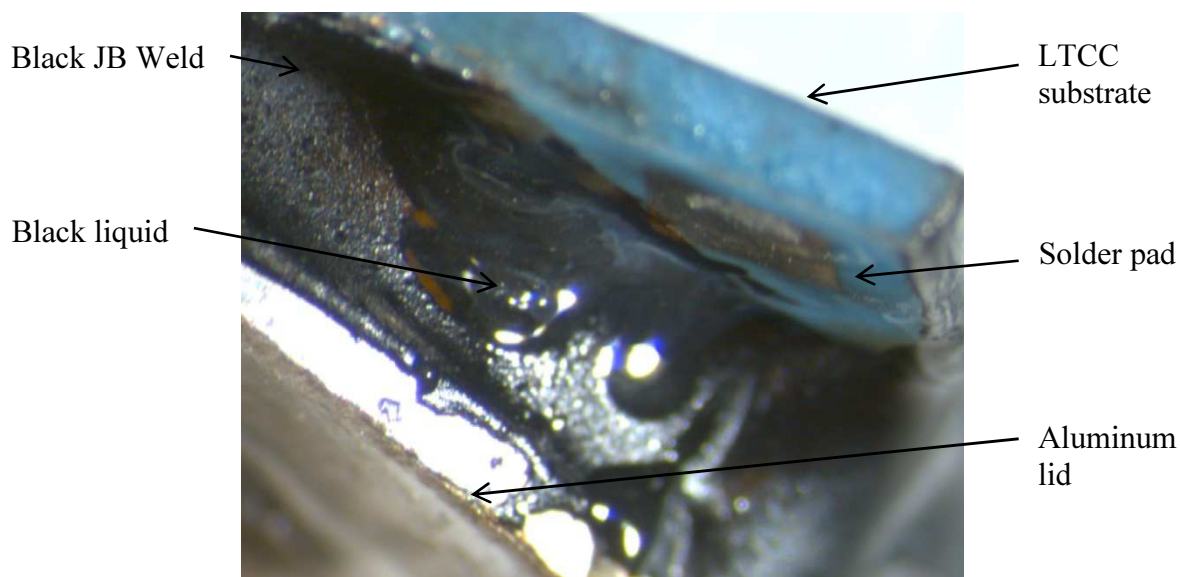


**Figure 21. LTCC post heat treatment**

During the test, when approximately 1200 (V) was applied, specimen 1 was observed to physically deflect upwards in the direction opposite the breach formed during initiation. The bottom portion of the initiator appeared to have fragmented and formed a well-defined crack following the boundary between ceramic and adhesive as presented in Figure 22. Immediately after breach of the initiator, an orange-yellow glow was observed to emanate from the underside of the initiator for a short period of time, potentially indicating that a combustion reaction depleted in oxygen occurred.

The spark gap trace lines seen in the upper middle portion of Figure 22 showed extensive burn damage with charring around the metallic trace. Recalling some of the spark gap tests, this appeared to also occur along the spark gap trace after the ark had been present

for several microseconds. This indicates that substantial damage to the spark gap may have occurred prior to initiation of the reactive compound.



**Figure 22. LTCC fully functional test specimen 1**

Specimen 2, shown in the Figure below, initially appeared as a “fail to fire” specimen which notably resulted in separation of one lead wire from the solder pad while at high voltage. It was thought that failure occurred due to loss of gas through the adhesive hole shown in the Figure 23 taken after the test had occurred.

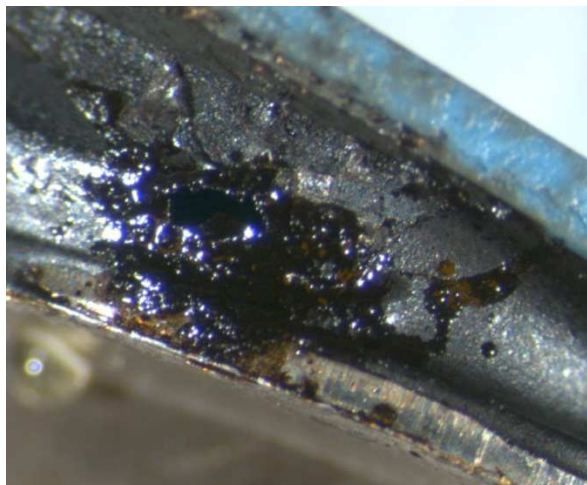


**Figure 23. Hole observe in test specimen 2**

To determine if the spark gap was successfully activated during the test, the top portion of lid was removed through a simple milling operation. While performing this operation, the interior of the device was contaminated by metal chips and likely some machining oil. Even with the contamination present, a visible decrease in the amount of material present in the cavity was observed. The magnified image of the internal cavity depicted by Figure 24 reveals scorch marks and damage to the spark gap and indicates that the gap successfully produced spark. Upon further analysis of video footage taken during the test a plume of smoke was observed exiting the initiator in the vicinity of a hole formed in the adhesive compound. This evidence, coupled with the observed loss of energetic compound and successful production of spark lends to the possibility of complete initiation and breach through the adhesive layer.

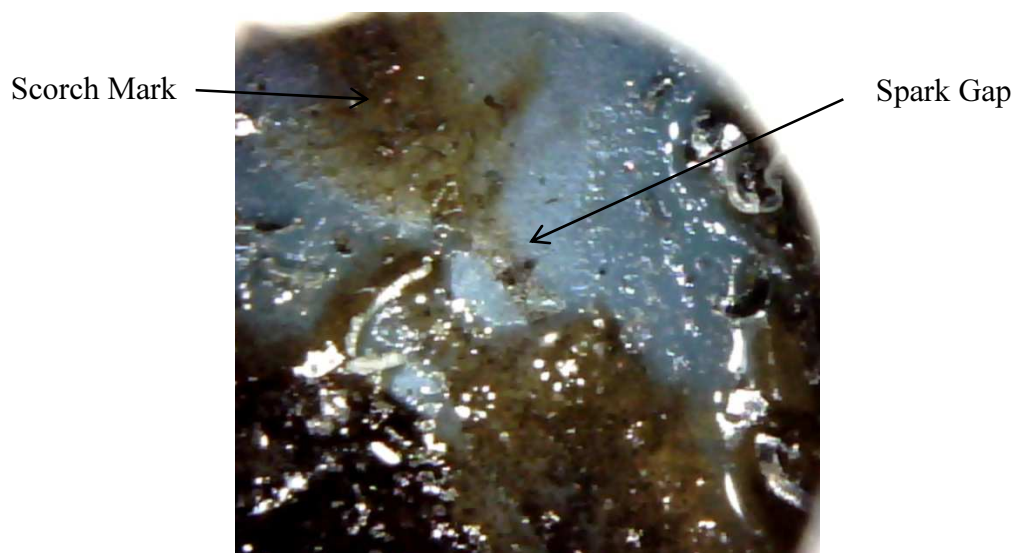


**Figure 24. Burnt remains of spark gap on interior of specimen 2**

The third specimen resulted in a no-fire situation and spark was observed to occur along the outer surface of the device. While increasing voltage to the initiator, a spark appeared between one of the solder pads and the adhesive. It is assumed that a small amount

of adhesive created the means for conduction between solder pads and the adhesive ring surrounding the internal cavity. This then gapped at along the path of least resistance and failed to initiate spark at the intended location.

A set of three control group specimens were tested without inclusion of the reactive compound. These tests were conducted to ensure that thermally induced expansion of the initiator cavity atmosphere coupled with the weakened ceramic during a sparking event was not the cause of breach. Two of the three specimens were accompanied by a slight glow observed along the underside of the specimens at an approximately 1000 (V). The glow is assumed to be the same occurrence observed during the imbedded spark gap tests discussed in Section 7.2.2. Following the tests, noticeable scorch marks appeared along the underside of each specimen, indicating that spark occurred in each case and that without inclusion of the energetic compound, the prototype initiator will not breach.

## Chapter 8. Conclusion

As a demonstration of proof-of-concept, fabrication of a fully functional thermally activated LTCC initiation device was successfully completed during the research conducted in this thesis. Upon test completion, two out of three initiators performed their intended function while control specimens reconfirmed the results. The materials utilized in the fabrication of a novel LTCC initiator proved the feasibility of a low cost, safe initiator design which could be fabricated with current manufacturing technology. However, as revealed through failed tests, much needed additional development in design is required to produce an initiator of higher quality.

Analysis of a series of small LTCC-via specimens identified the possibility of hermetic fabrication of LTCC cavities in excess of hermetic requirements currently imposed on production of electronic devices. However, due to equipment limitations, the possibility of leak rates between  $1 \times 10^{-4}$  and  $2 \times 10^{-6}$  ( $\text{atm cm}^3 \text{ s}^{-1}$ ) was unable to be accounted for. During this analysis the need for proper quality control associated with via fill operations and lamination was identified as the primary cause of hermetic failure. Due to the small sample population subject to gross leak analysis, no conclusions regarding the dependence of leak rate on the number of vias was able to be confirmed. A larger sample size and methods to eliminate the undefined leak region must be utilized to provide adequate conclusions on the hermetic properties of LTCC.

Development of a spark gap initiator based on screen printing and via-fill operations revealed the possibility of repeatable and successful fabrication of initiators. Furthermore, incorporation of imbedded spark gap features showed promise in development of additional designs. However, electrical transmission failure resulting from adhesive-solder pad contact

or large amounts of excess via paste also identified the need for proper quality control. Such problems could be eliminated through careful fabrication practices or development of designs eliminating the potential failure modes. Furthermore, human error resulting in improper alignment of multiple layers highlighted the benefit of computer automated processes for initiator fabrication. These processes are readily available for production scale fabrication and should be implemented in future development. Additional refinement of the successful novel initiator design is paramount to continued use of such a device.

## Chapter 9. Future work

The research conducted in the development of a thermally activated initiator has highlighted a need for further work in development of the design. Not only did the LTCC material reveal the potential for hermetic failure, but the initiator design itself showed a need for further modification to increase reliability. In either case, the results suggest multiple areas for continued research and development to provide a reliable, finalized design on par with current technology.

One area for improvement is a need to develop a reliable and repeatable method for via fill operations in LTCC specimens. While it is likely of little concern in production scale application, continual study with the crude methods used in prototyping must be addressed. The work conducted on LTCC via specimens resulted in multiple gross leakers as well as the potential for exceedingly hermetic devices. The contrast between the two indicates the potential for a highly hermetic design but also highlights the necessity for quality control on a level not achieved during the prototype fabrication. Additionally, further analysis of the interaction between LTCC and via fill material under thermal shock testing would prove useful for continued application of LTCC in initiator design. An in-depth analysis of high quality hermetic specimens under thermal loading would lay the groundwork for the continued use of LTCC as a packaging material for initiators.

As revealed during initiation testing of the fully functional initiators, considerations need to be taken to ensure the electric charge follows the desired path. Testing revealed that the conductive adhesive material provided a method for flow of electrons to arc along the outside of the device rather than at the designed spark gap. This failure mode can be eliminated by either modification to the initiator design, selection of a nonconductive

adhesive, or controlled application of adhesive on a level previously unachieved during prototype fabrication. In any case, a need to improve the initiator design has been revealed by the careful analysis conducted.

Specific areas of improvement in the initiator design are directly related to observed failure modes. The failure caused by the proximity of conductive adhesive to the spark gap wire system can be eliminated with the relocation of the surface solder pads. By placing the solder pad on the surface opposite the adhesive/lid interface, not only would this eliminated potential external gapping, but also completely prevent interference between any selected adhesive and the electrical system. While this may be a trivial issue with automated manufacturing, solder pad relocation would drastically reduce the time associated with sealing the initiators simply by making adhesive application easier in prototype fabrication.

Additionally, a few spark gap tests revealed that it may be possible to completely eliminate contact between vias and the internal cavity, thereby eliminating the potential leak path caused by via-LTCC interaction. By imbedding the spark gap between ceramic layers it may still be capable of initiating the reactive compound. This option could easily be explored in greater detail with simple modification to the existing design, potentially using preexisting equipment specific to the original design. Either of these design modifications would be relatively easy to implement and would eliminate multiple potential device failure modes.

Finally, a more comprehensive analysis of an adhesive compound required for application in the initiator device would be paramount for continued development of the initiator design on an industrial scale. The criteria outlined for adhesive selection are difficult to meet with readily available adhesives and an analysis of multiple adhesive types

subject to the conditions imposed on the initiator is of vast importance. While the selection utilized resulted in proof of an adhesive capable working with the initiator design concept, it has hardly been optimized for the design implemented. This design could greatly benefit from further analysis and assessment of each individual component, a study not practical for a proof of concept study in the development of an entire complex device.

## Bibliography

- [1] M. Gad-el-Hak, *The MEMS Handbook*, Boca Raton, FL: CRC Press, 2002.
- [2] J. W. Judy, "Microelectromechanical Systems (MEMS): Fabrication, Design and Applications," *Smart Mater. Struct.*, vol. 10, no. 6, Nov. 2001.
- [3] K. A. Peterson, K. D. Patel, C. K. Ho, S. B. Rohde, C. D. Nordquist, C. A. Walker, B. D. Wroblewski, and M. Okandan. "Novel Microsystem Applications with New Techniques in Low-Temperature Co-Fired Ceramics," *Int J. Appl. Ceram. Tec.*, vol. 2, no. 5, p. 345-63, 2005.
- [4] F. D. Barlow and A. Elshabini, *Ceramic Interconnect Technology Handbook*, Boca Raton, FL: CRC Press, 2007.
- [5] DuPont Microcircuit Materials, "951 Green Tape™: Thick Film Composition," MCM951 datasheet, 2001 [Revised Sept. 2003].
- [6] D. Plumlee, J. Steciak and A. Moll, "Development and simulation of an embedded hydrogen peroxide catalyst chamber in low temperature co-fired ceramics," *Int. J. Appl. Ceram. Tec.*, vol. 4., p. 406-14, Sep. 2007.
- [7] D.G. Plumlee, "Development of a monopropellant micro-propulsion device in low temperature co-fired ceramics," Ph.D. dissertation, Dept. Mech. Eng., Univ. Idaho, Moscow, 2007.
- [8] M. Wu, and P. Lin, "Design, fabrication and characterization of low-temperature co-fired ceramic gaseous bi-propellant microthruster," *J. of Micromech. Microeng.*, vol. 20, no. 8, Aug. 2010
- [9] K. Kim, Jung-Mu Kim, Jong-Man Kim, G. Hwang, C. Baek and Y. Kim, "Packaging method for RF MEMS devices using LTCC substrate and BCB adhesive layer," *J. of Micromech. Microeng.*, vol. 1, June 2005.
- [10] A. Jourdain, P. De Moor, S. Pamidighantam, and H. A. C. Tilmans, "Investigation of the hermeticity of BCB-sealed cavities for housing (RF-) MEMS devices," *J. MEMS*, Jan. 2001.
- [11] IsoVac Report R-4150-A, "the Charcoal Gettering Technology," IsoVac Engineering Inc. Glendale, Ca.
- [12] G. R. Neff et al. "Non-Hermetic Impulse Cartridge Failures: "A Case Study"," presented at the *Joint Propulsion Conference & Exhibit*, Sacramento, Ca., 2006. (c) IEEE. DOI: 10.2514/6.2006-4813

- [13] K. K. Rink, "Fundamental Considerations Concerning the Detection of Gross Leaks in Bridge-Wire Initiators," *Int. J. of Vehicle Safety*, vol. 1, no. 4, p. 253-66, Nov. 2006.
- [14] A. Goswami, B. Han, S. J. Ham, and B. G. Jeong. "Quantitative Characterization of True Leak Rate of Micro to Nanoliter Packages Using Helium Mass Spectrometer," *IEEE T. Adv. Packaging*, vol. 32, no. 2, p. 440-47, May 2009.
- [15] J. L. Murgatroyd, "Leak-Rate Determination Using Krypton 85." *IEEE T. Instrum. Meas.*, vol. 21, p. 41-48, Feb. 1972.
- [16] L. M. A. Ford, "Comparison and Evaluation of the Helium Pressurization and Radiflo Methods of Leak Rate Determination," Sandia Laboratory., Albuquerque, NM, Tech. Rep. SC-TM-66-2614, Jan. 1967.
- [17] C. P. Ballard, R. J. Eagan, and E. A. Kjeldgaard. "Glass Ceramics for Explosive Device Headers," Conference 7. international pyrotechnics seminar, Vail, CO, 1980.
- [18] D. M. Forman, "Automotive Initiator Technology," *presented at the 35th AIAA/ASME/SAE/ASEE Joint Propulsion Conference and Exhibit*, Los Angeles, CA, 1999, DOI: 10.2514/6.1999- 2422.
- [19] M. R. Maughan, R. R. Stephens, D. M. Blackketter and K. K. Rink, "Thermal Stresses Due to Laser Welding in Bridge-Wire Initiators," *J. Electronic Packaging*, vol. 131, no. 1. July 2007.
- [20] L. M. Thompson, M. R. Maughan, K. K. Rink, D. M. Blackketter and R. R. Stephens. "Thermal Induced Stresses in Bridge-Wire Initiator Glass-to-Metal Seals," *J. Electronic Packaging*, vol. 129, no.1, Nov. 2006.
- [21] C. J. Leedecke, P. C. Baird and K. D. Orphanides, "Glass-to-Metal Seals," HCC Aegis Inc., 1989.
- [22] A. W. Hull and E. E. Burger. "Glass-to-Metal Seals," *Physics* vol. 5, no. 12, Dec.1934
- [23] K. Kokini, and R. W. Perkins, "Thermal Stresses in Annular Glass-to-Metal Seals Under Thermal Shock," *AIAA J.*, vol. 22, no.10 p. 1472-77, 1983
- [24] M. B. Abrams and D.J. Green. "Prediction of Stable Crack Growth Geometry in Residually Stressed Glass," *Int. J. Fract.*, vol. 130, no.2, p.601-15. Nov. 2004.
- [25] C. K. Fischer, "Measurement and Analysis of Helium Leak Rates Through Cracked Glass-To-Metal Bridge-Wire Initiator Seals," M.S. thesis, Dept. Mech. Eng., Univ. Idaho, Moscow, 2007.

- [26] K. K. Rink, "Leakage Rates through LTCC Substrates for Extreme Environment Applications." Ed. Fred Barlow and Aicha Elshabini. *IMAPS*, 2008.
- [27] N. Harris, *Modern Vacuum Practices*, Maidenhead, England: McGraw-Hill Book company, 1989.
- [28] B. Cassen, and D. Burnham. "A Method of Leak Testing Hermetically Sealed Components Utilizing Radioactive Gas," *Int. J. Appl. Radiat. Is.*, vol. 9, no.1, p. 54-59, Dec. 1960.
- [29] S. Ruthberg, "Graphical Solution for the Back Pressurization Method of Hermetic Test," *National Bureau of Standards Special Publication*, p. 400-473, Nov.1982.
- [30] S. Dushman and J. M. Lafferty. *Scientific Foundations of Vacuum Technique*, 2nd ed., New York, NY: John Wiley & Sons, Inc., 1962
- [31] J. M. Lafferty *Foundations of Vacuum science and Technology*, New York, NY: Wiley, 1988.
- [32] M. Gad-el-Hak, "The Fluid Mechanics of Microdevices—The Freeman Scholar Lecture." *J. Fluids Eng.*, vol. 121, no.5, Mar. 1999.
- [33] E. A. Guggenheim, "The Kinetic Theory of Gases," in *The International Encyclopedia of Physical Chemistry and Chemical Physics*, vol. 1, J. E. Mayer, and F. C. Tompkins, eds. Oxford, England: Pergamon Press, 1960.
- [34] M. Knudsen, *The Kinetic Theory of Gases*, London, England: Mathuen & Company, 1950.
- [35] L. B. Loeb, *The Kinetic Theory of Gases*, New York, NY: Dover Publications, 1961.
- [36] P. D. Zeman, "Free Molecular Flow in the Sample Inlet to the Mass Spectrometer," *J. Appl. Phys.*, vol. 23, no. 8, p. 924-27, Aug. 1952
- [37] Method 1014.14, *Test Method Standard Microcircuits*, MIL-STD-883J, U.S. Dept. Defense, 2013.
- [38] Method 1071.6, *Test Methods for Standard Semiconductor Devices*, MIL-STD-750F, U.S. Dept. Defense, 2013.
- [39] S. Costello, M. P. Y. Phillipe and S. McCracken. "Review of Test Methods Used for the Measurement of Hermeticity in Packages," *IEEE Trans. Compon., Packag., Manuf. Technol.*, vol. 2, no. 3, p. 430-438, Jan. 2012.

- [40] P. F. Berry, and J.F. Cameron, "Detection and Measurement of Leaks in Hermetically Sealed Electrical Components Using Krypton 85." *Proceedings of the IEE Part A: Power Engineering*, vol. 109, no. 3, p. 172-175, 1962.
- [41] IsoVac Report R-4130, "How the Radiflo® Process Works," IsoVac Engineering Inc. Glendale, CA.
- [42] P. Malbrunot, D. Vidal, J. Vermesse, R. Chahine, and T. K. Bose. "Adsorption Measurements of Argon, Neon, Krypton, Nitrogen, and Methane on Activated Carbon up to 650 MPA," *Langmuir*, vol. 8, no.2, p. 577-80, Feb.1992.
- [43] G. Constabaris, J. H. Singleton and G. D. Halsey, Jr. "A Precision Adsorption Apparatus for the Study of the Interactions Between Gas Atoms and Surfaces," *J. Phys. Chem.*, vol. 63, no. 9, Sept. 1959.
- [44] P. O. Moore, *Nondestructive Testing Handbook*, 3rd ed., C. N. Jackson Jr., and C. N. Sherlock, eds. American Society for Nondestructive Testing, 1998.
- [45] J. F. McLaughlin, P. G. Schneider and M. H. Eager. U.S. DOE Report Y-2230 "Residual Contaminants in Dye-Penetrant Testing," Oak Ridge, TN. Apr. 13 1981.
- [46] S. Ruthberg, G. R. Neff and B. D. Martin. "Radioisotope Hermetic Test Precision," *IsoVac Engineering Inc.* [www.isovac.com/home/technical\\_information](http://www.isovac.com/home/technical_information)
- [47] K. J. Shultis and R. E. Faw. *Fundamentals of Nuclear Science and Engineering*, Boca Raton, FL: CRC Press, 2008.
- [48] G. R. Neff, "Hybrid Hermeticity And Failure Analysis," *Hybrid Circuit Technol.*, Apr.1986.
- [49] "Alcatel ASM 180T Manual," *Laco Technologies Creating Vacuum and Leak Testing Solutions*. LACO, 2013.

## **Appendix A**

Previous Iterations of Initiator LTCC Cavity

Prior to the designs utilized for this initiator, some initial work was accomplished by electrical engineering graduate student Brian Patterson. However, this project was outside of his area of research leading to less time and effort allotted to the development of an LTCC initiator. The designs he produced consisted of a multilayered square cavity with renditions of both a smaller square and circular shaped openings capping off the upper surface. The cavity was designed to minimize the contact area between the metal lid and the ceramic while maximizing the internal volume. By minimizing the necessary contact adhesive area, the area available to adhesive based leakage can also be minimized.

The cavity design had some flaws that were not addressed before Patterson diverted his attention back to his graduate studies and primary focus of research. As depicted in the figures below, cracking can be seen along the upper edges of each cavity and in some cases protruding towards the center of the cavity's circular ceramic lid piece. Furthermore, cracking can be observed along the bottom surface of the ceramic components as well. This failure was directly related to the firing orientation of the ceramic as the elevated temperatures would induce thermal creep in the ceramic and lead to deformation of the upper lid. With larger cavities present in the LTCC, material suspended over open space, i.e. all the material directly above the primary cavity, collapses into the lower cavity surface due to lack of support at the elevated temperatures. Once hardening neared completion, crack would form along stressed locations leading to catastrophic failure of the ceramic components.

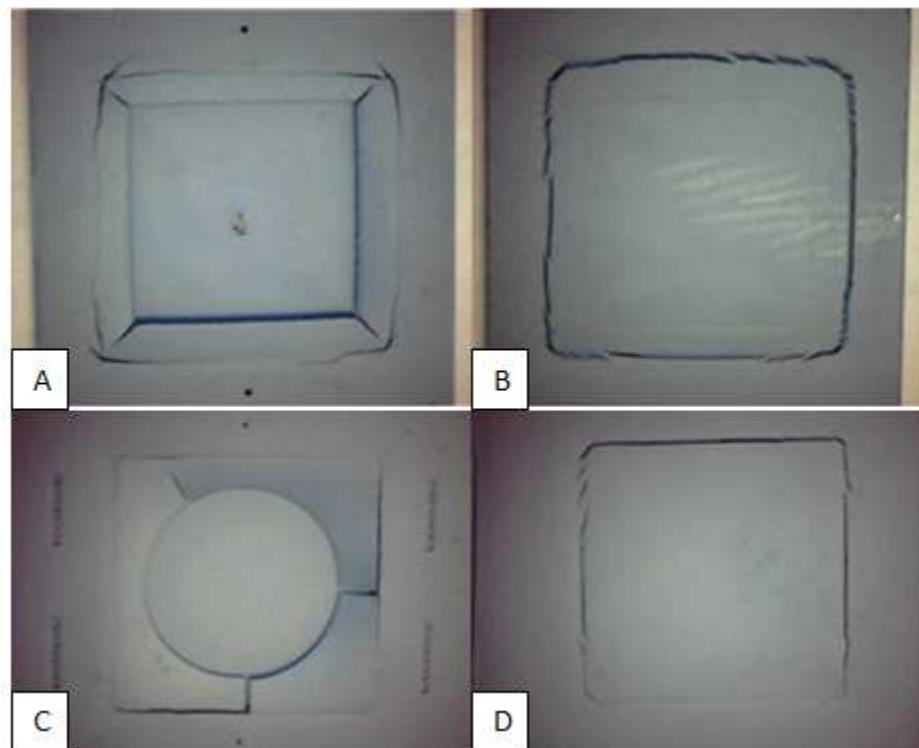


**Figure 25. Square top cavity front: (A), Square top cavity back: (B), Circular top cavity front: (C), Circular top cavity back: (D)**

One method to cope with these issues is to insert a sacrificial carbon material below the top layer to serve as a support structure. This would reduce the likelihood of cracking by providing additional support and eliminating the sagging which occurs otherwise. However, the sacrificial material would also not change dimensionally at the same rate leading to the possibility of failure by added stress on the ceramic due to contact between the carbon and LTCC material. The issue of top layer sagging was mitigated by making the top layer the same as the interior layers and thus eliminating the “overhang” that is observed in Figure 25A and Figure 25C. Additionally, the cavity was changed in favor of a circular design rather than rectangular in an effort to limit potential stress concentrations that could have resulted in crack initiation observed at locations along the lower surface of the ceramic components.

## **Appendix B**

Complete Assembly Process for LTCC Initiator:

### LTCC Assembly Process

- Design each layer to specifications with provided AutoCAD software
- Utilize a rapid punching process to create the desired geometry effects in each layer
- Fill each via with the desired metal interconnect material
- Screen print each of the metallic components onto the surface of the ceramic layers
- Cut out each individual layer and stack for lamination process
- Cut out individual pieces prior to firing
- Fire the layers to create single piece hard ceramic components

Once a sufficient number of ceramic components have been completed:

- Introduce chemical compound to become reactive at a later time
- Apply specific adhesive type to bond lid and upper ceramic surface
- Cure the adhesive following the cure guidelines specific to each adhesive

Once the adhesive is completely cured:

- Perform elevated heat treatment for initiation reactive compound
- Solder lead wires onto the respective soldering pads for each initiator
- Connect lead wires to current/high voltage source depending on initiation type
- Switch the power to the on position
- Observe initiation

## **Appendix C**

Complete Operation Procedure for Radiflo®

The Radiflo® leak detection system involves two basic stages for testing leak rates in material by way of the back pressurization technique. The two basic systems are: (a) A pressurization system which contains diluted mixture of nitrogen and  $^{85}\text{Kr}$  gas; and (b) a scintillation crystal system that is used to record measurements of the radioactive signature of any  $^{85}\text{Kr}$  associated with a leaking device [41].

Differ to the machines operations manual for information pertaining to the initial startup and installation of the device if necessary. The Radiflo® is serviced by a trained technician and should be in a pre-calibrated state ready for turnkey operation. The machine should be started up and cycled through its actions prior to attempting a test to ensure that operation occurs smoothly when required.

#### Step 1

The devices(s) to be tested are placed in a suitable metal fixture and lowered into the pressurization tank where the lid is lowered and locked into place. At this time, if the components and fixture are relatively small, it may be desirable to insert a piece of bulk material to volumetrically displace the atmosphere in the tank and thus decrease the amount of tracer gas needed for the test. This has no ill effect on the test results and can be performed simply by placing some bulk metal (typically aluminum) in the pressure tank along with the devices and fixture.

#### Step 2

The Radiflo® system is programed to run at a pressure and time previously calculated through the use of the Radiflo® equation. The pressure and time are selected based on the material and time constraints associated with the test. The leak rate sensitivity is directly related to the use of these parameters.

### Step 3

The machine is started and a pump-down procedure is automatically initiated where the atmosphere inside the pressure tank is evacuated. Following evacuation, the tracer gas mixture ( $^{85}\text{Kr}/\text{Air}$ ) is allowed to fill the tank and maintained at the specified pressure for the allotted amount of time.

### Step 4

Once the preset time has been achieved, the machine automatically evacuates the tracer gas mixture and relocates it into a shielded holding tank. The chamber is filled with air to equalize the pressure and the tank lid can be opened.

### Step 5

The components are removed from the pressure chamber and placed in/on the scintillation counting device. A measurement of the radioactivity for each device is taken individually to determine the activity of  $^{85}\text{Kr}$  present in the potentially leaker. Background radiation readings are consistently noted and applied when necessary.

## **Appendix D**

### Leak Rate Analysis Procedure

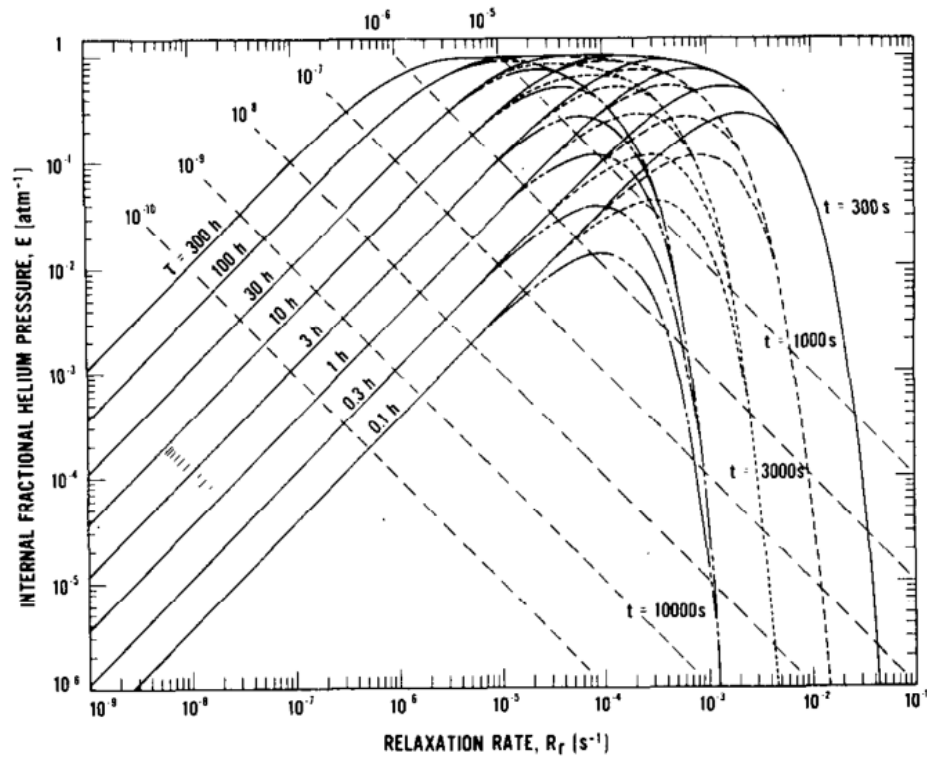


**Figure 26. Ruthberg standards plot [29]**

The procedure for identifying and quantifying a leak associated with the helium mass spectrometer back pressurization technique utilized by Ruthberg [29] operates as follows:

With known input parameters:

$V$  = Internal free volume ( $\text{cm}^3$ )

$P_e$  = Helium partial pressure (atm)

$T$  = Bomb time (h)

$T$  = Dwell time (s)

$R$  = Indicated leak rate ( $\text{atm cm}^3 \text{ s}^{-1}$ )

Compute:

$$R_r \cdot E = \frac{R}{(P_o \cdot VP_e)}$$

This provides a linear slope on or between test lines provided in the figure above, Find the intersection with the test line relating to the Dwell time, or approximate linearly. Determine the value of  $R_r$  at the intersection. Apply Equation (5a) from [29]:

$$R_r = \frac{L}{P_o V}$$

Solve for the leak rate “L” and apply the conversion factor between leak rate of air and leak rate of helium to have the final fine leak rate.

Follow the  $R_r \cdot E$  line to the line associated with the dwell time  $t$ , determine the value for  $R_r$  and apply Equation (5a) from Ruthberg [29] to solve for leak rate  $L$ . This provides a calculation for the potential gross leak rate. To determine which of the leaks actually describes the system, a follow up test should be employed. If the leak rate is drastically different, the device has a gross leak. If the leak rate appears similar to the original, a fine leak is present.

## **Appendix E**

Derivation of MIL-STD 883J HMS Leak Rate Equation

The molecular flow leak rate equation used in MIL-STD 883J is derived from the bounded integration of the general form equation for flow through an orifice called Equation 3.4.4 in the text.

$$Q = F(p_2 - p_1) \quad (\text{E.1})$$

$Q$  = the flow rate ( $\text{Pa m}^3 \text{s}^{-1}$ ) ( $\text{atm cm}^3 \text{s}^{-1}$ )

$F$  = flow conductance ( $\text{m}^3 \text{s}^{-1}$ ) ( $\text{cm}^3 \text{s}^{-1}$ )

$p_1$  = downstream tracer gas partial pressure (Pa) (atm)

$p_2$  = upstream tracer gas partial pressure (Pa) (atm)

The flow rate is equivalent to the change in pressure per change in time of a fluid inside a specific volume with the assumption that the system is isothermal and behaves as an ideal gas.

$$V \frac{dp}{dt} = F(p_e - p) \quad (\text{E.2})$$

Additionally, if the flow is assumed to be in the molecular region, the flow conductance becomes a function only of the flow geometry which is assumed to be constant with respect to the isothermal, ideal gas system. Therefore, some leak rate  $L$  (essentially a specific  $Q$  value divided by a differential pressure of 1 (atm)) is equivalent to the flow conductance by substitution of  $L$  for  $Q$  and  $P_o$  for the pressure terms in Equation E.1:

$$F = \frac{L}{p_o} \quad (\text{E.3})$$

This can be substituted back into Equation E.2 yielding Equation 3.6.3 from the text:

$$V \frac{dp}{dt} = \frac{L}{p_o} (p_e - p) \quad (\text{E.4})$$

“ $p_e$ ” is treated as the partial pressure of tracer gas in the bombing chamber. “ $p$ ” is treated as the initial internal tracer gas partial pressure at any given time. Separation of

variables and integration from an initial internal partial pressure of “0” to some final internal partial pressure of “ $p_f$ ” during the bombing time (0 to T) yields:

$$V \frac{dp}{dt} = \frac{L}{p_o} (p_e - p)$$

$$\int_0^{p_f} \frac{1}{p - p_e} dp = \int_0^T \frac{-L}{P_o V} dt$$

$$\ln \left( \frac{p_e - p_f}{p_e} \right) = \frac{-LT}{P_o V}$$

$$p_f = p_e \left[ 1 - \exp \left( \frac{-LT}{P_o V} \right) \right] \quad (E.5)$$

This represents the partial pressure inside the part at the time it is extracted from high pressure bombing. Immediately afterwards the device is assumed to begin leaking in the opposite direction. Therefore the value of “ $p$ ” is treated as the new initial partial pressure and an additional integration occurs over the length of the dwell time. “ $p_e$ ” is treated as the external partial pressure of tracer gas at time “0” when the device is exposed to atmospheric conditions and is assume to be negligible. “ $p_f$ ” is treated as the initial internal tracer gas partial pressure discussed above. Separation of variables and integration with from an initial internal partial pressure of “ $p_f$ ” to some final partial pressure of “ $p_n$ ” during the dwell time (0 to t) yields:

$$V \frac{dp}{dt} = \frac{L}{p_o} (0 - p)$$

$$\int_{p_f}^{p_n} \frac{1}{p} dp = \int_0^t \frac{-L}{P_o V} dt$$

$$\ln \left( \frac{p_n}{p_f} \right) = \frac{-Lt}{P_o V}$$

$$p_n = p_f \left[ \exp \left( \frac{-Lt}{P_o V} \right) \right]$$

Substituting Equation E.5 for “ $p_f$ ” yields an equation which incorporates dwell time and bombing time.

$$p_n = p_e \left[ 1 - \exp \left( \frac{-LT}{P_o V} \right) \right] \left[ \exp \left( \frac{-Lt}{P_o V} \right) \right] \quad (E.6)$$

If an initial tracer gas partial pressure is present in the cavity due to a previous test or some other means, it should be accounted for. This is done by incorporating a term for the initial partial pressure ( $p'$ ) as an initial condition applied to integration bounds of Equation E.4. Integration with the initial partial pressure term with respect to the bombing time leads to an expression of the internal partial pressure at the end of the bombing period. This is expressed as:

$$\begin{aligned} V \frac{dp}{dt} &= \frac{L}{p_o} (p_e - p) \\ \int_{p'}^{p_f} \frac{1}{p - p_e} dp &= \int_0^T \frac{-L}{P_o V} dt \\ \ln \left( \frac{p_e - p_f}{p_e - p'} \right) &= \frac{-LT}{P_o V} \\ p_f &= (p - p') \left[ \exp \left( \frac{-LT}{P_o V} \right) \right] \end{aligned}$$

This can be rewritten in the form expressed above:

$$p_f = p' + (p_e - p') \left[ 1 - \exp \left( \frac{-LT}{P_o V} \right) \right] \quad (E.7)$$

The same operation conducted to produce Equation E.6 is applied to Equation E.7 yielding an expression for the partial pressure of a tracer gas inside in internal cavity with respect to the bombing time, dwell time, and an initial internal pressure:

$$p_f = \left[ p' + (p_e - p') \left[ 1 - \exp\left(\frac{-LT}{P_o V}\right) \right] \right] \left[ \exp\left(\frac{-Lt}{P_o V}\right) \right] \quad (\text{E.8})$$

The ramifications of failure to utilize Equation E.8 when an initial tracer gas partial pressure is present are discussed in Section 3.7.

## **Appendix F**

NASA CEA Stoichiometric Analysis

NASA-GLENN CHEMICAL EQUILIBRIUM PROGRAM CEA2, FEBRUARY 5, 2004  
 BY BONNIE MCBRIDE AND SANFORD GORDON  
 REFS: NASA RP-1311, PART I, 1994 AND NASA RP-1311, PART II, 1996

\*\*\*\*\*

prob case=LEEF1057 uv

rho,g/cc = 1.5

reac

name C2H2,acetylene mole = 1 t,k= 298.15

name N2O mole = 3 t,k= 298.15

output trace=1e-5

end

OPTIONS: TP=F HP=F SP=F TV=F UV=T SV=F DETN=F SHOCK=F REFL=F INCD=F  
 RKT=F FROZ=F EQL=F IONS=F SIUNIT=T DEBUGF=F SHKDBG=F DETDBG=F TRNSPT=F

TRACE= 1.00E-05 S/R= 0.000000E+00 H/R= 0.000000E+00 U/R= 0.000000E+00

SPECIFIC VOLUME,M\*\*3/KG = 6.666667E-04

REACTANT	MOLES	(ENERGY/R),K	TEMP,K	DENSITY	EXPLODED FORMULA
N: C2H2,acetylene	1.000000	0.271478E+05	298.15	0.0000	C 2.00000 H 2.00000
N: N2O	3.000000	0.957014E+04	298.15	0.0000	N 2.00000 O 1.00000

SPECIES BEING CONSIDERED IN THIS SYSTEM  
 (CONDENSED PHASE MAY HAVE NAME LISTED SEVERAL TIMES)  
 LAST thermo.inp UPDATE: 9/09/04

g 7/97 *C	tpis79 *CH	g 4/02 CH2
g 4/02 CH3	g 11/00 CH2OH	g 7/00 CH3O
g 8/99 CH4	g 7/00 CH3OH	srd 01 CH3OOH
g 8/99 *CN	g 12/99 CNN	tpis79 *CO
g 9/99 *CO2	tpis91 COOH	tpis91 *C2
g 6/01 C2H	g 1/91 C2H2,acetylene	g 5/01 C2H2,vinylidene
g 4/02 CH2CO,ketene	g 3/02 O(CH)2O	srd 01 HO(CO)2OH
g 7/01 C2H3,vinyl	g 9/00 CH3CN	g 6/96 CH3CO,acetyl
g 1/00 C2H4	g 8/88 C2H4O,ethylen-o	g 8/88 CH3CHO,ethanal
g 6/00 CH3COOH	srd 01 OHCH2COOH	g 7/00 C2H5
g 7/00 C2H6	g 8/88 CH3N2CH3	g 8/88 C2H5OH
g 7/00 CH3OCH3	srd 01 CH3O2CH3	g 7/00 CCN
tpis91 CNC	srd 01 OCCN	tpis79 C2N2
g 8/00 C2O	tpis79 *C3	n 4/98 C3H3,1-propynl
n 4/98 C3H3,2-propynl	g 2/00 C3H4,allene	g 1/00 C3H4,propyne
g 5/90 C3H4,cyclo-	g 3/01 C3H5,allyl	g 2/00 C3H6,propylene
g 1/00 C3H6,cyclo-	g 6/01 C3H6O,propylox	g 6/97 C3H6O,acetone
g 1/02 C3H6O,propanal	g 7/01 C3H7,n-propyl	g 9/85 C3H7,i-propyl
g 2/00 C3H8	g 2/00 C3H8O,1propanol	g 2/00 C3H8O,2propanol
srd 01 CNCOCN	g 7/88 C3O2	g tpis *C4
g 7/01 C4H2,butadiyne	g 8/00 C4H4,1,3-cyclo-	n10/92 C4H6,butadiene
n10/93 C4H6,1butyne	n10/93 C4H6,2butyne	g 8/00 C4H6,cyclo-
n 4/88 C4H8,1-butene	n 4/88 C4H8,cis2-buten	n 4/88 C4H8,tr2-butene

n 4/88 C4H8,isobutene	g 8/00 C4H8,cyclo-	g10/00 (CH3COOH)2
n10/84 C4H9,n-butyl	n10/84 C4H9,i-butyl	g 1/93 C4H9,s-butyl
g 1/93 C4H9,t-butyl	g12/00 C4H10,n-butane	g 8/00 C4H10,isobutane
g 6/01 C4N2	g 8/00 *C5	g 5/90 C5H6,1,3cyclo-
g 1/93 C5H8,cyclo-	n 4/87 C5H10,1-pentene	g 2/01 C5H10,cyclo-
n10/84 C5H11,pentyl	g 1/93 C5H11,t-pentyl	n10/85 C5H12,n-pentane
n10/85 C5H12,i-pentane	n10/85 CH3C(CH3)2CH3	g 2/93 C6H2
g11/00 C6H5,phenyl	g 8/00 C6H5O,phenoxy	g 8/00 C6H6
g 8/00 C6H5OH,phenol	g 1/93 C6H10,cyclo-	n 4/87 C6H12,1-hexene
g 6/90 C6H12,cyclo-	n10/83 C6H13,n-hexyl	g 6/01 C6H14,n-hexane
g 7/01 C7H7,benzyl	g 1/93 C7H8	g12/00 C7H8O,cresol-mx
n 4/87 C7H14,1-heptene	n10/83 C7H15,n-heptyl	n10/85 C7H16,n-heptane
n10/85 C7H16,2-methylh	n 4/89 C8H8,styrene	n10/86 C8H10,ethylbenz
n 4/87 C8H16,1-octene	n10/83 C8H17,n-octyl	n 4/85 C8H18,n-octane
n 4/85 C8H18,isoctane	n10/83 C9H19,n-nonyl	g 3/01 C10H8,naphthale
n10/83 C10H21,n-decyl	g 8/00 C12H9,o-bipheny	g 8/00 C12H10,biphenyl
g 6/97 *H	g 6/01 HCN	g 1/01 HCO
tpis89 HCCN	g 6/01 HCCO	g 6/01 HNC
g 7/00 HNCO	g10/01 HNO	tpis89 HNO2
g 5/99 HNO3	g 4/02 HO2	tpis78 *H2
g 5/01 HCHO,formaldehy	g 6/01 HCOOH	g 8/89 H2O
g 6/99 H2O2	g 6/01 (HCOOH)2	g 5/97 *N
g 6/01 NCO	g 4/99 *NH	g 3/01 NH2
tpis89 NH3	tpis89 NH2OH	tpis89 *NO
g 4/99 NO2	j12/64 NO3	tpis78 *N2
J12/64 N2O	g 6/01 NCN	g 5/99 N2H2
tpis89 NH2NO2	g 4/99 N2H4	g 4/99 N2O3
tpis89 N2O4	g 4/99 N2O5	tpis89 N3
g 4/99 N3H	g 5/97 *O	g 4/02 *OH
tpis89 *O2	g 8/01 O3	g 12/0 THDCPD,endo
g 12/0 THDCPD,exo	g11/99 N2H4(L)	n 4/83 C(gr)
n 4/83 C(gr)	n 4/83 C(gr)	n12/84 CH3OH(L)
n12/84 C2H5OH(L)	n 4/85 C6H14(L),n-hexa	n12/88 C6H5NH2(L)
n10/86 C6H6(L)	g11/99 H2O(cr)	g 8/01 H2O(L)
g 8/01 H2O(L)		

O/F = 0.000000

	EFFECTIVE FUEL	EFFECTIVE OXIDANT	MIXTURE
INTERNAL ENERGY	u(2)/R	u(1)/R	u0/R
(KG-MOL)(K)/KG			
	0.35336408E+03	0.00000000E+00	0.35336408E+03

KG-FORM.WT./KG	bi(2)	bi(1)	b0i
*C	0.12652168E-01	0.00000000E+00	0.12652168E-01
*H	0.12652168E-01	0.00000000E+00	0.12652168E-01
*N	0.37956503E-01	0.00000000E+00	0.37956503E-01
*O	0.18978251E-01	0.00000000E+00	0.18978251E-01

POINT ITN T C H N O

THERMODYNAMIC EQUILIBRIUM COMBUSTION PROPERTIES AT ASSIGNED

VOLUME

CASE = LEEF1057

REACTANT		MOLES	ENERGY	TEMP
NAME			KJ/KG-MOL	K
C2H2,acetylene		1.0000000	225721.029	298.150
N2O		3.0000000	79571.029	298.150

O/F= 0.00000 %FUEL= 0.000000 R,EQ.RATIO= 1.666667 PHI,EQ.RATIO= 0.000000

#### THERMODYNAMIC PROPERTIES

P, BAR	24485.4
T, K	5094.61
RHO, KG/CU M	1.5000 3
H, KJ/KG	4570.41
U, KJ/KG	2938.05
G, KJ/KG	-38474.9
S, KJ/(KG)(K)	8.4492
M, (1/n)	25.950
(dLV/dLP)t	-1.01389
(dLV/dLT)p	1.1180
Cp, KJ/(KG)(K)	2.2088
GAMMAS	1.2011
SON VEL,M/SEC	1400.2

#### MOLE FRACTIONS

CH3	1.7939-5
CH4	1.2402-5
*CN	9.5595-5
*CO	2.7650-1
*CO2	4.6049-2
COOH	4.9964-4
CH2CO,ketene	1.1733-5
OCCN	1.2445-5
*H	1.0796-2
HCN	1.5098-3
HCO	1.5547-3
HNC	7.0462-4
HNCO	6.6839-4
HNO	2.9795-4
HNO2	2.9206-5
HO2	7.9967-5
*H2	5.5906-2
HCHO,formaldehy	1.7449-4
HCOOH	2.6748-4
H2O	9.0109-2
H2O2	4.7562-5
*N	1.8330-4
NCO	1.5160-4
*NH	4.1974-4
NH2	6.5798-4
NH3	7.0681-4
*NO	1.0581-2
NO2	2.7851-5

*N2	4.8435-1
N2O	8.4828-5
*O	1.4812-3
*OH	1.5077-2
*O2	8.7114-4

\* THERMODYNAMIC PROPERTIES FITTED TO 20000.K

## **Appendix G**

Iterative Solution to Helium Mass Spectrometer Analysis

### Primary function: accept inputs and process data

```

function GraphRvals = HMSLeakRate2(varargin)

if length(varargin)~=6
    disp('For specific input data follow procedure below')
    disp('function requires inputs of T,t,R,P_b,g_p,V in specified order')
    disp('T = bombing time of specimen(seconds)')
    disp('t = dwell time of specimen (input as t = [1 2 3 ... n])')
    disp('R = indicated leak rate (input as as R = [1 2 3 ... n])')
    disp('P_b = external bombing pressure of specimen(atm absolute)')
    disp('g_p = helium gas purity (in decimal form)')
    disp('V = internal free volume of tested specimen(cm^3)')
    disp('-----')
    disp('Copy and paste HMSLeakRate(T,t,R,P_b,g_p,V) for input form')
    disp('-----')
    error('Wrong number of inputs to final bounds, 6 inputs required');
else
    close all
    T=varargin{1};           % Helium Bombing time (sec)
    t=varargin{2};           % Dwell time for individual parts
    R=varargin{3};           % Indicated leak rate (displayed on HMS)
    P_b=varargin{4};         % Helium Bombing Pressure (Atm)
    g_p=varargin{5};         % Helium gas purity percentage (decimal form)
    V=varargin{6};           % Internal Free Volume of test specimen
    P_e=g_p*P_b;             % Partial pressure of helium during bombing.
    P_o = 1;                 % Standard atmospheric pressure
    He_Air = (1/2.69);       % Leak Rate conversion between air and helium
end

loginc = 100;           n = 0;
lowerbound = 1E-9;     upperbound = 1E0;
R_r(1) = lowerbound;

for m=2:900*abs((log10(upperbound)-log10(lowerbound)))
    R_r(m)=R_r(m-1)+lowerbound*(1/loginc);
    if m==n+901
        n=n+900;
        lowerbound=lowerbound*10;
    end
end

Rvals = findallbounds(T, t, R, P_e, V);

for i=1:length(T)
    for k= 1:length(t)
        sign = 1;   lastsign = 1;
        for j = 2:length(R_r)
            E(k,1) = (1/P_o)*(1-exp(-1E-9*T(i)))*exp(-1E-9*t(k));
            EC(k,1) = R(k)/(P_o*V*P_e*R_r(1)) ;
            E(k,j) = (1/P_o)*(1-exp(-R_r(j)*T(i)))*exp(-R_r(j)*t(k));
            EC(k,j) = R(k)/(P_o*V*P_e*R_r(j)) ;
            if EC(k,j) ~= E(k,j)
                sign = (EC(k,j)-E(k,j))/abs(EC(k,j)-E(k,j));
            end
        end
    end
end

```

```

        if sign ~= lastsign
            EC1 = [ EC(k,j) R_r(j) ];
            EC2 = [ EC(k,j-1) R_r(j-1) ];
            loglog(R_r(j-1),EC(k,j-1),'r+'); hold on;
            loglog(R_r(j),EC(k,j),'r+')
        end
    end
    lastsign = sign;
end

for pl=1:4
    Ep(pl) = (1/P_o)*(1-exp(-Rvals(k).bounds(pl)*T))*...
        exp(-Rvals(k).bounds(pl)*t(k));
    ECp(pl) = R(k)/(P_o*V*P_e*Rvals(k).bounds(pl));
    rpl(pl) = Rvals(k).bounds(pl);
end
loglog(rpl,ECp,'bo')
loglog(rpl([2 4]),ECp([2 4]),'b-')
loglog(rpl,Ep,'r.')
loglog(rpl([2 4]),Ep([2 4]),'r-')
loglog(R_r,E(k,:), 'k'); hold on;
loglog(R_r,EC(k,:), 'k');
end
end

for i=1:length(t)
    F_leak(i) =
        ((Rvals(i).bounds(1,1)+Rvals(i).bounds(1,2))/2)*P_o*V*He_Air;
    G_leak(i) =
        ((Rvals(i).bounds(2,1)+Rvals(i).bounds(2,2))/2)*P_o*V*He_Air;
end

allboundsdata(T, t, R, P_b, g_p, V, P_e, F_leak, G_leak);
axis([1E-9 1 1E-6 1]); grid on;
xlabel('Relaxaton Rate R_r(s^-1)')
ylabel('Internal Fractional Helium Pressure E (atm^-1)')
GraphRvals = [F_leak G_leak];

```

### Secondary function: refine data point associated error

```

function Rvals = findallbounds(varargin)
% inputs to the function should be none, or in the order: T,t,R,P_e,V

%-----
-
%
%
if nargin == 0
    error('function requires T,t,R,P_e,V inputs to operate');
else
    if length(varargin)~=5
        disp('function requires T,t,R,P_e,V inputs')
        error('Wrong number of inputs to findallbounds()');
    end
end

```

```

else
    T=varargin{1};
    t=varargin{2};
    R=varargin{3};
    P_e=varargin{4};
    V=varargin{5};
end
end
P_o = 1 ;
R_r = logspace(-9,0,1000);
for k=1:length(t)
    Rind = 2;
    E1 = (1/P_o)*(1-exp(-R_r(1)*T))*exp(-R_r(1)*t(k));
    E2 = R(k)/(P_o*V*P_e*R_r(1));
    sign = (E1-E2)/abs(E1-E2);
    lastsign = sign;
    inters = 1;
    lastR = 5;
    while inters < 3
        E1 = (1/P_o)*(1-exp(-R_r(Rind)*T))*exp(-R_r(Rind)*t(k));
        E2 = R(k)/(P_o*V*P_e*R_r(Rind));
        if E1 ~= E2
            sign = (E1-E2)/abs(E1-E2);
            if sign ~= lastsign
                Rvals(k).bounds(inters,:) = [lastR R_r(Rind)];
                inters = inters+1;
            end
            lastR = R_r(Rind);
        else
            lastR = R_r(Rind-1);
        end
        lastsign = sign;
        Rind = Rind+1;
    end
end
end

for rvi = 1:length(Rvals)
    for bi = 1:size(Rvals(rvi).bounds,1)
        bounds = Rvals(rvi).bounds(bi,:);
        other.R = R(rvi);
        other.P_o = P_o;
        other.V = V;
        other.P_e = P_e;
        other.t = t(rvi);
        other.T = T;
        boundsep = abs(bounds(1)-bounds(2));
        lastbound = bounds;
        while boundsep > 1e-10
            newbound = refinebound(bounds,other);
            if isempty(newbound)
                break;
            else
                if newbound >= lastbound
                    break
                end
                lastbound = newbound;
            end
        end
    end
end

```

```

        boundsep = abs(newbound(1)-newbound(2));
    end
end
if isempty(newbound)
    warning(sprintf('Error in bound refinement. Returned empty
bound for Rvals(%d).bounds(%d)', rvi, bi));
end
Rvals(rvi).bounds(bi,:) = lastbound;
end
end
end

function newbound = refinebound(bounds, other)
    Vn = other.V;
    Rn = other.R;
    P_on = other.P_o;
    P_en = other.P_e;
    tn = other.t;
    Tn = other.T;
    flip=0;
    rind = 2;
    lastr=5;
    newbound = [];
    R_rn = logspace(log10(bounds(1)), log10(bounds(2)), 1000);
    En1 = (1/P_on)*(1-exp(-R_rn(1)*Tn))*exp(-R_rn(1)*tn);
    En2 = Rn/(P_on*Vn*P_en*R_rn(1));
    nsign = (En1-En2)/abs(En1-En2);
    nlsign = nsign;
    while ~flip
        En1 = (1/P_on)*(1-exp(-R_rn(rind)*Tn))*exp(-R_rn(rind)*tn);
        En2 = Rn/(P_on*Vn*P_en*R_rn(rind));
        if En1 ~= En2
            nsign = (En1-En2)/abs(En1-En2);
            if nsign ~= nlsign
                newbound = [lastr R_rn(rind)];
                flip=1;
            end
            lastr = R_rn(rind);
        else
            lastr = R_rn(rind-1);
        end
        nlsign = nsign;
        rind = rind+1;
        if rind > 1000
            break
        end
    end
end
end
end

```

### Secondary function: export data to excel document

```

function Rdata = allboundsdata(varargin)

    T = varargin{1};
    t = varargin{2};
    R = varargin{3};
    P_b = varargin{4};
    g_p = varargin{5};
    V = varargin{6};
    P_e = varargin{7};
    F_leak = varargin{8};
    G_leak = varargin{9};
    testnum = zeros(1,max(size(R)));
    date=datestr(floor(now),'mmmmddyyyy','local');

    try exist([date '.xls'],'file');
        num=xlsread([date '.xls'],'TestNum','A3');
        num=num+1;
        xlswrite(date,num,'TestNum','A3');
    catch
        num=1;
        TestNumTitle={'Number of Separate Tests on: '; date };
        xlswrite(date,TestNumTitle,'TestNum','A1');
        xlswrite(date,num,'TestNum','A3');
    end

    for j = 1:max(size(R));
        testnum(j) = j;
    end

    Heading = {'Daily Test #' num ' ';
               'Date' datestr(floor(now),'mmmm-dd-yyyy','local') ' ';
               'Gas Purity' 100*g_p '%';
               'Bomb Pressure' P_b 'Atm';
               'He Partial Pressure' P_e 'Atm';
               'Volume' V 'cc';
               'Bomb Time' T 'sec'} ;
    titleline = {'Test #','Dwell Time','Indicated Leak','Fine
    Leak','Gross Leak'};

    xlswrite(date,Heading,int2str(num),'A1');
    xlswrite(date,titleline,int2str(num),'A8');
    xlswrite(date,testnum,int2str(num),'A9');
    xlswrite(date,t,int2str(num),'B9');
    xlswrite(date,R,int2str(num),'C9');
    xlswrite(date,F_leak,int2str(num),'D9');
    xlswrite(date,G_leak,int2str(num),'E9');

    Rdata='success';
end

```

## **Appendix H**

Iterative Solution to Radioisotope Leak Detection Code

```

% Radiflo leak equation correlation
%% Function parameters (necessary input data is required)
function GraphRvals = Radiflo(varargin)

if length(varargin)~=8
    disp('For specific input data follow procedure below')
    disp('function requires inputs of P_e, t, V, Lrej, R_o, Rrej, K, S')
    disp('t = dwell time of specimen (input as t = [1 2 3 ... n])')
    disp('V = internal free volume of sample (cc)')
    disp('Lreject = test sensitivity (atm*cc/s)')
    disp('R_o = background activity (counts/min)')
    disp('Rreject = set reject level (counts/min)')
    disp('K = crystal counting efficiency (counts/min*muCi)')
    disp('S = specific activity of Kr used (muCi/atm*cc)')
    disp('P_e = bombing pressure (atm absolute)')
    disp('-----')
    disp('Copy and paste HMSLeakRate(T,t,R,P_b,g_p,V) for input form')
    disp('-----')
    error('Wrong number of inputs to final bounds, 6 inputs required');
else
    close all
    P_e = varargin{1};           % Bombing time
    t = varargin{2};           % Dwell time for individual parts
    V = varargin{3};           % internal volume of sample
    Lrej = varargin{4};        % test sensitivity
    R_o = varargin{5};        % background level
    Rrej = varargin{6};        % reject level
    K = varargin{7};           % counting efficiency
    S = varargin{8};           % specific activity
    %P_e = varargin{9};        % bombing pressure

end

%% Constant parameters
t_c = 3600 ;                   % Conversion between seconds and hours
P_o = 1 ;                      % Atmospheric pressure (atm)
Kr_Air = (1/1.71);            % Leak Rate conversion between air and Kr
% Technically, (M_air/M_Kr)^(1/2)=(1/1.71), simplified for equations
EC = Rrej/(P_o*V*P_e*S*K);
Rr = (100)*Lrej*(Kr_Air);
T=-(log(1-(EC/P_o)))/(Rr*t_c);

%% Create the R space based on logarithmic decades (900 points per log
set)
loginc = 100;                 n = 0;
lowerbound = 1E-9; upperbound = 1E0;
R_r(1) = lowerbound;

for m=2:900*abs((log10(upperbound)-log10(lowerbound)))
    R_r(m)=R_r(m-1)+lowerbound*(1/loginc);
    if m==n+901
        n=n+900;
        lowerbound=lowerbound*10;
    end
end
end

```

```

for i=1:length(T)
    sign = 1;    lastsign = 1;
    for k= 1:length(t)
        for j = 2:length(R_r)
            E(k,1) = (1/P_o)*(1-exp(-1E-9*T(i)*t_c))*exp(-1E-9*t(k));
            E(k,j) = (1/P_o)*(1-exp(-R_r(j)*T(i)*t_c))*exp(-R_r(j)*t(k));
            if EC ~= E(k,j)
                sign = (EC-E(k,j))/abs(EC-E(k,j));
                if sign ~= lastsign;
                    EC1 = [ EC R_r(j) ] ;
                    EC2 = [ EC R_r(j-1) ] ;
                    loglog(R_r(j-1),EC,'bo'); hold on;
                    loglog(R_r(j),EC,'bo');
                end
            end
            lastsign = sign;
        end
        loglog(R_r,E(k,:), 'k');
    end
end

%% Graphing parameters
lowerbound = 1E-9;    upperbound = 1E0;
loglog([lowerbound,upperbound],[EC,EC], 'r'); hold on
loglog([Rr,Rr],[lowerbound,10*EC], 'b')
axis([1E-9 1 1E-6 1]);    grid on;
xlabel('Relaxaton Rate R_r(s^-1)')
ylabel('Internal Fractional Helium Pressure E (atm^-1)')
GraphRvals=P_o;

```